1983

Rheological and other properties of some novel thermotropic liquid crystalline polyesters.

Debra Ann Simoff
University of Massachusetts Amherst

RHEOLOGICAL AND OTHER PROPERTIES OF SOME NOVEL THERMOTROPIC LIQUID CRYSTALLINE POLYESTERS

A Thesis Presented

By

Debra Ann Simoff

Submitted to the Graduate School of the
University of Massachusetts in partial fulfillment
of the requirements for the degree of

MASTER OF SCIENCE

February 1983

Polymer Science and Engineering Department

RHEOLOGICAL AND OTHER PROPERTIES OF SOME NOVEL THERMOTROPIC LIQUID CRYSTALLINE POLYESTERS

A Thesis Presented

By

Debra Ann Simoff

Approved as to style and content by:

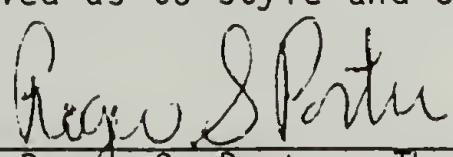

Prof. Roger S. Porter, Thesis Advisor

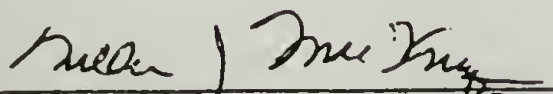

Prof. William J. MacKnight, Department Head
Polymer Science and Engineering Department

DEDICATION:

To Mom

Dad

Terry

Diane

Celeste

Nick

and Toby

ACKNOWLEDGEMENTS

I extend my deepest thanks and appreciation to the two persons most responsible for making this thesis possible: Dr. Oliver Deex of Monsanto Company, who provided the novel liquid crystalline polyesters on which the thesis was based, and my thesis advisor, Dr. Roger S. Porter for his guidance, support, and encouragement.

I also thank Dr. Morris Ort and Dr. Robert Mendelson of Monsanto Company. Dr. Ort provided the sample of non-liquid crystalline polyester which was used as a reference, and Dr. Mendelson provided background rheological data for this reference polymer.

A number of researchers working in the field of polymer liquid crystal rheology were very helpful in discussing their work with me, and/or providing preprints of as-yet unpublished articles. These include Dr. K.F. Wissbrun, Prof. J.L. White, Prof. D.G. Baird, Prof. G.L. Wilkes, Prof. M.T. Shaw, and Dr. G. Kiss.

Several people in the PSE Department provided special assistance in obtaining data. I would particularly like to thank Cameron Murray and William McCarthy for help with x-ray crystallinity mesurement, Robert Briber for obtaining wide-angle x-ray scattering photographs, Louis Raboin for assistance with scanning electron microscopy, and Steve Allen for help with tensile testing.

Sincere appreciation and thanks are extended for the combined cooperation of Ms. Dottie Swan, Ms. Marylin Cummings, and Ms. Marilyn Putnam in typing the manuscript, and Ms. Nan Finkenaur, who prepared the majority of the original figures.

A special thank you is reserved for my friend, Roger Doerpholz, for his companionship and encouragement throughout my graduate studies.

TABLE OF CONTENTS

LIST OF FIGURES

LIST OF TABLES

C H A P T E R I

INTRODUCTION

Background

A "liquid crystal" is a substance whose properties are intermediate between those of a crystalline solid and an isotropic liquid. The molecules within a liquid crystal are partially ordered, but they are able to translate easily in at least one direction.

Various types of liquid crystalline order exist (eg., "nematic," "smectic," "cholesteric," "discotic," etc.), but only nematic liquid crystals will be discussed. Nematic liquid crystals contain rod-shaped molecules (or segments of molecules) which tend to align with their axes parallel to each other. Locally, the rods point in a preferred direction, but they can translate easily along that direction.

Currently there is much interest in nematic liquid crystalline polymers (LCPs) - that is, those polymers which exhibit a nematic state. This is because the rod-like molecules orient easily with little mechanical stress, offering the potential for forming fibers of ultra-high strength and modulus. Numerous nematic LCP compositions have produced fibers which are stronger than steel on a per unit weight basis (1). The best known example is duPont's Kevlar

(poly-p-phenylene-terephthalamide), which is available commercially. The mechanical properties of Kevlar 49 (a particular commercial grade) are compared with those of stainless steel and other fibers in Table 1 (2).

"Thermotropic" LCPs are those which form a liquid crystalline phase upon heating from the semi-crystalline state. This class is increasingly being investigated for alternative fiber candidates to "lyotropic" polymers (such as Kevlar), which require solvent for formation of the mesophase. From a manufacturing standpoint, the necessity for solvent handling and removal is undesirable. In addition, the majority of lyotropic fiber candidates have been relatively insoluble, requiring rather aggressive, unpleasant solvents. Kevlar, for example, is spun from sulfuric acid solution. Thermotropic LCPs circumvent the need for solvent, providing the opportunity for use of additional fabricating techniques, such as injection molding, film blowing, and sheet or profile extrusion.

The first thermotropic LCPs to be recognized appear to be the copolyesters of poly(ethylene terephthalate) (PET) and p-hydroxy benzoic acid (PHB), studied by Jackson, Kuhfuss, and co-workers of Tennessee Eastman Company (3,4). Injection molded specimens of copolyesters having 60 mole % PHB were shown to have superior strength and modulus along the flow direction to commercial glass-reinforced polyesters, although properties in the across-flow direction were weak.

A new family of aromatic polyesters - some of which are thermotropic - has recently been introduced in the patent literature

Table 1

Mechanical Properties of Kevlar 49 compared with Other Fibers and Stainless Steel

	Kevlar 49 Aramid	DuPont Nylon Type 728	Dacron Polyester Type 68	"E" Glass	Stainless Steel
Tensile Strength, GPa.	2.8**	1.0**	1.1**	2.4***	1.7
Tensile Modulus, GPa.	124	6	14	69	200
Elongation to Break, %	2.5	18.3	14.5	3.5	2.0
Density, g/cm^3	1.44	1.14	1.38	2.55	7.86
Specific Tensile Strength*, cm	20	8.8	8.3	9.7	2.2
Specific Tensile Modulus*, 10^8 cm	8.8	0.49	1.0	2.8	2.6

* Absolute property divided by density.
** Unimpregnated twisted yarn test - ASTM D2256
*** Impregnated strand test - ASTM D2343

by Monsanto Company (5). These are polyesters of 1,2-bis-(4-hydroxy phenyl) ethane (called Bisphenol E and designated BPE) with one or more aromatic dicarboxylic acids. Within this family, thermotropic behavior is observed in the copolymer of BPE with a mixture of 80:20 isophthalic acid:2,6-naphthalene dicarboxylic acid, while isotropic behavior is observed in the homopolymer of BPE with isophthalic acid alone (containing no naphthyl groups). Samples from these two members of the BPE family - one being thermotropic and the other not (for comparison) - were obtained for this thesis investigation.

The focus in this investigation has been to examine and compare the rheology of the two BPE polymers. Their rheology was of particular interest because: 1.) relatively little is known about the rheology of thermotropic polymers, 2.) previous studies of lyotropic polymers, as well as the few existing studies of thermotropic polymers, have revealed very unusual rheological behavior compared to isotropic polymer fluids, and 3.) understanding of LCP rheology should aid the optimization of processing conditions in the production of ultra-high-strength, ultra-high-modulus materials.

In this report, the melt rheological behavior of the BPE-isophthalate-co-naphthalate liquid crystalline copolyester is compared with that of the non-liquid-crystalline BPE-isophthalate homopolyester using capillary rheometric techniques. In contrast to the reference hompolyester, the behavior of the thermotropic copolyester is observed to be unusual - particularly in 1.) the temperature dependence of viscosity, and 2.) the magnitude of extrudate swelling.

Other unusual behavior for the thermotropic polymers was observed in the molecular weight-dependence of viscosity. In comparing two separate batches of the BPE-isophthalate-co-naphthalate which had unintentionally been polymerized to different molecular weights, the higher-molecular weight polymer was found to have lower melt viscosity! This anomalous behavior compared to conventional polymers led to an investigation of possible compositional differences between the two copolyester batches, which is discussed in Chapter V.

In addition to the rheological and compositional studies, other properties of the BPE polymers were investigated to further understand their overall behavior. Characterization techniques included differential scanning calorimetry, measurement of melt turbidity and stir opalescence, x-ray determinations of crystallinity, characterization of extrudate orientation by x-ray and scanning electron microscopy, and measurement of tensile modulus.

Before turning to those chapters of the thesis in which experimental results are reported, key findings from the literature are reviewed which had particular relevance to the observed rheology of the BPE polymers.

Literature Review

Until recently little was known about the rheology of rod-like thermotropic polymers (6,7). A review by Baird (6) in 1978 cited a single published investigation - that of Jackson and Kuhfuss (3) on copolyesters of poly(ethylene terephthalate) (PET) and p-hydroxy-

benzoic acid (PHB). A review in 1981 by Wissbrun (7) noted relatively few additional studies (4,8,9,10) - all of which again dealt with copolyesters of PET and PHB, but two which also included work on other rod-like thermotropic polyesters (4,10). However, interest in the rheology of rod-like thermotropic polymers is growing rapidly, as evidenced by the number of recent papers (11-18).

Studies of other types of liquid crystals are more numerous - especially low molecular weight liquid crystals and lyotropic polymers. The rheology of these systems has been reviewed elsewhere (6,10,19) and will not be discussed here in detail. However, many similarities in behavior have been observed between rod-like thermotropic polymers and these other types of liquid crystals, and some comparisons will be made.

A variety of unusual behavior patterns have been observed in the rheology of liquid crystals as compared to isotropic fluids. Examples of unconventional behavior which have been observed in rod-like thermotropic polymers include: 1.) minima in viscosity as a function of mesogen concentration (3,4,14); 2.) minima or plateaus in viscosity as a function of temperature (12,13,15-18); 3.) negative normal forces (10,11,14,17); 4.) negligible, and perhaps even negative, extrudate swell (9-13,17,18); 6.) history-dependent viscosity (10,15); 7.) secondary maxima in shear stress during start-up of steady shear (10,17); and 8.) incomplete stess-relaxation after cessation of steady shear (17).

In this review discussion will be limited to those topics which

were found to be particularly relevant in studies of the Bisphenol E-isophthalate-co-naphthalate polymers. These are: 1.) temperature dependence of viscosity, 2.) the nature of normal stresses and extrudate swell in shear flow, and 3.) the effect of molecular weight on viscosity.

Temperature dependence of viscosity. Porter and Johnson (19) noted in a 1967 review that low molecular weight rod-like (nematic) liquid crystals exhibit a "characteristic and unique" dependence of viscosity upon temperature. In the review article, the general flow behavior of the nematic mesophase was illustrated using the data shown in Figure 1, which was taken from earlier literature (20). Porter and Johnson noted that "the higher-temperature isotropic phase has a characteristically higher viscosity than the nematic mesophase at lower adjacent temperature." The region of steepest viscosity increase was associated with the nematic-isotropic transition. By contrast, viscosity of isotropic liquids normally decreases monotonically with increasing temperature.

The lower viscosity of the nematic mesophase vs the isotropic state has been attributed to the alignment of rod-like molecules (or segments), which orient readily in the direction of flow. These aligned molecules (or segments) dissipate less frictional energy than randomly arranged ones, presumably either by 1.) sliding easily past one another due to their parallel arrangement, or 2.) flowing together as units (clusters, domains) so that less surface area is

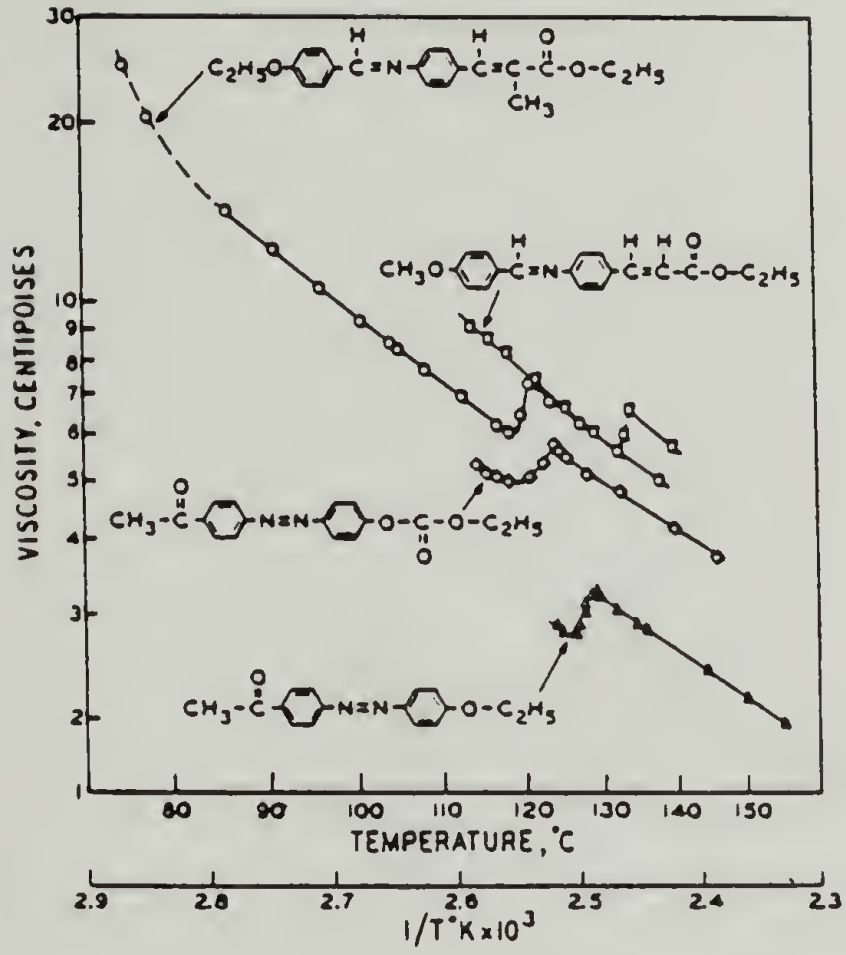

Fig. 1. Viscosity change with temperature for low molecular weight nematic liquid crystals (19).

involved in shearing. In either case, less dissipation of frictional energy results in a lower viscosity.

Solutions of many lyotropic polymers have also shown the same characteristic dependence of viscosity upon temperature which is exhibited by low molecular weight liquid crystals. However, with lyotropic polymers, behavior is furthur complicated by an unusual dependence of viscosity upon concentration. The interactive dependence of viscosity upon temperature and concentration has been depicted by Berry (21) using data for a polybisbenzoxazole (PBO), poly(p-benzamide) (PBA), and poly(p-phenylene diamine terephthalamide) (PPTA), as shown in Figure 2.

Until recently, such unusual temperature dependence of viscosity had not been reported for rod-like thermotropic polymers. The earliest and most widely-studied thermotropic polymers - copolyesters of PET and PHB - did not, at first, reveal any unusual temperature dependence (3,4,7-11). Typical early viscosity data for these copolyesters (as presented in the original papers) is shown in Figures 3 and 4 (8,9). Subsequent investigations by Baird (17), however, have indicated a region from 250-260°C where viscosity of a 60% PHB/PET copolyester does not decrease monotonically with temperature, but is nearly constant.

In the past year, three other research groups have reported either plateaus or local minima/maxima in viscosity as a function of temperature for rod-like thermotropic polymers. These are 1.) White et al with thermotropic hydroxypropyl cellulose (HPC) and ethyl cellu-

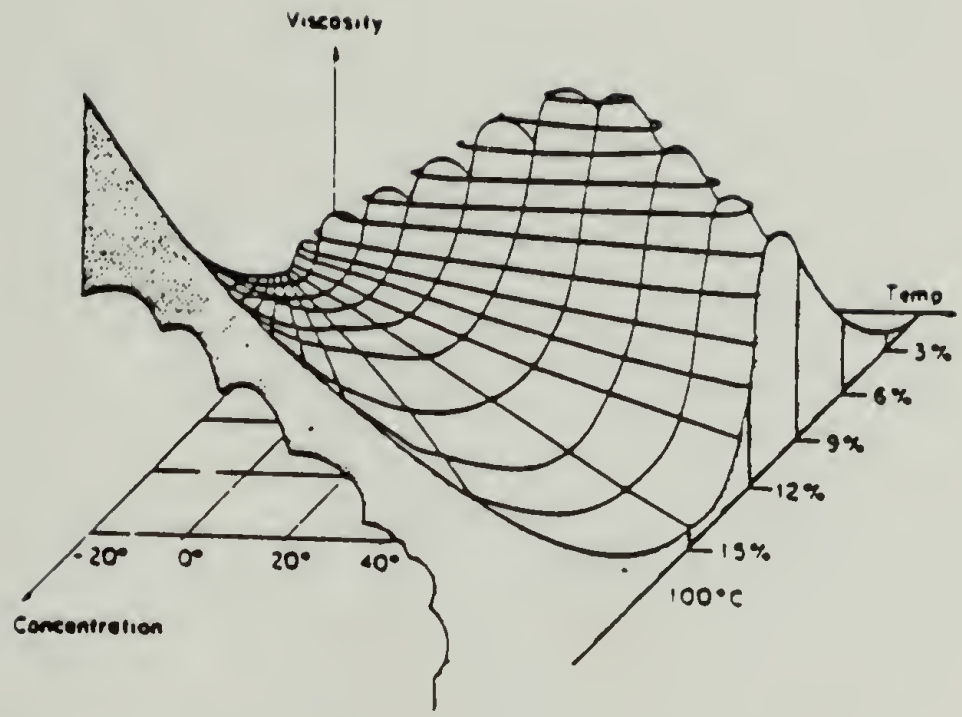

Fig. 2. Schematic diagram of the interactive dependence of viscosity on temperature and concentration for rod-like lyotropic polymers (21).

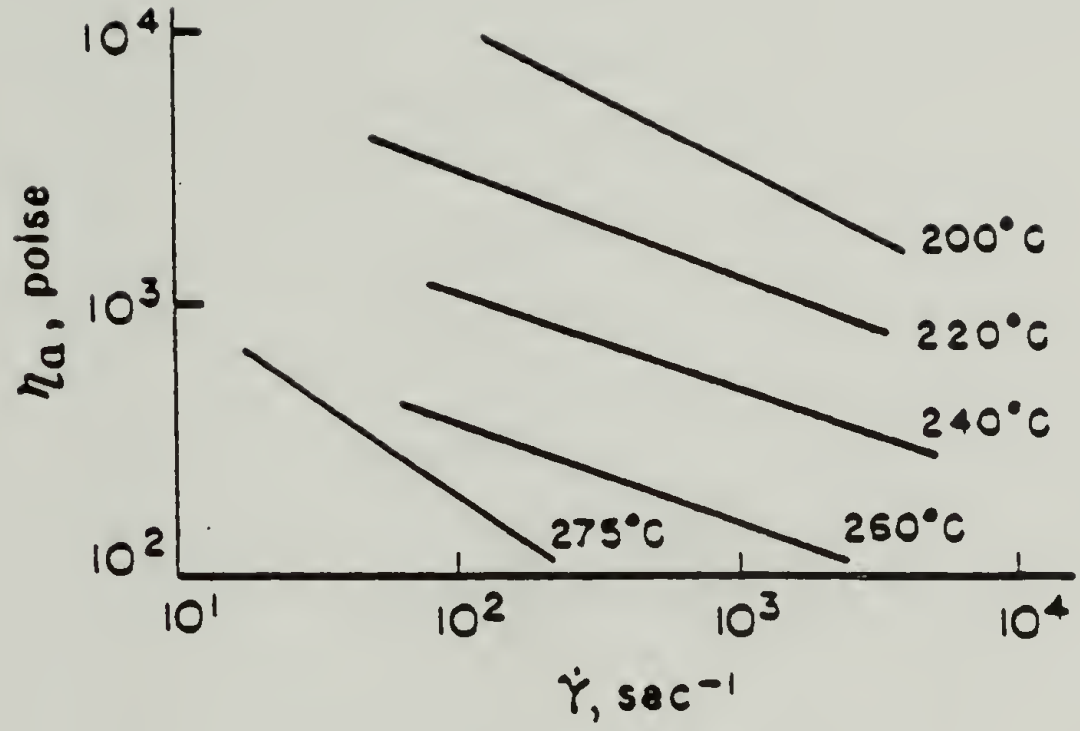

Fig. 3. Apparent melt viscosity of polyester X7G (8).

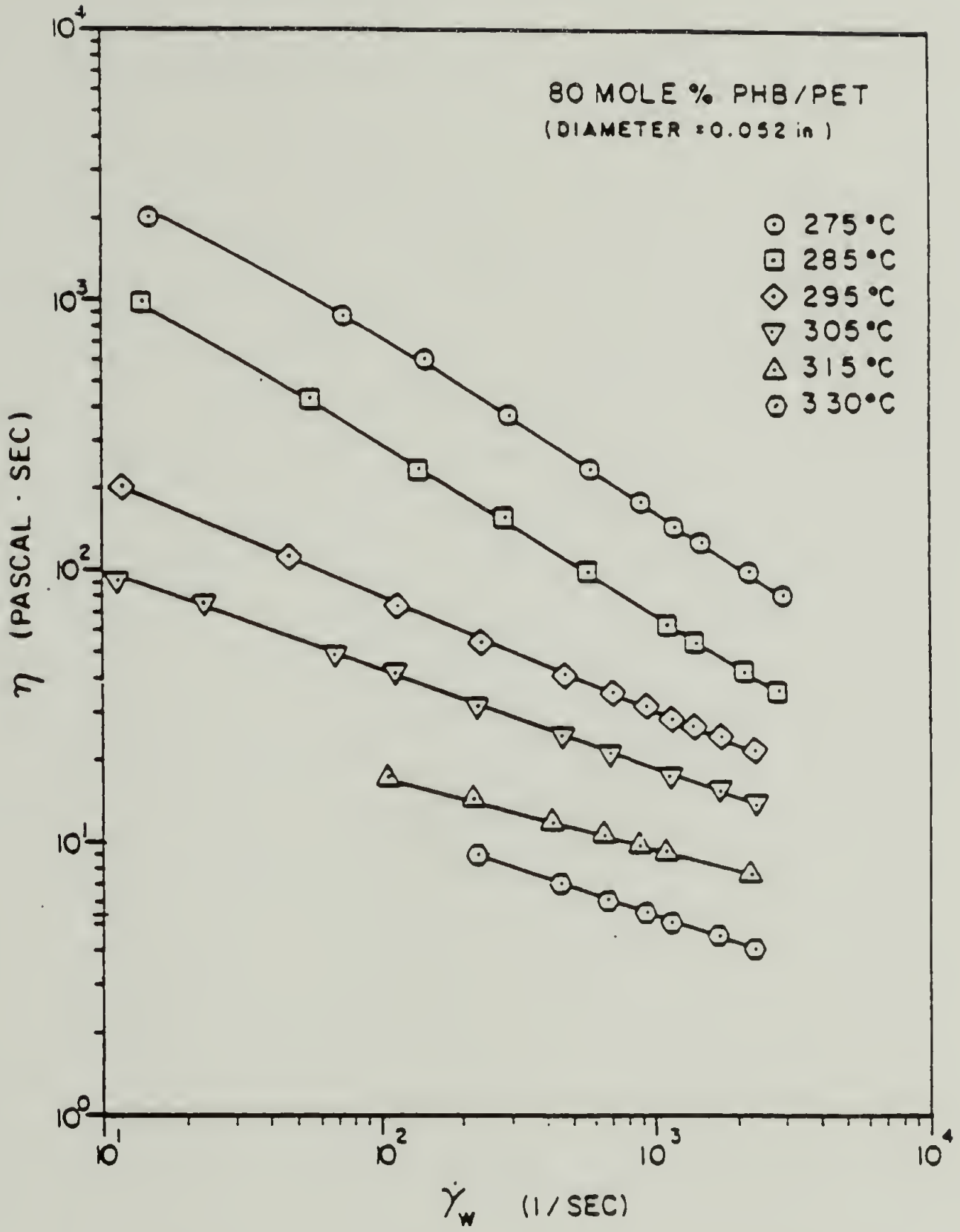

Fig. 4. Viscosity vs wall shear rate for 80 mole % PHB/PET as a function of temperature (9).

lose (EC) (12,13,18); 2.) Wissbrun and Griffin with a partially aliphatic copolyester in which both nematic and isotropic states are accessible for testing (15); and 3.) Bickel, Shaw, and Samulski with a novel thermotropic copolyester (16). In all three studies, the change in temperature dependence of viscosity corresponded to a transition from the liquid crystal to the isotropic fluid, as determined by differential scanning calorimetry and/or light scattering.

To illustrate the unusual temperature dependence of viscosity, data from two of these studies is reproduced in Figures 5 and 6. In Figure 5, viscosity-shear rate data for HPC and EC have been plotted at various temperatures, with dashed lines indicating the regions where the temperature dependence of viscosity changes (13). In Figure 6, data for the copolyester studied by Bickel et al show a plateau in viscosity as a function of temperature (16).

Minima in viscosity with temperature for rod-like thermotropic polymers were documented as early as 1977 in a patent assigned to Tennessee Eastman Co. (22) covering copolyesters of the terephthalate-isophthalate-hydroquinone type (Figure 7). Their data were somewhat hidden in the literature, however, since the patent did not explicitly state the thermotropic liquid crystalline nature of the polymers.

Unusual temperature dependence of viscosity has also been reported for carbonaceous mesophase pitches as compared to isotropic pitches (23). Normally, isotropic pitch does exhibit a minimum and increase in viscosity at high temperature, but this is due to the onset of cross-linking (coke formation). Mesophase pitches, on the

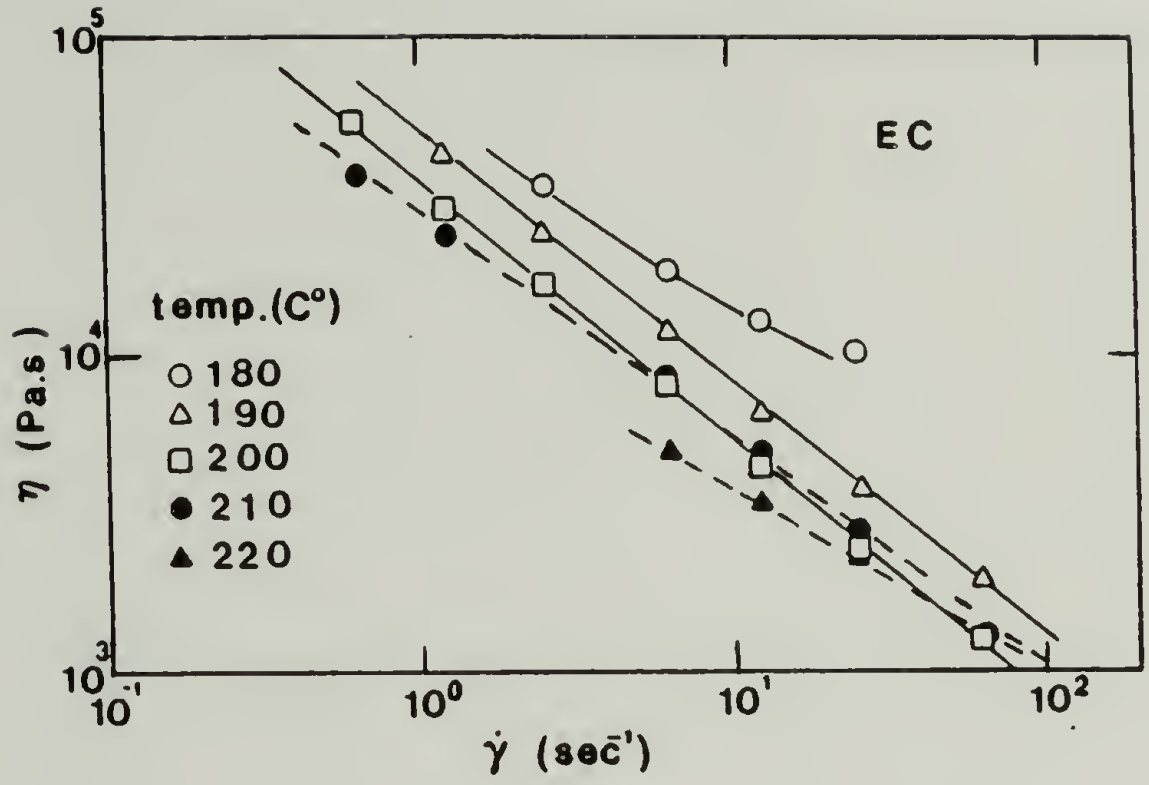

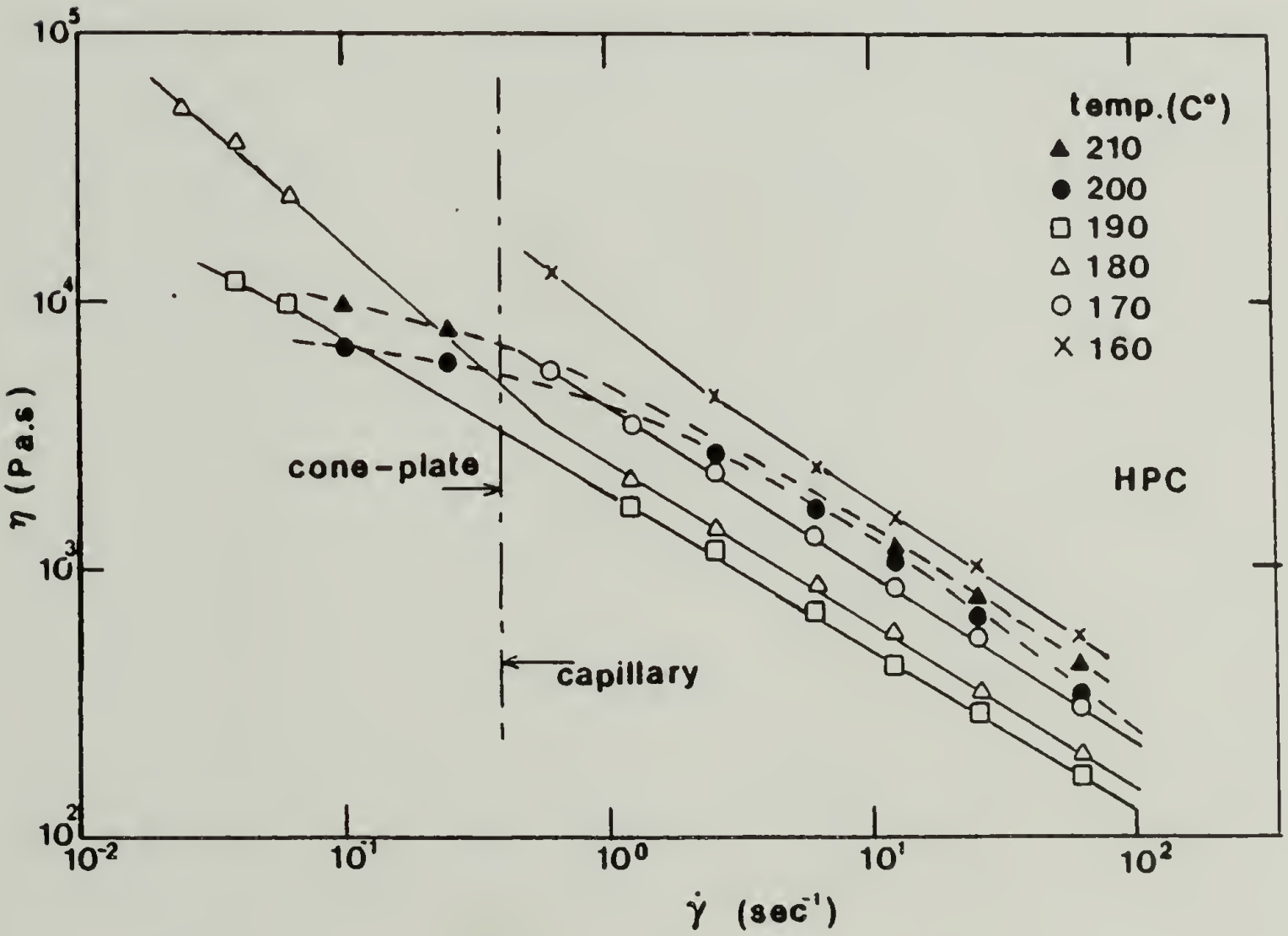

Fig. 5. Viscosity vs shear rate at various temperatures for thermotropic cellulose derivatives. Upper figure: ethyl cellulose; Lower figure: hydroxypropyl cellulose (13).

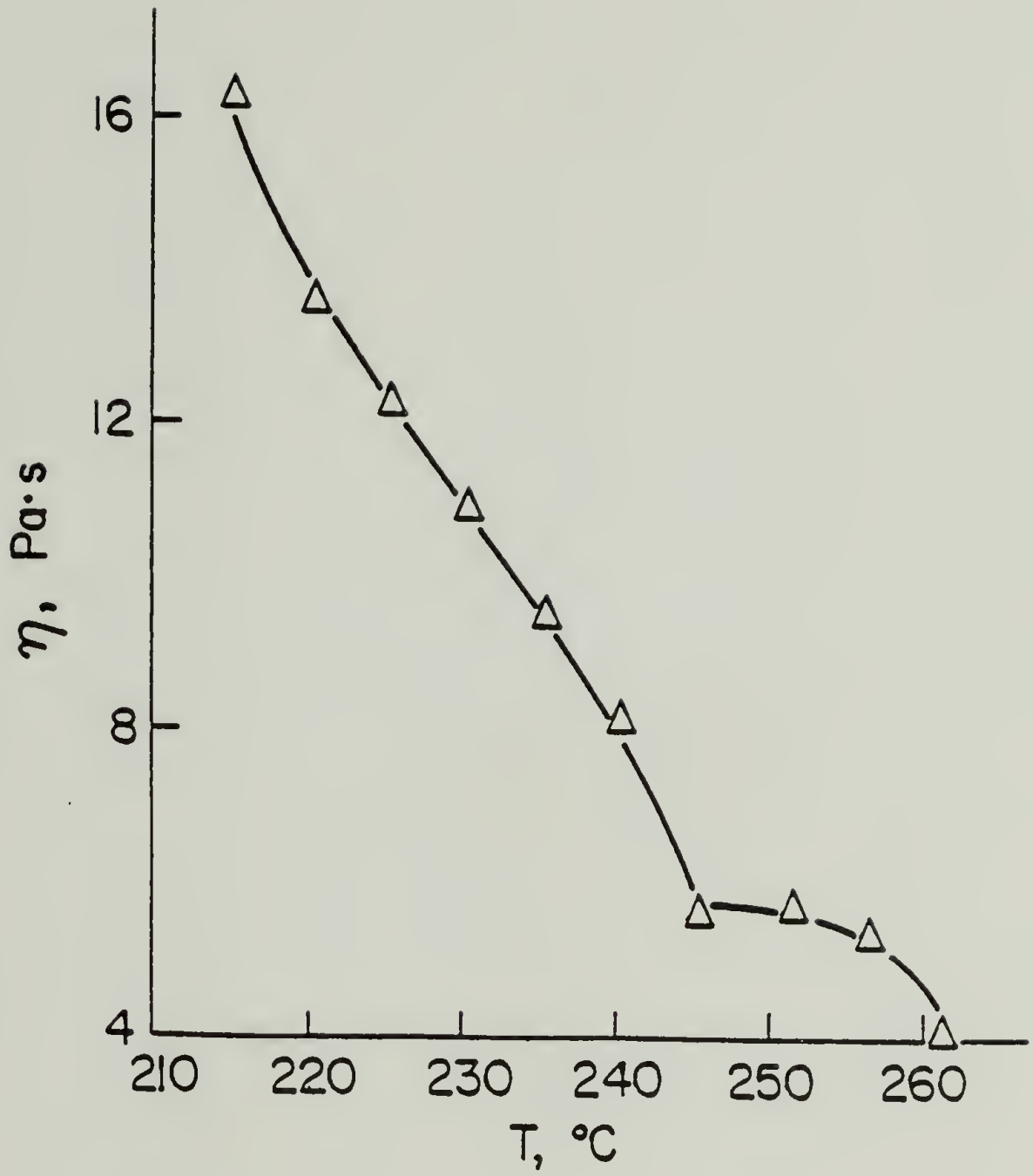

Fig. 6. Temperature dependence of viscosity for a novel thermotropic copolyester (16).

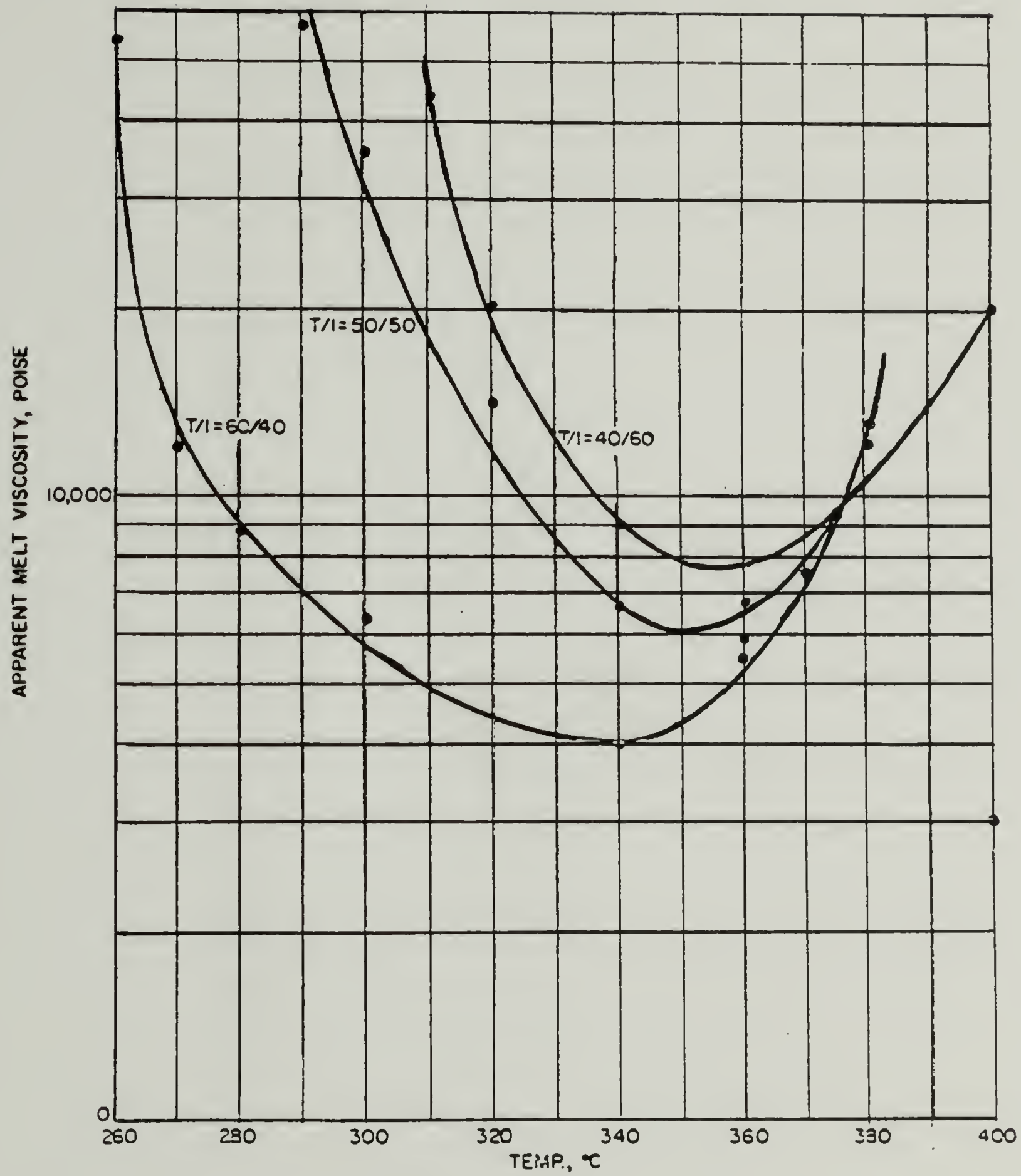

Fig. 7. Temperature dependence of viscosity for copolyesters of the terephthalate-isophthalate-hydroquinone type (22).

other hand, can exhibit two minima in viscosity with increasing temperature - the first of which is believed to accompany a transition from the mesophase to an isotropic phase, and the second corresponding to the onset of cross-linking. Mesophase pitch differs from the thermotropic polymers discussed earlier in having lower molecular weight and having a molecular structure that is more planar or disc-shaped ("discotic") than rod-like (nematic).

Evidence now suggests that a plateau or local minimum/maximum in viscosity as a function of temperature near the liquid crystal-isotropic transition will be characteristic of rod-like thermotropic polymers, equivalent to the behavior manifested by low-molecular weight nematics. If true, some explanation should be given for the phenomena not being observed in the early studies of thermotropic polymers. Most likely, the appropriate temperature range was not studied, or temperature increments were spaced too widely. In some of the polymers the higher nematic-iostropic transition temperature may not have been accessible due to degradation, since many thermotropic aromatic polyesters begin to degrade at temperatures too low for an isotropic transition to occur. Alternatively, the unusual viscosity-temperature relationship may not have been noticeable in particular polymers because their mesogen concentration were too low, or because their transitions were broadened by molecular weight distributions and/or compositonal distributions.

Primary normal stress differences and extrudate swell in shear flow of rod-like polymers. Conventional behavior for polymers is to exert a positive primary normal stress difference, $\tau_{11} - \tau_{22}$, when subjected to shearing. As noted earlier, the highly unusual phenomena of negative $\tau_{11} - \tau_{22}$ has been observed with some liquid crystalline polymers.

Kiss and Porter (24,25,26), in studies of lyotropic polypeptide solutions, were the first to observe consistent, time-independent negative $\tau_{11} - \tau_{22}$ in liquid crystalline polymers. An example using polybenzylglutamate in m-cresol is shown in Figure 8. The negative $\tau_{11} - \tau_{22}$ were observed for several different polypeptides in a number of different geometries, but were restricted to discreet ranges of shear rates and concentrations. The phenomenon was not observed with isotropic polymers in the same apparatus and has been attributed to the liquid crystalline nature of the polymer solutions studied.

Time-independent negative $\tau_{11} - \tau_{22}$ in thermotropic polymers have also recently been reported by Prasadarao, Pearce, and Han (14) for copolyesters of poly(ethylene terephthalate) (PET) and p-acetoxybenzoic acid (PAB) plus hydroquinone diacetate/ tetramethylterephthalic acid (HQTM), and by Baird (11,17) for copolyesters of PET and PHB. The data by Prasadarao et al is shown in Figure 9. They noted that the phenomena appeared to be associated with yield behavior, but did not yet understand its origin.

The review by Wissbrun (7) listed other systems where transient, as opposed to the above-mentioned time-independent, negative $\tau_{11} - \tau_{22}$

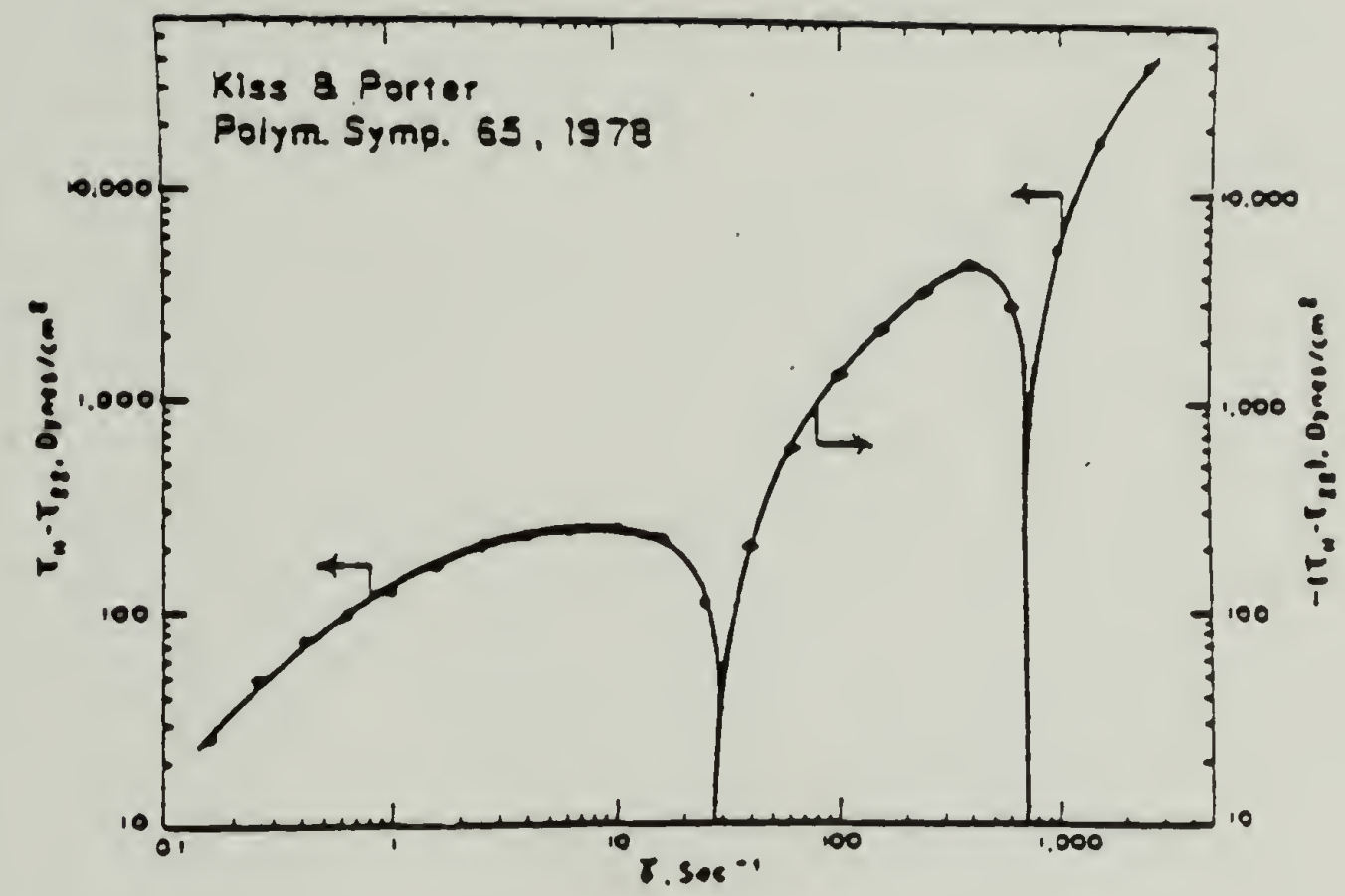

Fig. 8. First normal stress difference versus shear rate for polybenzyl glutamate in m-cresol (16.4 wt%) (25).

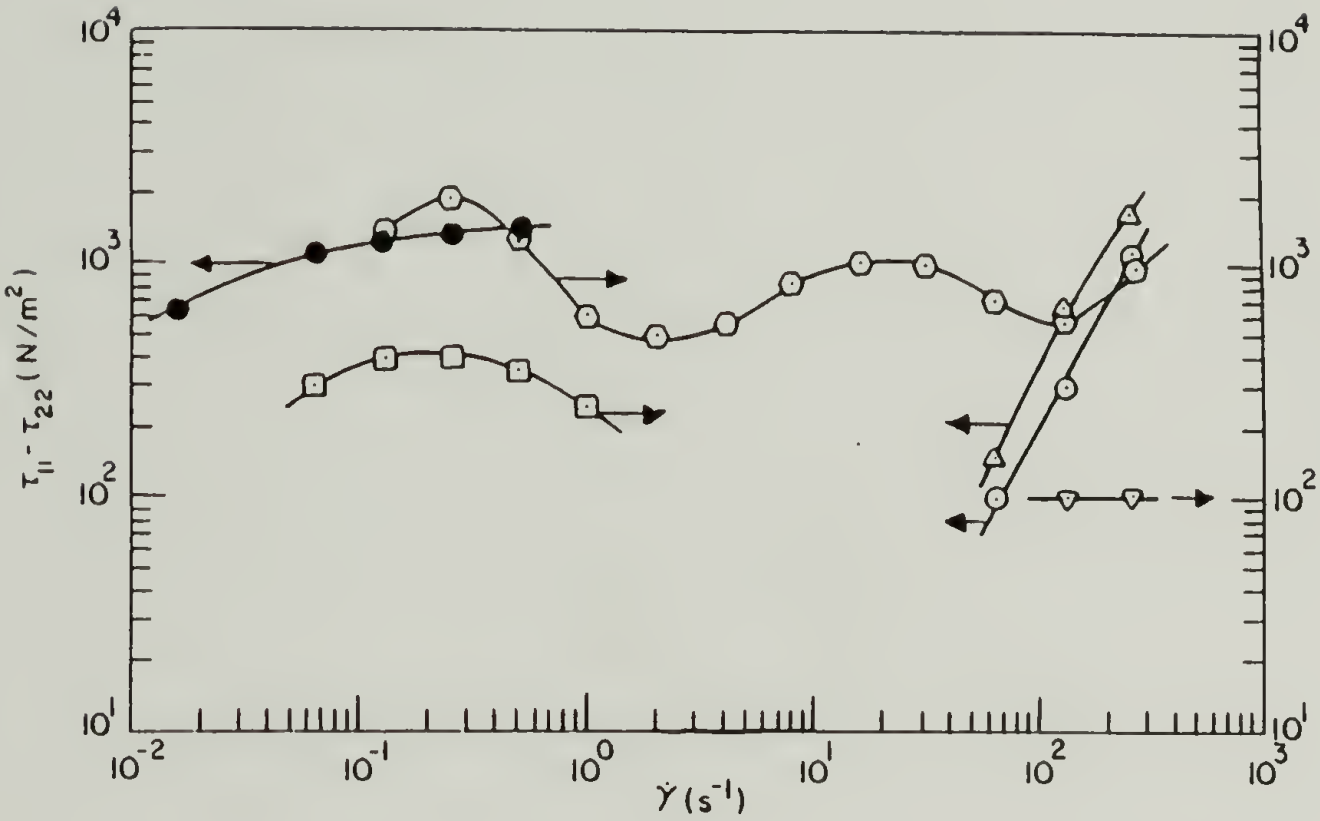

Fig. 9. First normal stress difference vs shear rate for copolyesters of PET and (PAB+HQTM): (⊙) PET homopolymer; (△) PET/(PAB+HQTM) = 82/18 (molal ratio); (⊡) PET/(PAB+HQTM) = 54/46; (▽) PET/(PAB+HQTM) = 43/57; (⬡) PET/(PAB+HQTM) = 33/67; (●) PET/PAB+HQTM) = 25/75 (14).

have been observed: by Hutton (27) with lubricating greases; by Duke and Chapoy (28) for liquid crystalline lecithin solutions; by Huang (29,30) with a block copolymer; and by Wissbrun (10) for a number of thermotropic polyesters. The origin of the negative normal stresses is not yet understood, though Wissbrun (10) has summarized possible mechanisms and notes that the Leslie-Ericksen continuum theory (31) for rod-like molecules can account for negative $\tau_{11} - \tau_{22}$ in simple shear flow.

Regardless of the origin of the negative normal stresses, their occurence has led to speculation that one might observe negative extrudate swell in capillary flow of liquid crystalline polymers. $\tau_{11} - \tau_{22}$ and extrudate swell are generally correlated, and both manifest elastic character in fluids (the tendency to recover from deformation)(32).

"Negative die swell" - that is, a die swell ratio ($B = D_e/D_o$) less than 1 - has, in fact, been reported by Jerman and Baird (9) for thermotropic copolyesters of PET and PHB. An example for 80 mole % PHB/PET is shown in Figure 10. A die swell ratio less than unity has also been observed by Suto, White, and Fellers (13) in capillary flow of thermotropic hydroxypropyl cellulose (HPC), leading them to suggest that this could be a general characteristic of liquid crystalline polymers. Their data for HPC have been reproduced in Figure 11.

In both of the above studies, swelling was observed to increase and become positive at higher temperatures where the polymers became isotropic. Although the reason for the negligible swelling in the liquid crystalline state is not yet fully understood, it is believed

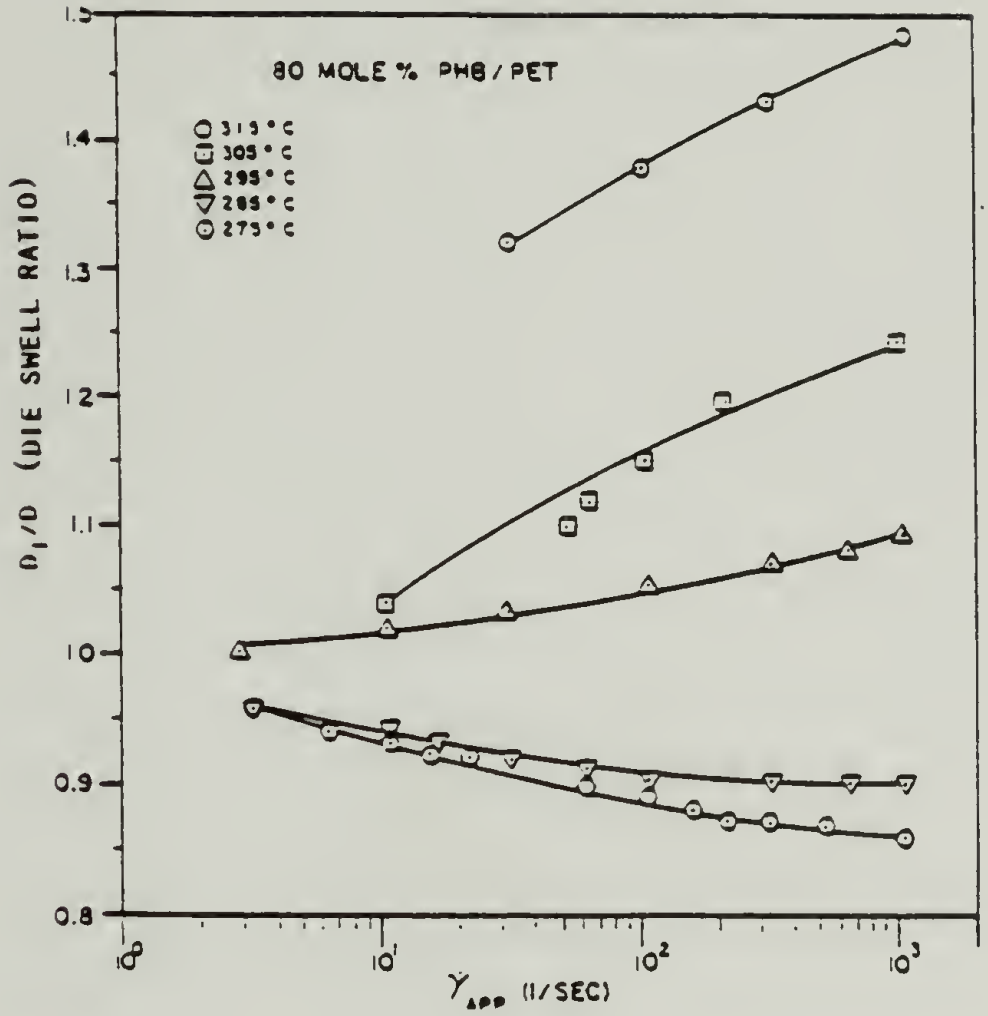

Fig. 10. Die swell versus apparent shear rate for 80 mole % PHB/PET at various temperatures. L/D = 40 (9).

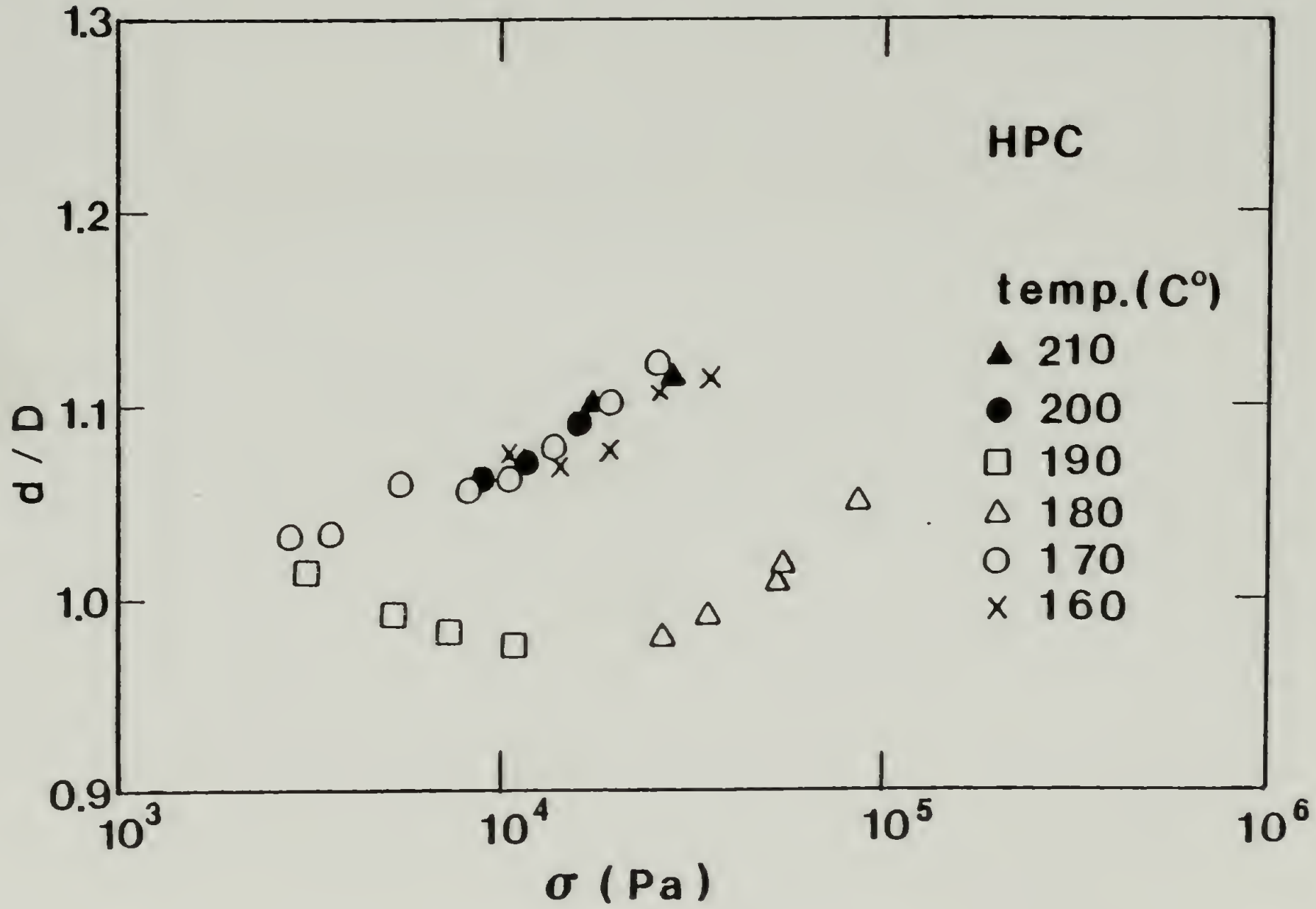

Fig. 11. Extrudate swell ($B = D_e/D_o$) of hydroxypropylcellulose as a function of die wall shear rate and temperature (13).

to result from 1.) an inherently low elastic nature of the liquid crystals, 2.) the existence of negative normal forces, or 3.) from an obstruction to elastic recovery resulting from a yield stress (9).

Molecular weight effects. There do not yet appear to be any reports in the literature concerning the effect of molecular weight on melt viscosity for rod-like thermotropic polymers. However, a number of studies have been made of the molecular weight dependence of solution viscosity for rod-like lyotropic polymers (7).

Papkov et al (33) studied the viscosity of solutions of lyotropic poly(para-benzamide) (PBA) in dimethyl acetamide (DMAC) as a function of both concentration and molecular weight. Data from their study is shown in Figures 12a and 12b. Figure 12a shows solution viscosity as a function of polymer concentration for PBA samples of four different molecular weights. Figure 12b contains the same data, but is plotted as viscosity vs molecular weight at four different concentrations.

At each molecular weight, the PBA solutions exhibited the classic viscosity-concentration dependence that has come to be expected of lyotropic polymers: viscosity passed through a maximum with concentration near the isotropic-to-liquid crystal transition. This behavior was illustrated previously in Figure 2.

When polymer concentration was held constant, viscosity similarly passed through a maximum with molecular weight, as shown in Figure 12b. That is, there was a critical molecular weight for formation of the anisotropic phase. Above the critical value, viscosity decreased with increasing molecular weight!

Fig. 12a. Concentration dependence of viscosity at 20°C for solutions of PBA of four different molecular weights (33).

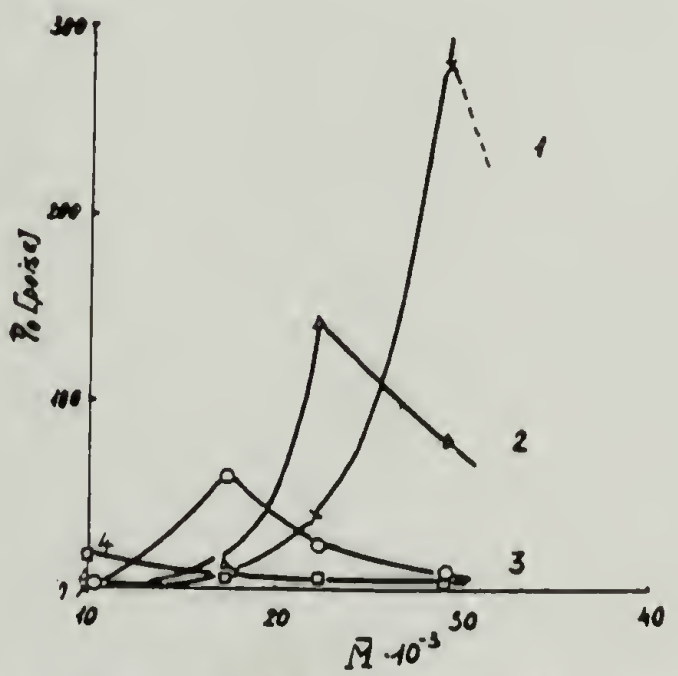

Fig. 12b. Dependence of solution viscosity on average molecular weight of PBA. Concentrations: curve 1, 5%; curve 2, 6.7%; curve 3, 8.2%; curve 4, 13% (33).

The point being made is this: for rod-like polymers - at a constant temperature and constant mesogen concentration - viscosity can decrease with increasing molecular weight. Although this behavior has, as yet, been observed only with lyotropic polymers, it is conceivable that a similar decrease in viscosity with molecular weight could occur in thermotropic liquid crystalline polymer melts, as well.

C H A P T E R II

POLYMERS

Source

All polyesters in this study were received from researchers at Monsanto Company. Liquid crystalline copolyesters were provided by Dr. Oliver Deex, Monsanto Co., St. Louis, Missouri. A non-liquid crystalline reference homoplyester was received from Dr. Morris Ort, Monsanto Co., Indian Orchard, Massachusetts.

Compositions

The polyesters were prepared from 1,2-bis(4-acetoxy phenyl) ethane (commonly called Bisphenol E diactetate; designated here as BPE) and one or more aromatic diacids. The compositions and polymerization conditions are covered by U.S. Patent 4,102,864 (5).

Poly(Bisphenol E isophthalate). A non-liquid crystalline hompolyester which served as a reference for the liquid crystalline copolyesters was comprised of Bisphenol E diacetate and isophthalic acid (I) in a monomer mole ratio of 50:50 BPE:I (Fig. 13). This poly(Bisphenol E isophthalate) is referred to as BPE/I.

BPE/I is a semi-crystalline polmer having a melting point at 285-310°C. Its properties are similar - and in many respects superior - to engineering thermoplastics such as poly(butylene

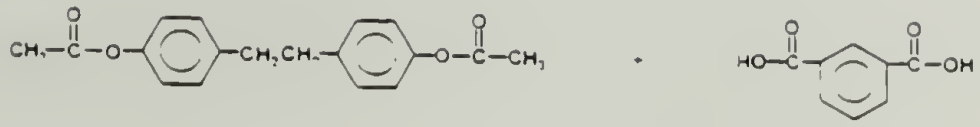

Bisphenol E diacetate Isophthalic acid

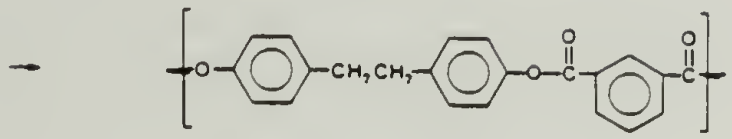

Poly(Bisphenol E isophthalate)

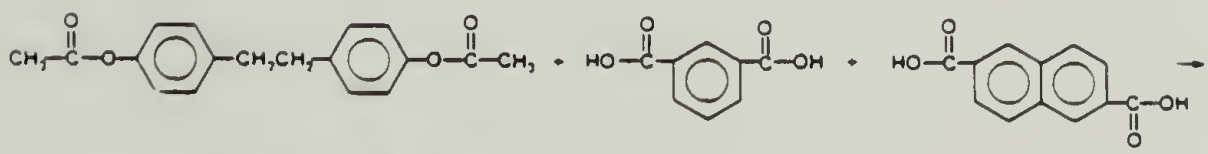

Bisphenol E diacetate Isophthalic acid 2,6-Naphthalene dicarboxylic acid

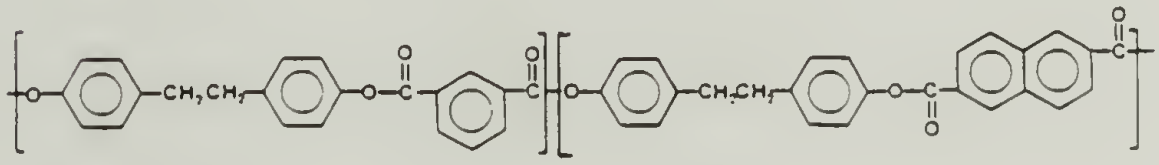

Poly(Bisphenol E isophthalate-co-naphthalate)

Fig. 13. Reaction equations for BPE/I and BPE/I/N-20 polyesters.

terephthalate) and aliphatic nylons (5). Key properties claimed in the Monsanto patent include inherently low flammability, high extended-use temperature, excellent chemical resistance, and minimal warpage in molded parts due to rapid crystallization.

Poly(Bisphenol E isophthalate-co-naphthalate). Six thermotropic liquid crystalline copolyesters were received, all having the same composition but differing in molecular weight (n_{inh}). These were prepared from Bisphenol E diacetate, isophthalic acid (I), and 2,6-naphthalene dicarboxylic acid (N) in a monomer mole ratio of 50:40:10 BPE:I:N (Fig. 13). This poly(Bisphenol E isophthalate-co-naphthalate) composition was designated BPE/I/N-20, where the "N-20" referred to the 80:20 I:N ratio of the two diacids.

The BPE/I/N-20 composition was determined by Monsanto to be thermotropic, exhibiting a transition from a semi-crystalline solid to an anisotropic fluid at ~284°C. A transition to the isotropic state at higher temperatures is not usually observed, since pyrolysis occurs before that state can be reached. The exception has been a low molecular weight prepolymer (n_{inh} ~0.38 dl/gm) in which a clearing temperature at ~380°C was observed (See "Melt turbidity/stir opalescence").

The BPE/I/N-20 mesophase (liquid crystalline state) is presumed to be nematic, based upon 1.) its appearance between cross-polarized lenses, 2.) the tendency to form fibrillar structures during extrusion or injection molding, and 3.) the similarity of its molecular structure to other nematic polymers (34). The mesogen (structural unit

which, due to its rod-like shape and/or polar nature causes formation of the mesophase) is presumably built around the naphthyl moiety. The naphthyl rings, flanked by ester groups which are in turn attached to para-substituted phenyl rings, form rigid rod-like segments having sufficiently high aspect ratio to act as mesogens. The mesogens in this polymer occur in the main chain, in contrast to being attached as pendant groups in some other liquid crystalline polymers.

Initially, only two samples of BPE/I/N-20 were studied. These were BPE/I/N-20 #1 and BPE/I/N-20 #2, which differed principally in apparent molecular weight (inherent viscosity). Later, due to unexplained differences in rheology and differential scanning calorimetry between these two samples, an additional set of four samples was prepared in order to investigate molecular weight effects. These latter four samples were less thoroughly investigated, and are discussed primarily in Chapter X.

Polymerizations by Monsanto

Polymerizations were accomplished by Monsanto using a two-step batch polycondensation procedure. The first step consisted of preparation of low-molecular weight prepolymer (η_{inh} ~ 0.38 dl/gm) by reacting the monomers under vacuum to temperatures as high as ~260°C, with removal of acetic acid distillate. The second step involved granulation of the prepolymer and continued polymerization under higher vacuum to higher molecular weight (η_{inh} ~ 0.55-1.00 gm/ml) in

the solid state - ie., above Tg but below Tm. Solid-state polymerization (SSP) temperatures varied, but were typically in the range 260-280°C.

The polymers were not all prepared on the same scale. The BPE/I/N-20 copolyesters were prepared in laboratory scale reactors, and were provided in powder form. The BPE/I homopolyester, on the other hand, was prepared in a pilot plant scale reactor, and was provided in the form of extruded pellets. Previous work by Monsanto, however, has shown that rheological and mechanical properties of BPE/I produced on the two scales are equivalent (35).

Initial Characterization

Prior to beginning capillary flow studies, the BPE/I, BPE/I/N-20 #1, and BPE/I/N-20 #2 polyesters were characterized as to physical appearance, inherent viscosity, and thermal transitions. The results are summarized in Table II and are discussed below.

Appearance. The BPE/I was received in the form of extruded pellets which were amber in color and translucent-to-opaque. After melting and cooling, the BPE/I ranged from being transparent to opaque depending upon the degree of crystallinity.

The BPE/I/N-20 copolyesters were received as finely-ground powders, though BPE/I/N-20 #2 was somewhat more coarsely ground than BPE/I/N-20 #1. BPE/I/N-20 #1 was off-white in color, as were the four

Table 2

Initial Characterization of Polyesters

	BPE/I	BPE/I/N-20 #1	BPE/I/N-20 #2
Monsanto reference number	E-100 1007 3-10-2	1382189	1974271
Physical appearance, as received	Amber translucent pellets	Off-white opaque powder	Tan opaque powder
η_{inh}, dl/gm 0.5% in 60/40 phenol/1,1,2,2-tetrachloroethane	0.85	0.90	0.60
DSC transitions*			
1st heating:			
Tg onset, °C	214	111-120	111
T_m peak, °C	310	286	286,310
ΔH, cal/gm polymer	17.0	5.3	5.3
2nd heating:			
Tg onset, °C	137	110	110
T_m peak, °C	288	284	250,285,293
ΔH, cal/gm polymer	~7	~4.0	~3.6
Temperature range for melt turbidity and stir opalescence, °C	None	~290 to > 400	~290 to > 400

*Data taken from Chapter X. Heating rates and cooling rates extrapolated to 0°C/min.

BPE/I/N-20 copolyesters received later. The BPE/I/N-20 #2, however, was darker in color ("tan") - indicating the possibility of greater oxidation during polymerization, or perhaps a greater content of impurities in the starting monomers.

The BPE/I/N-20 powders were opaque as received. These polyesters also were opaque after melting and cooling under any conditions tested, including heating and cooling on various kinds of hot stages. Extrudates obtained in the capillary flow studies (Chapters III,IV) were opaque, as well.

Inherent Viscosity. Inherent viscosities were determined using the mixed solvent of 60/40 wt% phenol/1,1,2,2-tetrachloroethane.[a] Determinations were made at a concentration of 0.5 gm/100ml using a size 150 Ubbelohde viscometer and a constant temperature bath at 25°C. Difficulty in dissolving the polyesters due to their crystallinity required heating under reflux at 120°C for one to two hours. Inherent viscosity was calculated as

$$\eta_{inh}\ (dl/gm) = \ln(ET/ST)/C \qquad ---1$$

where ET is sample efflux time, ST is solvent efflux time, and C is sample concentration in gm/dl.

The inherent viscosities obtained were ~0.85 dl/gm for BPE/I, ~0.90 dl/gm for BPE/I/N-20 #1, and ~0.60 dl/gm for BPE/I/N-20 #2. The

a. Purchased from Aquair, P.O. Box 7048, Charlotte, NC 28217.

BPE/I and BPE/I/N-20 #1 were thus expected to have comparable molecular weights, although the Mark-Houwink coefficients - which relate inherent viscosity to molecular weight - have not been determined for BPE/I/N-20.

The inherent viscosity of BPE/I/N-20 #2 was unexpectedly low, since it had originally been intended to be equivalent to BPE/I/N-20 #1. A discussion with Dr. Deex (34) confirmed that some difficulty had been encountered in polymerizing the BPE/I/N-20 #2. That polymer was even subjected to a second SSP treatment in an attempt to raise its inherent viscosity.

The reason for the low η_{inh} of BPE/I/N-20 #2 is not certain, but three possibilities were suggested. First, a small amount of an experimental catalyst was included in BPE/I/N-20 #1 which was omitted from BPE/I/N-20 #2. Lack of the catalyst in BPE/I/N-20 #2 may have slowed its rate of polymerization, though Dr. Deex expressed doubt that there would have been a significant effect on final molecular weight. Secondly, the BPE/I/N-20 #2 powder was somewhat more coarsely ground than the BPE/I/N-20 #1. This could have reduced the rate of diffusion of acetic acid out of the polymer during SSP treatment, thus reducing the molecular weight. Finally, there may have been a slight deficiency in the mole fraction of diacetate monomer during the polymerization of BPE/I/N-20 #2 which would have limited its attainable molecular weight. This third possibility received some support from analysis of composition via ^1H NMR (Chapter V.)

Differential scanning calorimetry. Enthalpic transitions in the polyesters were examined using a Perkin-Elmer DSC-2 differential scanning calorimeter equipped with a Thermal Analysis Data Station (TADS). Only a brief description of the thermal behavior will be included here, since more detailed results are provided in Chapter VII.

Thermograms for the BPE/I, BPE/I/N-20 #1, and BPE/I/N-20 #2 as-received polyesters (obtained at a heating rate of 10°C/min) are shown in Figure 14. All three polymers exhibited relatively narrow endotherms at temperatures in the range 280-320°C. The magnitudes of the transition peaks in Figure 14 may be directly compared, since the TADS was used to normalize the data on a per-unit-weight basis.

The BPE/I exhibited the highest endotherm (~311°C), corresponding to its crystalline melting point, T_m. It also had a relatively high glass transition temperature, T_g (~230°C) and large enthalpy-of-fusion, (ΔH_m ~17 cal/gm of polymer). These high temperatures and ΔH_m in the as-received BPE/I reflected an elevated degree of crystallinity induced by solid-state polymerization. The properties dropped significantly after melting, cooling, and reheating, to T_m~288°C, T_g~135°C, and ΔH_m ~7 cal/gm of polymer, respectively.

The BPE/I/N-20 endotherms occurred at lower temperatures (~287°C) than in the as received BPE/I. These peaks have been labelled $T_{C \rightarrow N}$ (crystal-nematic transition temperature) since they correspond to the transition from a semi-crystalline solid to an anisotropic melt. However, it is not clear from this data whether the molecular structure undergoing a change in enthalpy involves the mesogenic units, or

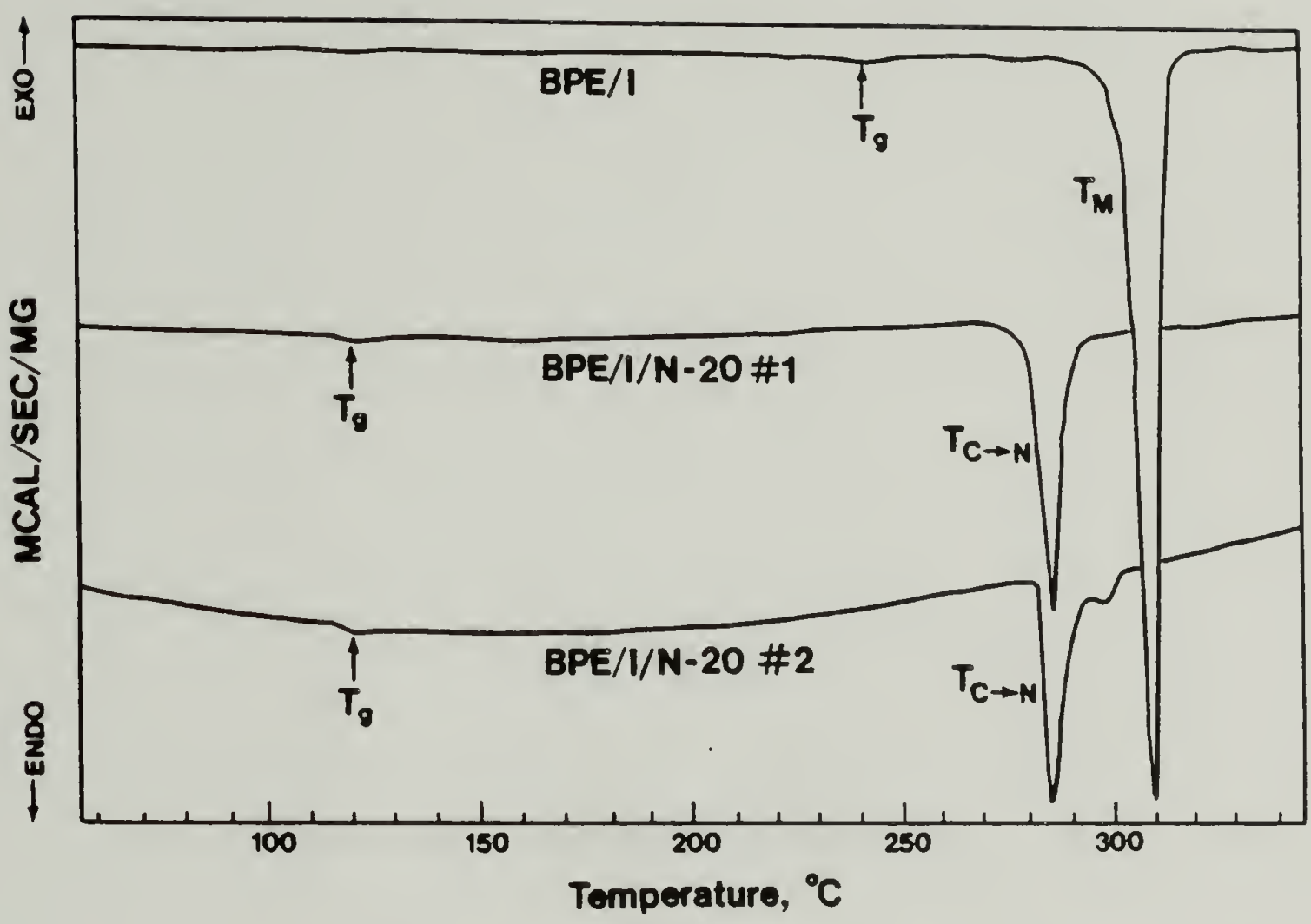

Fig. 14. Comparison of BPE/I, BPE/I/N-20 #1, and BPE/I/N-20 #2 via differential scanning calorimetry (Heating Rate 10°C/min).

simply crystals of BPE/I sequences whose T_m has been lowered by the presence of the naphthalate groups - or some combination of both. It would seem likely that crystals of pure BPE/I should be present in the BPE/I/N-20 copolyesters, since 90 mole % of their composition is identical to BPE/I.

The T_g's and enthalpies-of-transition for the BPE/I/N-20 copolyesters were lower than those for BPE/I: T_g's ~ 120°C and ΔH's ~ 5.5 cal/gm of polymer. After melting and cooling the as-received BPE/I/N-20 powders, their T_g's, $T_{C\rightarrow N}$'s and ΔH's decreased slightly (as with the BPE/I) to T_g ~ 110°C, $T_{C\rightarrow N}$ ~ 285°C, and ΔH ~3.6-4.0 cal/gm of polymer.

A difference in the two BPE/I/N-20 polymers was noticed in that BPE/I/N-20 #2 exhibited a high-temperature shoulder, or second endotherm. An explanation for this was provided by data from the four BPE/I/N-20 polyesters received later (See Chapter X). Multiple endotherms were observed to characterize BPE/I/N-20 prepolymer (n_{inh} ~ 0.38 dl/gm) prior to solid-state polymerization. As the SSP process is carried out and the polymer is raised to higher molecular weight, the multiple endotherms merge - suggesting a possible homogenization of the composition at higher molecular weight. The shoulder apparently exists in the BPE/I/N-20 #2 because that polyester has lower molecular weight. The shoulder is probably associated with domains in the BPE/I/N-20 #2 in which the crystals contain predominantly BPE/I.

The thermograms of the polyesters in Figure 14 show behavior only

to ~345°C. No other significant thermal transitions were noted until ~380-420°C, where very irregular endothermic response indicated the onset of severe degradation (See Chapter VII).

Melt turbidity/stir opalescence. Melt turbidity and stir opalescence (a "shimmering" reflection of light when sheared) are indications of liquid crystallinity. Monitoring of these properties as a function of temperature can complement differential scanning calorimetry in the detection of liquid crystalline transitions, since those transitions are not always accompanied by large changes in enthalpy.

Melt turbidity and stir opalescence were investigated by heating a few milligrams of each polyester between glass slides on a Fisher-Johns melting point apparatus. Slight pressure and a shearing motion were applied to the glass slides. The polyesters were heated to temperatures as high as 400°C, the upper limit of the apparatus. The occurence and temperature ranges of melt turbidity/stir opalescence are noted in Table 2.

The BPE/I/N-20 copolyesters all exhibited turbid melts/stir opalescence above ~290°C. These characteristics persisted to temperatures as high as 400°C, with the exception of a low-molecular weight polymer (η_{inh} ~ 0.38 dl/gm) described in Chapter X. That polymer showed an apparent clearing temperature at ~380°C; above 380°C it had a transparent melt.

The clearing temperature for this low-molecular weight BPE/I/N-20 was difficult to observe, since it coincided with rapid degradation,

evidenced by severe bubble formation - almost boiling. None of the higher molecular weight BPE/I/N-20 samples exhibited a clearing transition, but all showed signs of degradation at temperatures above ~370°C, manifested by yellowing and bubble formation. The finding that a clearing transition was observed only in the lowest molecular weight polymer should not be surprising, since studies of other nematic polymers have shown that the nematic-isotropic transition temperature can increase with molecular weight (36).

The BPE/I homopolyester did not exhibit any melt turbidity or stir opalescence. It melted at ~290-315°C to a transparent melt, indicative of an isotropic fluid. At higher temperatures (~380°C), some degradation was observed (as with the BPE/I/N-20 polymers), evidenced by darkened color and bubble formation.

CHAPTER III

CAPILLARY FLOW STUDIES

Methods

All bulk viscosity measurements were made using a Sieglaff-McKelvey Model R-64 capillary rheometer manufactured by the Tinius Olsen Testing Machine Company. The instrument was operated exclusively in the constant shear rate mode. Extrusion experiments were conducted at a series of constant temperatures from 288-370°C. Although a number of capillary geometries and sizes were investigated, generally measurements were made with one of two capillaries. One had a nominal L/D of 20/1 (25.4 mm length, L, X 1.296 mm diameter, D, with 180° entrance angle); the other had a nominal L/D of 15/1 (19.05 mm length X 1.290 mm diameter, also with 180° entrance angle).

A 2000-lb. load cell was used for the bulk of the experiments with the BPE/I and BPE/I/N-20 #2 polymers. However, due to the extremely low viscosity of the BPE/I/N-20 #1, a 200-lb. load cell was used for this polymer. This allowed a 10-fold increase in measurement sensitivity. Both load cells were calibrated with dead weights, with results between the two cells agreeing well.

Copper-beryllium piston tips were used to prevent backflow in the rheometer during viscosity measurements. In the as-received condition

these tips contributed greater than 10 lb_f (44.5 Newtons) in frictional resistance against the barrel wall. Modifications were made by sanding the tips lightly with medium sandpaper, so that friction was reduced to only 0-2 lb_f (0-9 Newtons), as observed during travel of the piston-plus-tip through an empty barrel at the test temperature.

Polyesters in general are known to be extremely sensitive to hydrolytic and oxidative degradation at high temperatures, so that certain precautions were necessary to minimize exposure to moisture and oxygen. Prior to viscosity measurements, samples were dried in a vacuum oven at 110°C for 48 hours. After drying, the oven was opened with a nitrogen purge. Samples were transferred to the rheometer while hot; the barrel was purged with nitrogen during this sample loading.

After sample loading, the polymer was allowed to heat-soak for at least ten minutes prior to initiating viscosity measurements. The attainment of thermal equilibrium during testing was checked by the following procedure: shear stress was measured at a number of different shear rates, with the sequence of shear rates being randomized. Measurements were repeated at selected shear rates. Thermal equilibrium was considered to be reached if all shear stress-vs-shear rate data from a given run produced a smooth, consistent curve.

Shear stress at the wall, τ_w (Pascals), and apparent shear rate at the wall $\dot{\gamma}_{app}$ (s^{-1}) were determined from conventional expressions (Eg.,32):

$$\tau_w = R_c \, \Delta P/2 \, L_c \qquad \text{---2}$$

$$= 6895 \quad FD_c/\pi D_p{}^2 L_c$$

$$\dot{\gamma}_{app} = 4Q/\pi R_c{}^3 \qquad \text{---3}$$

$$= 2 \, v_p D_p{}^2/15 D_c{}^3 \quad .$$

F is the force (lb_f) on the driving piston as measured by a load cell; v_p is the velocity of the piston (in/min) as measured by a linear velocity transducer; D_c, L_c, and R_c are the diameter, length, and radius of the capillary (in.), respectively; D_p is the diameter of the piston (~0.307 in); and 6895 is the conversion factor from psi to Pascals.

Bagley corrections to the shear stress for entrance pressure losses were not, in general, applied. However, plots of ΔP vs capillary length-to-radius ratio for the two primary capillaries were made, to at least estimate the magnitude of this correction.

Corrections to the shear rate for a non-parabolic velocity profile were applied according to the Rabinowitsch method:

$$\dot{\gamma} = \dot{\gamma}_{app} \left(\frac{3}{4} + \frac{1}{4n}\right) \qquad \text{---4}$$

where $$n = \frac{d(\log \tau_w)}{d(\log \dot{\gamma}_{app})} \quad . \qquad \text{---5}$$

Values of n were determined visually as the slope at each shear rate from a plot of log τ_w vs log $\dot{\gamma}_{app}$. Melt viscosity was then determined as:

$$\eta_a = \tau_w / \dot{\gamma}$$

$$= \frac{\tau_w}{\dot{\gamma}_{app}} \left(\frac{3}{4} + \frac{1}{4n}\right)^{-1} \quad . \qquad \text{---6}$$

Results

Data obtained for the three polyesters - BPE/I, BPE/I/N-20 #1, and BPE/I/N-20 #2 - are presented in several ways to emphasize different aspects of the observed behavior.

Shear stress-shear rate relationships. In Figures 15-17, shear stresses obtained at selected temperatures are plotted as a function of shear rate for the three polymers. Actual data points are presented (as opposed to averaged values), with isothermal curves being hand-fitted to the data. Equal numbers of data points were not obtained at all temperatures. Temperatures where data were most heavily replicated are 312 and 320°C for BPE/I, and 295, 310, and 340°C for the two BPE/I/N-20 polymers. The dashed lines in Figures 16 and 17 highlight regions where shear stress increases with temperature - an unusual feature to be discussed later.

Bagley end corrections. Bagley end corrections were not applied to the shear stresses. However, the magnitudes of end effects were estimated using two capillaries having different L/D values. In Figures 18-20 the pressure drop at various shear rates has been plotted vs L/R (= 2 L/D). Extrapolations have been made to zero pressure drop to show the effective length of capillary which is contributed by entrance pressure losses. Data is presented for those temperatures mentioned previously as the ones where data was most heavily

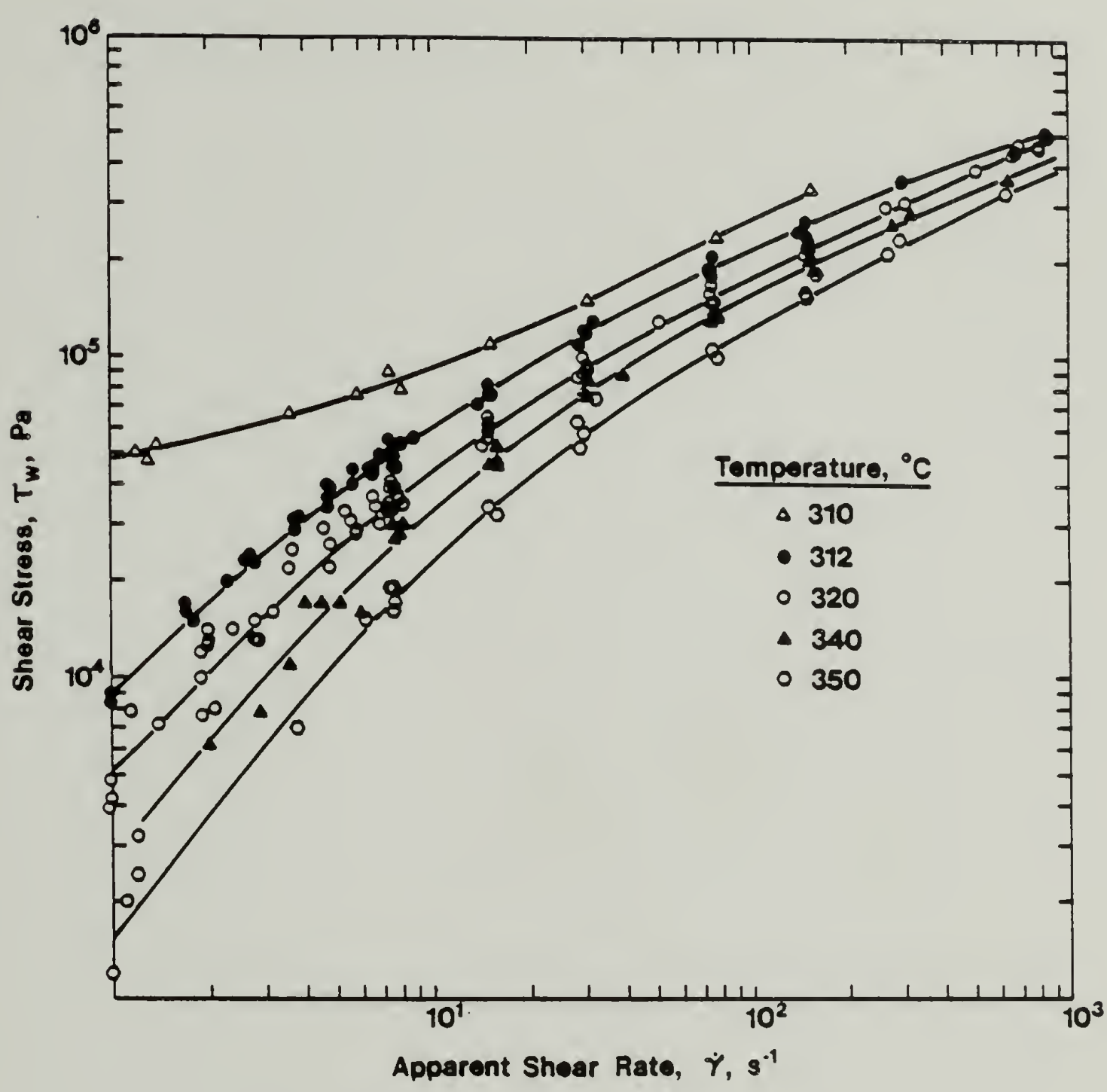

Fig. 15. Shear stress vs apparent shear rate for BPE/I.

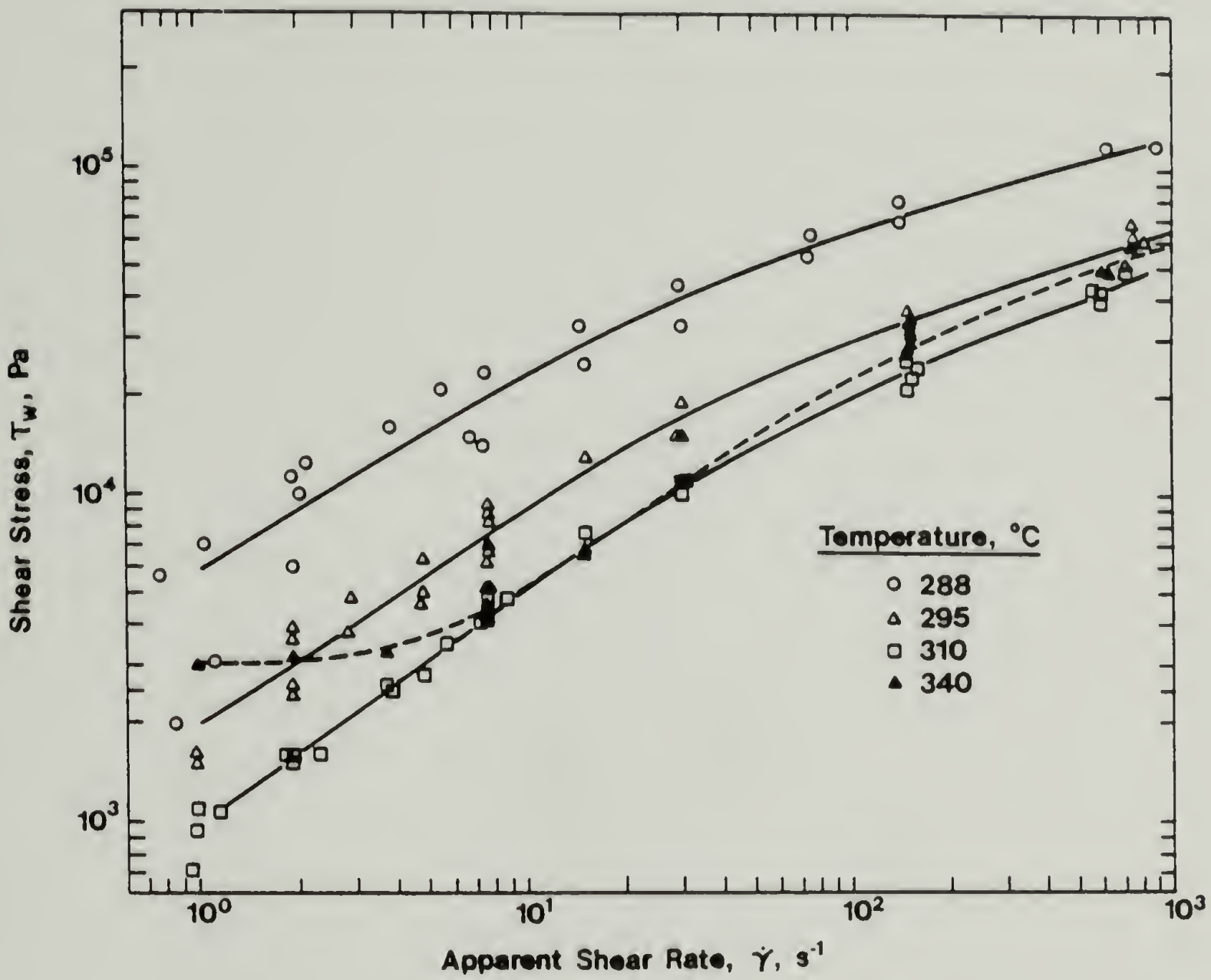

Fig. 16. Shear stress vs apparent shear rate for BPE/I/N-20 #1.

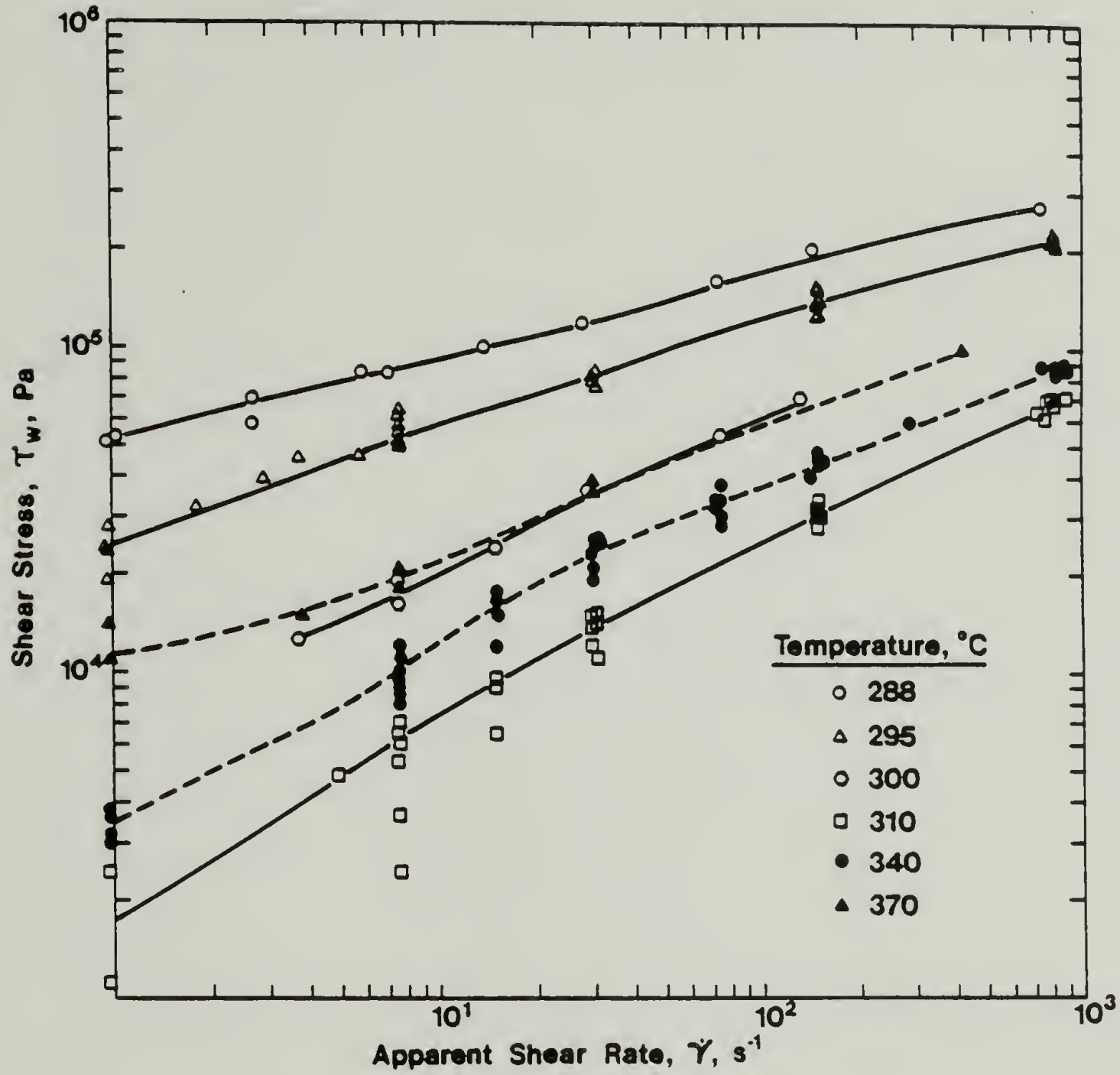

Fig. 17. Shear stress vs apparent shear rate for BPE/I/N-20 #2.

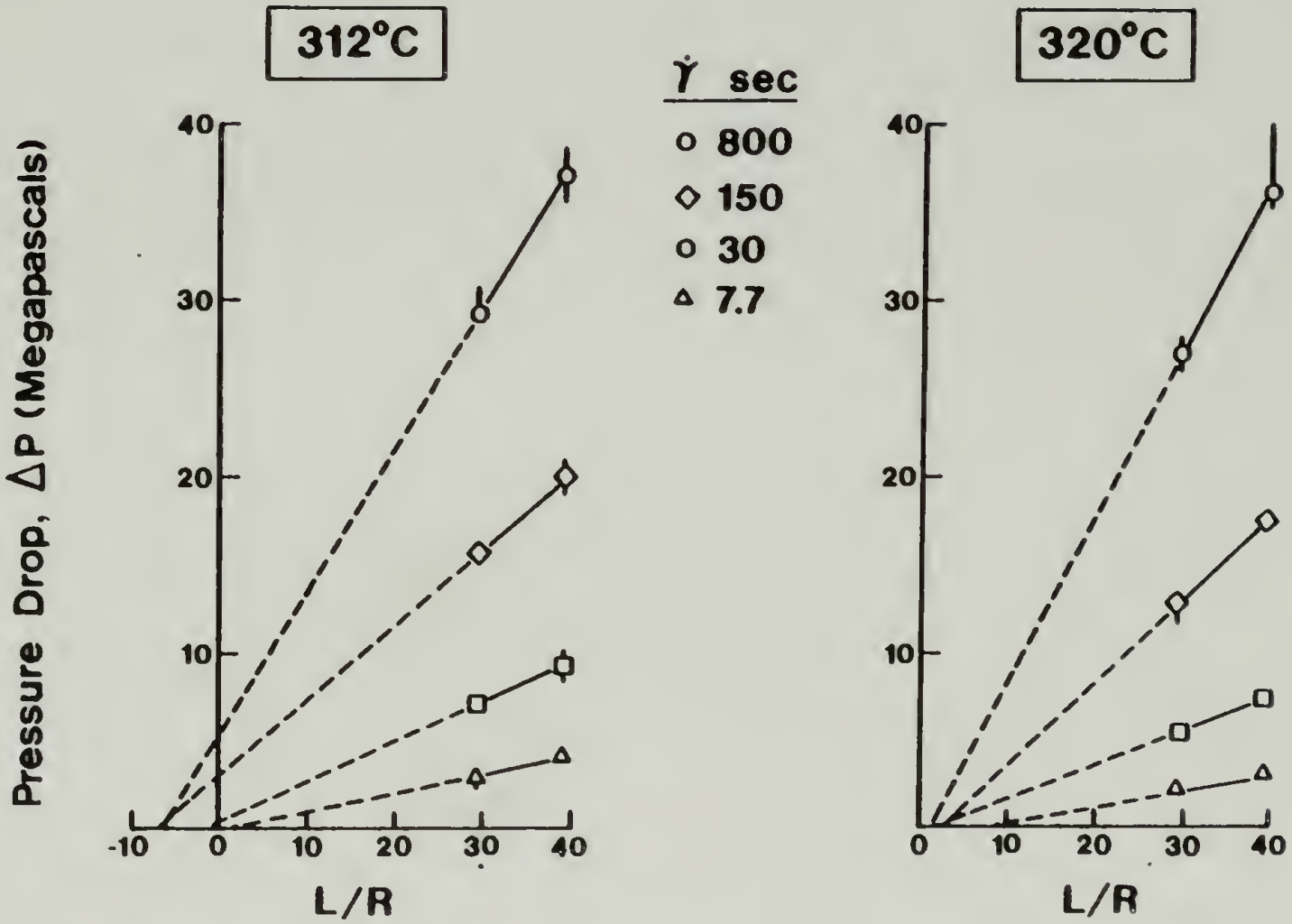

Fig. 18. Bagley end correction plots for BPE/I.

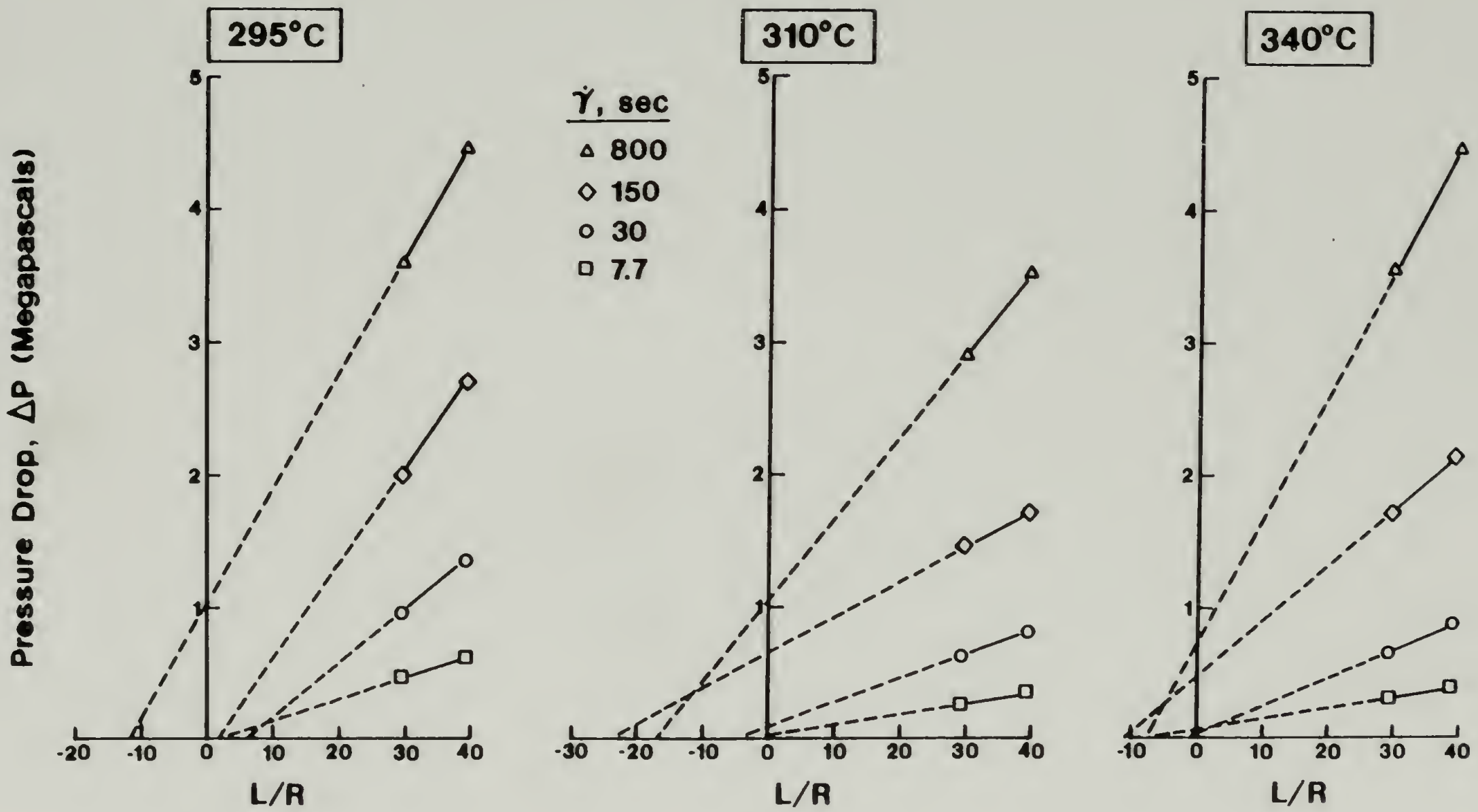

Fig. 19. Bagley end correction plots for BPE/I/N-20 #1.

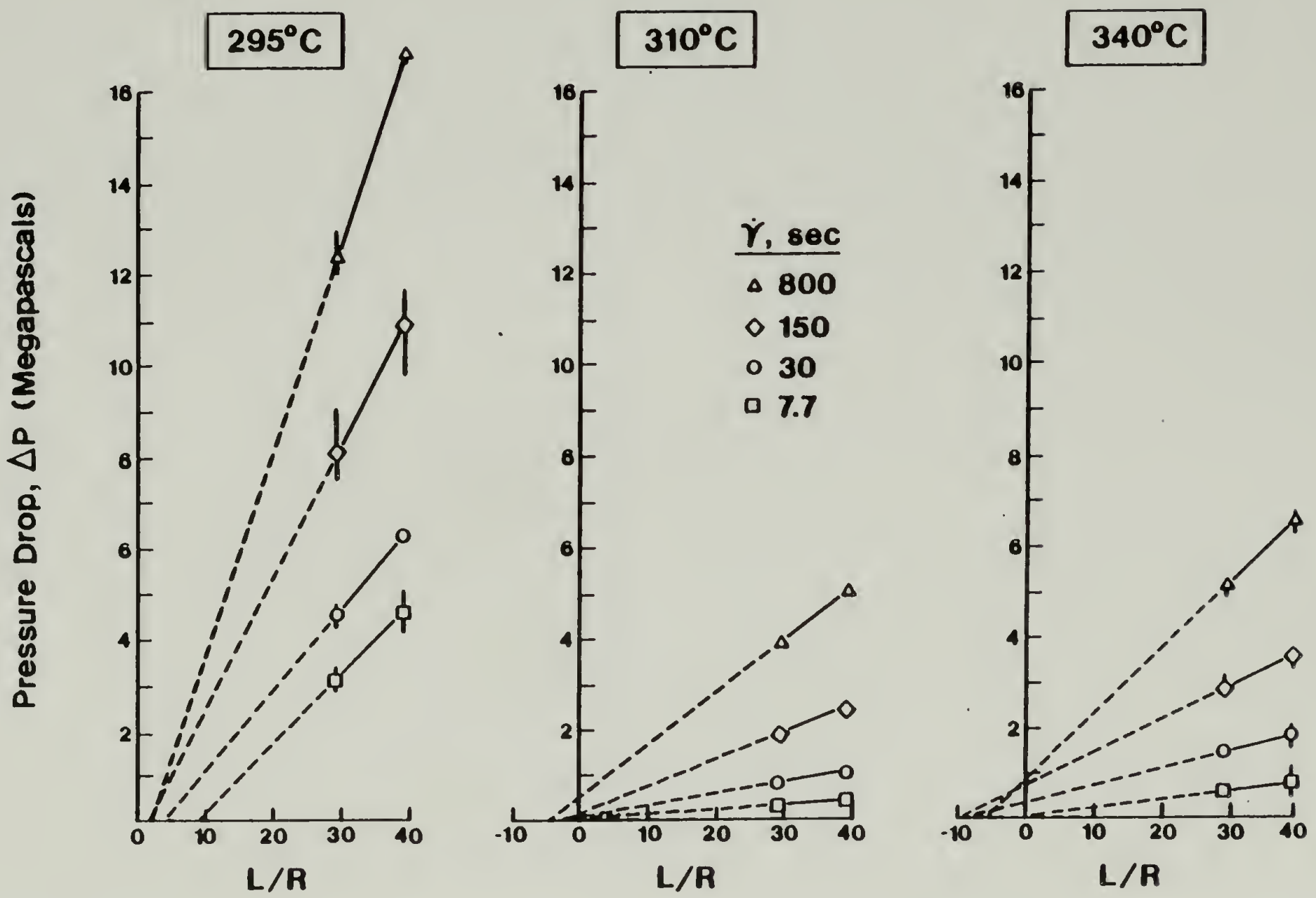

Fig. 20. Bagley end correction plots for BPE/I/N-20 #2.

replicated. Each data point in Figures 18-20 represents an average from at least three, and as many as six, experimental trials. The vertical error bars represent the ranges of observed pressure drops - as opposed to standard deviations or other statistical measures of error.

Viscosity - shear rate relationships. Melt viscosities were computed from Equations 4, 5, and 6 including Rabinowitsch corrections. Viscosities for the three polyesters are plotted as a function of corrected shear rate in Figures 21-23. As before, dashed lines represent regions where shear stress - and, thus, viscosity - increases with temperature.

Viscosity - temperature relationships. The temperature dependence of viscosity for the three polyesters is presented in Arrhenius fashion in Figures 24-26. The logarithm of viscosity at constant shear stress (as opposed to constant shear rate) is plotted vs the reciprocal of extrusion temperature, $1/T(K^{-1})$. Although all data were obtained at constant shear rates, viscosities at constant shear stresses were cross-plotted from Figures 21-23, where lines of constant τ_w are given by lines of constant $\eta\dot{\gamma}$. Data at additional temperatures is presented in the Arrhenius plots that were omitted from the viscosity-shear rate figures to avoid confusion from overlapping data.

A fourth Arrhenius plot is provided in Figure 27, in which the three polyesters are compared at a constant shear stress of 20 kPa.

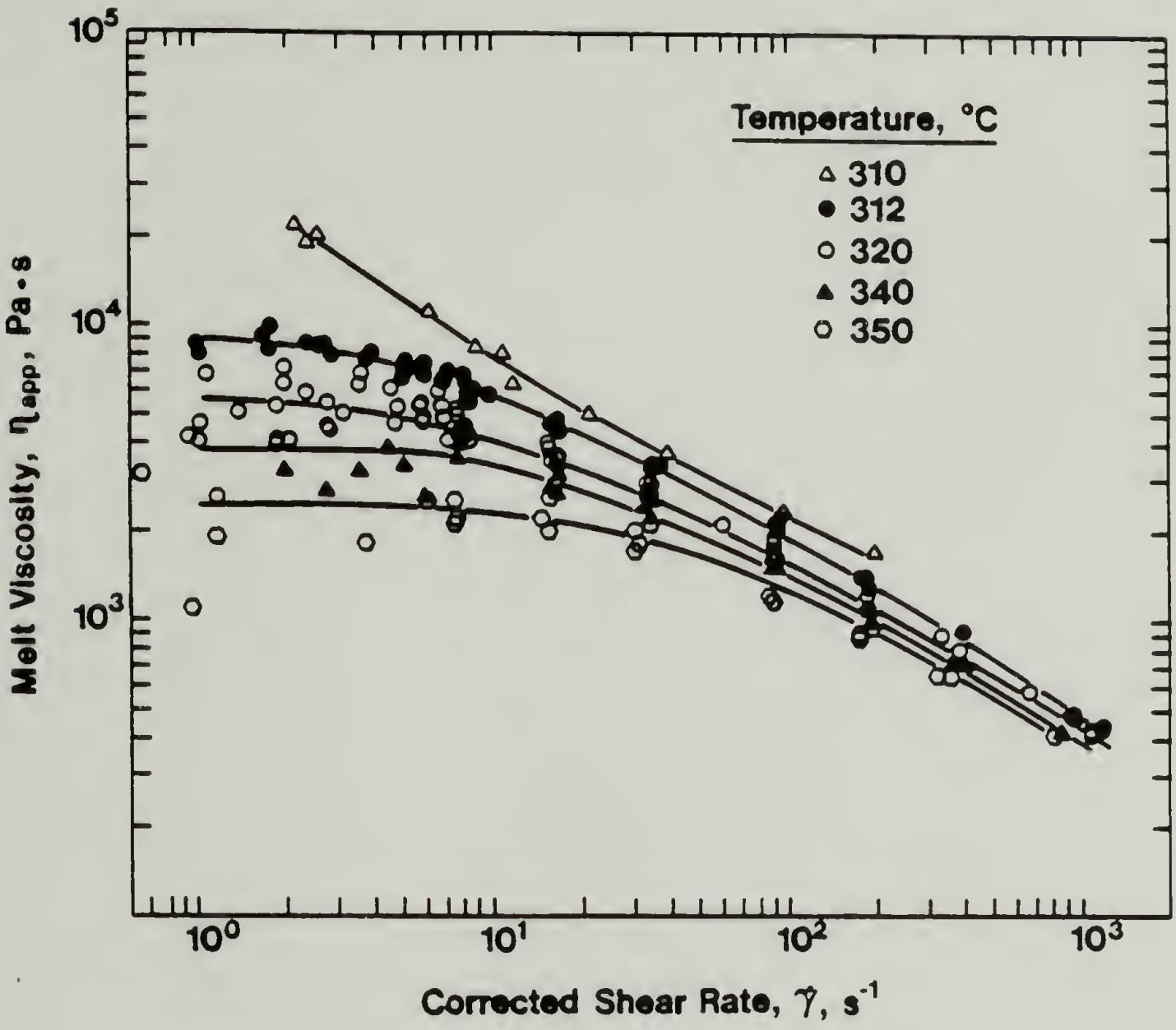

Fig. 21. Melt viscosity vs corrected shear rate for BPE/I.

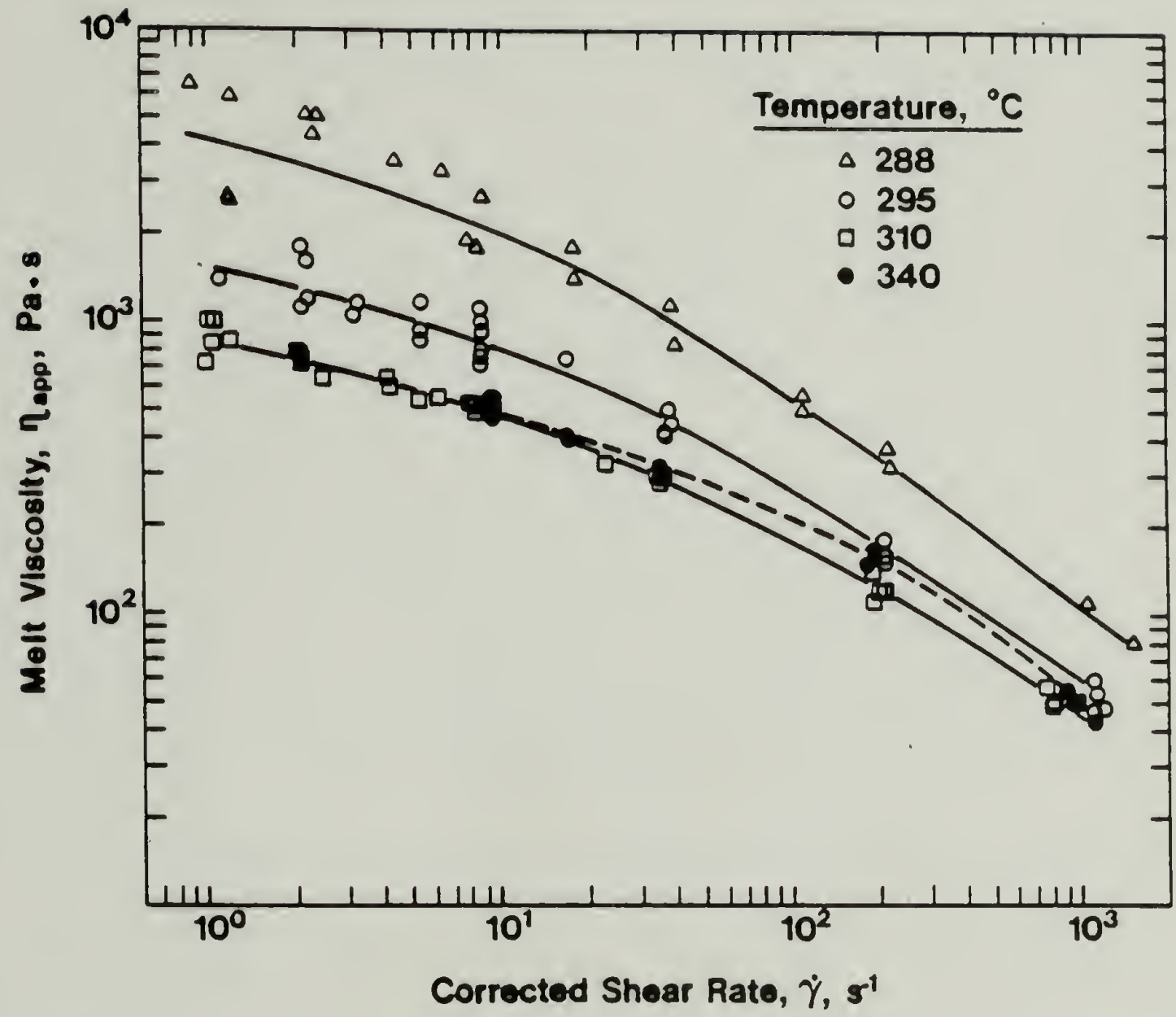

Fig. 22. Melt viscosity vs corrected shear rate for BPE/I/N-20 #1.

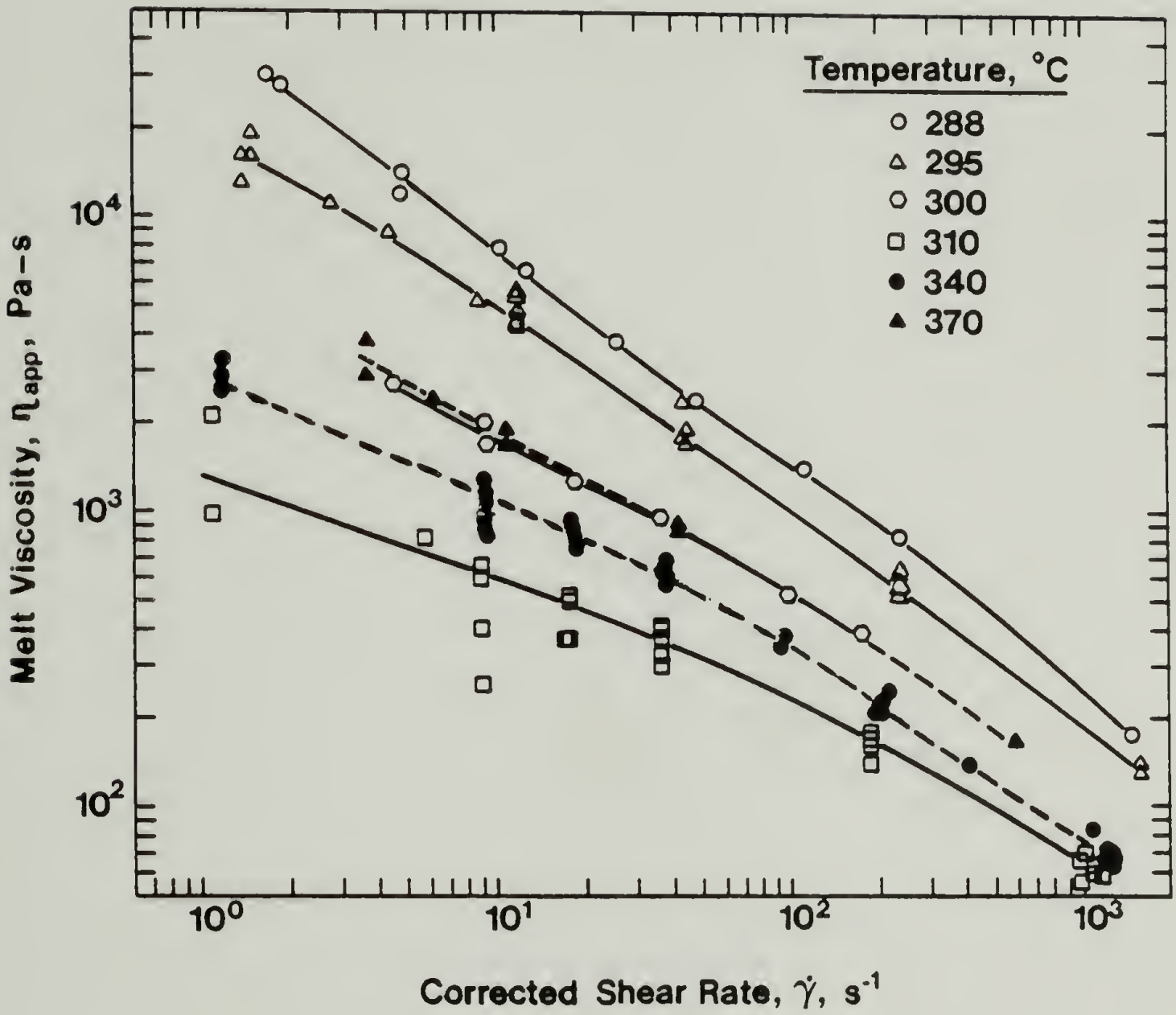

Fig. 23. Melt viscosity vs corrected shear rate for BPE/I/N-20 #2.

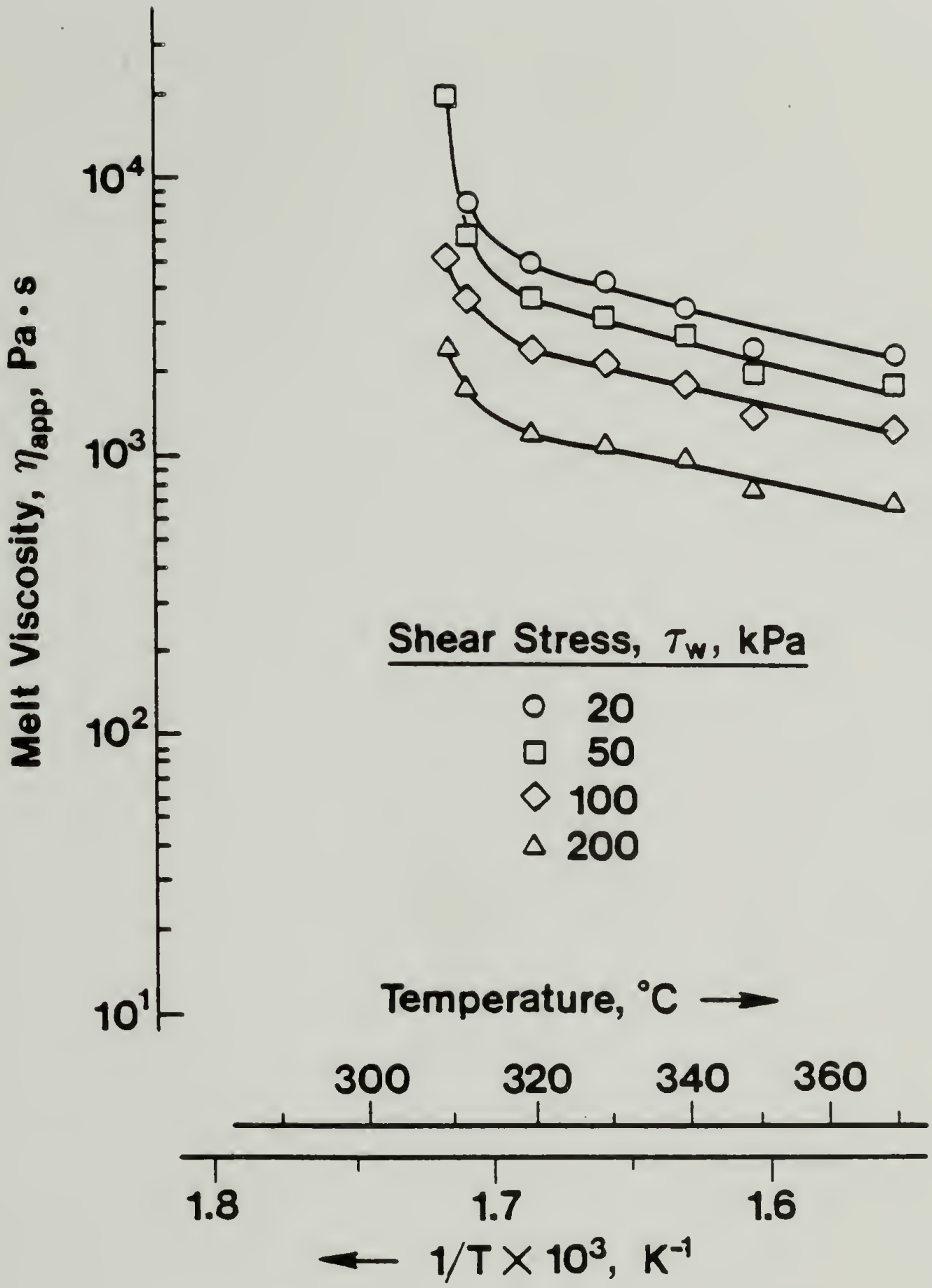

Fig. 24. Temperature dependence of viscosity at constant shear stress for BPE/I.

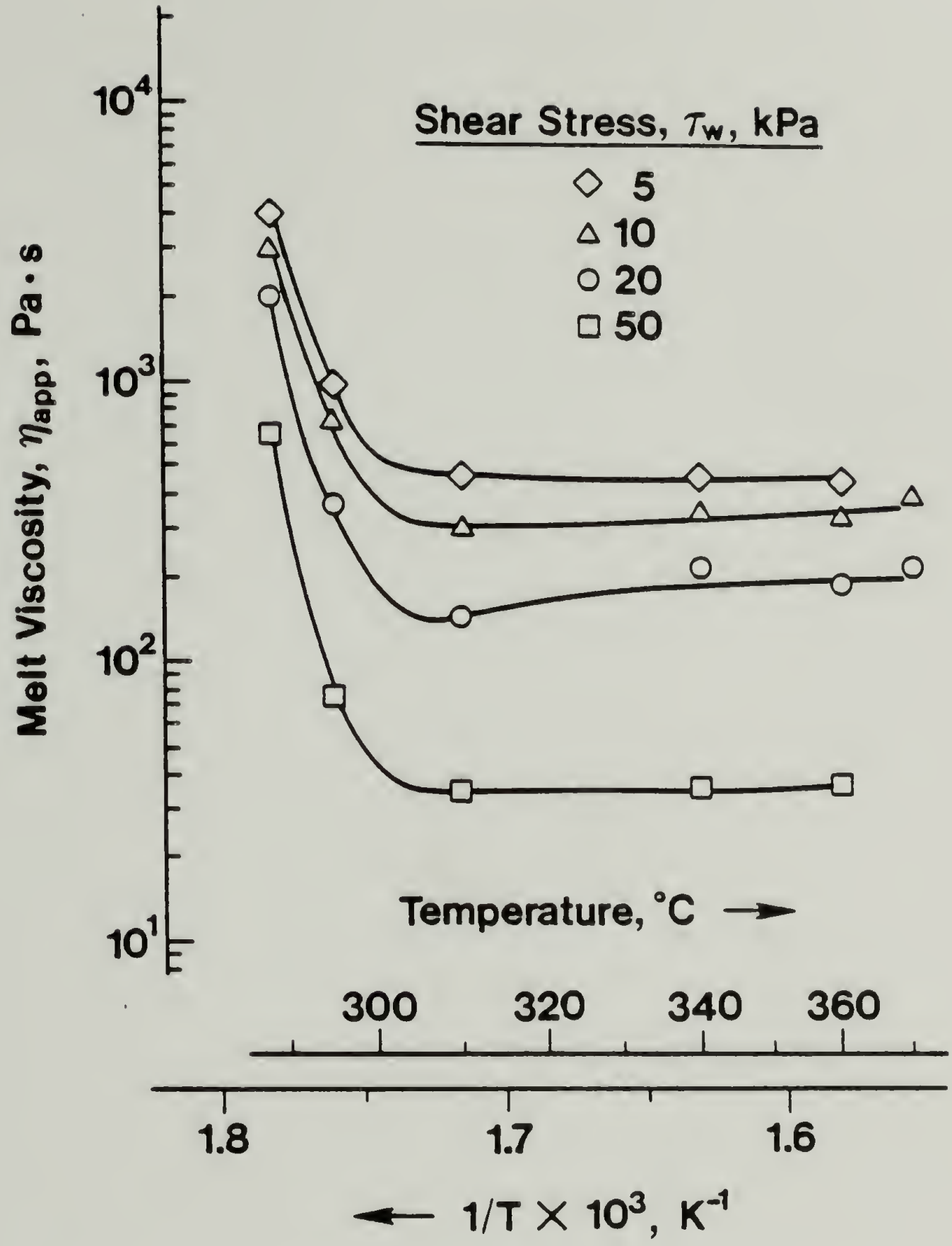

Fig. 25. Temperature dependence of viscosity at constant shear stress for BPE/I/N-20 #1.

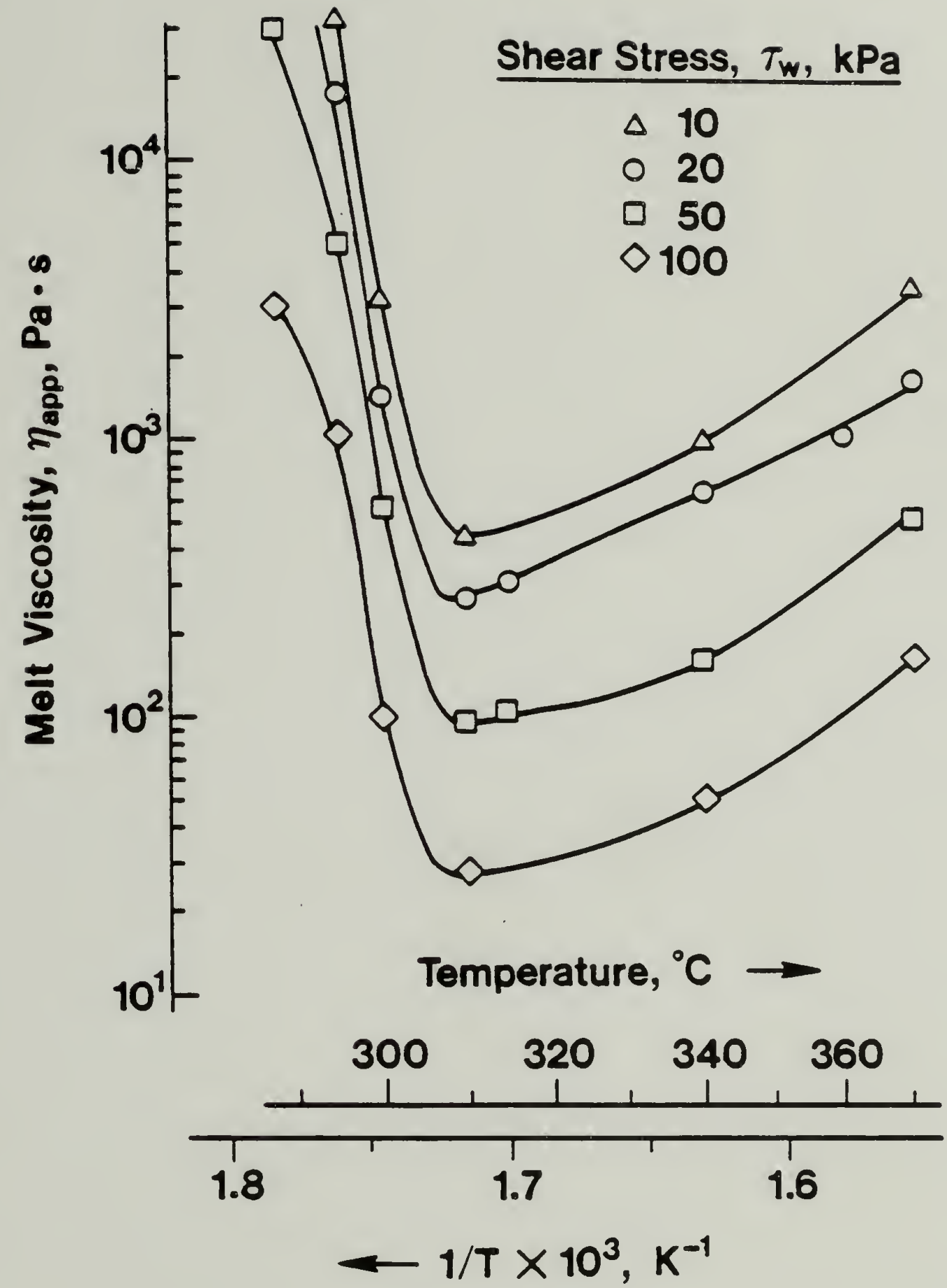

Fig. 26. Temperature dependence of viscosity at constant shear stress for BPE/I/N-20 #2.

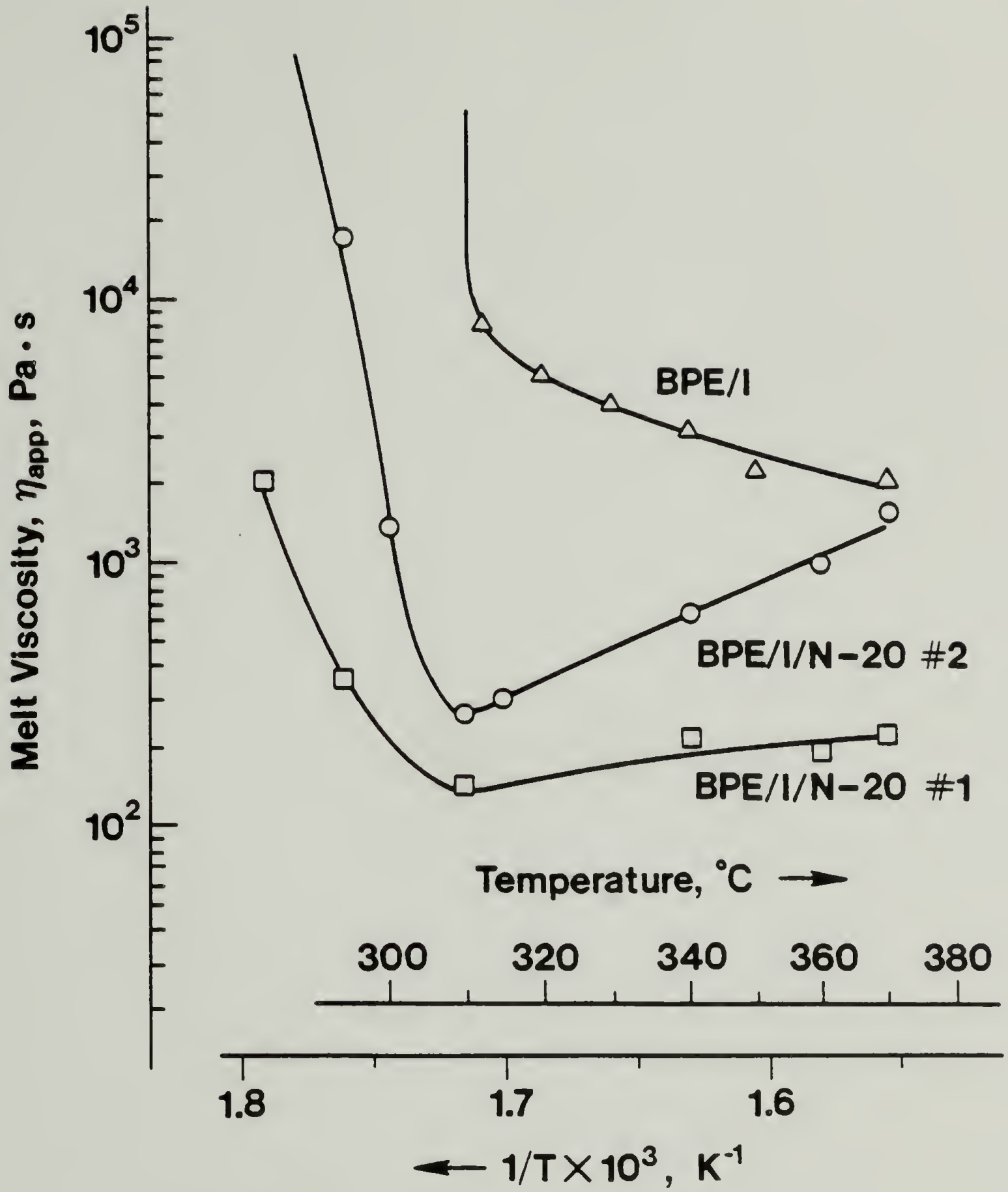

Fig. 27. Comparison of the temperature dependence of viscosity for BPE/I, BPE/I/N-20 #1, and BPE/I/N-20 #2 at constant shear stress, τ_w = 20kPa.

Degradation study. Despite vacuum drying of samples and purging the rheometer with nitrogen during sample loading, some degradation of the polyesters during testing was evident from yellow-brown color formation and the production of small bubbles in extrudates. These phenomena worsened with exposure to higher temperatures and longer times in the rheometer. Efforts were made to collect data before the severity of degradation could affect the viscosity. Degradation was judged to be minimal if the individual extrusion pressures and plunger velocities had reached steady-state values on the strip chart recorder, and if all data from a given run produced a smooth, consistent curve.

The extent of degradation was further monitored by measuring the inherent viscosities of selected extrudates as a function of extrusion temperature. Extrudates were selected from the middles of runs, usually at points where $\dot{\gamma}_{app} \sim 30\ s^{-1}$, but a few were taken at $\dot{\gamma}_{app} \sim 150\ s^{-1}$. Extrudates were dissolved at concentrations of 0.5 g/dl in 60/40 wt% phenol/1,1,2,2 - tetrachloroethylene, under reflux for 1-2 hours at ~120°C. Inherent viscosities were determined using size 150 Ubbelhode viscometers in a 25°C constant temperature bath. The results are given in Figure 28, where inherent viscosities for the three polyesters are plotted as a function of extrusion temperature. Measurements for the two BPE/I/N-20 copolyesters were replicated at least three times for the original powders and for extrudates at 295, 310, and 340°C. Error bars represent the range of data. Data for the BPE/I were not replicated, since previous

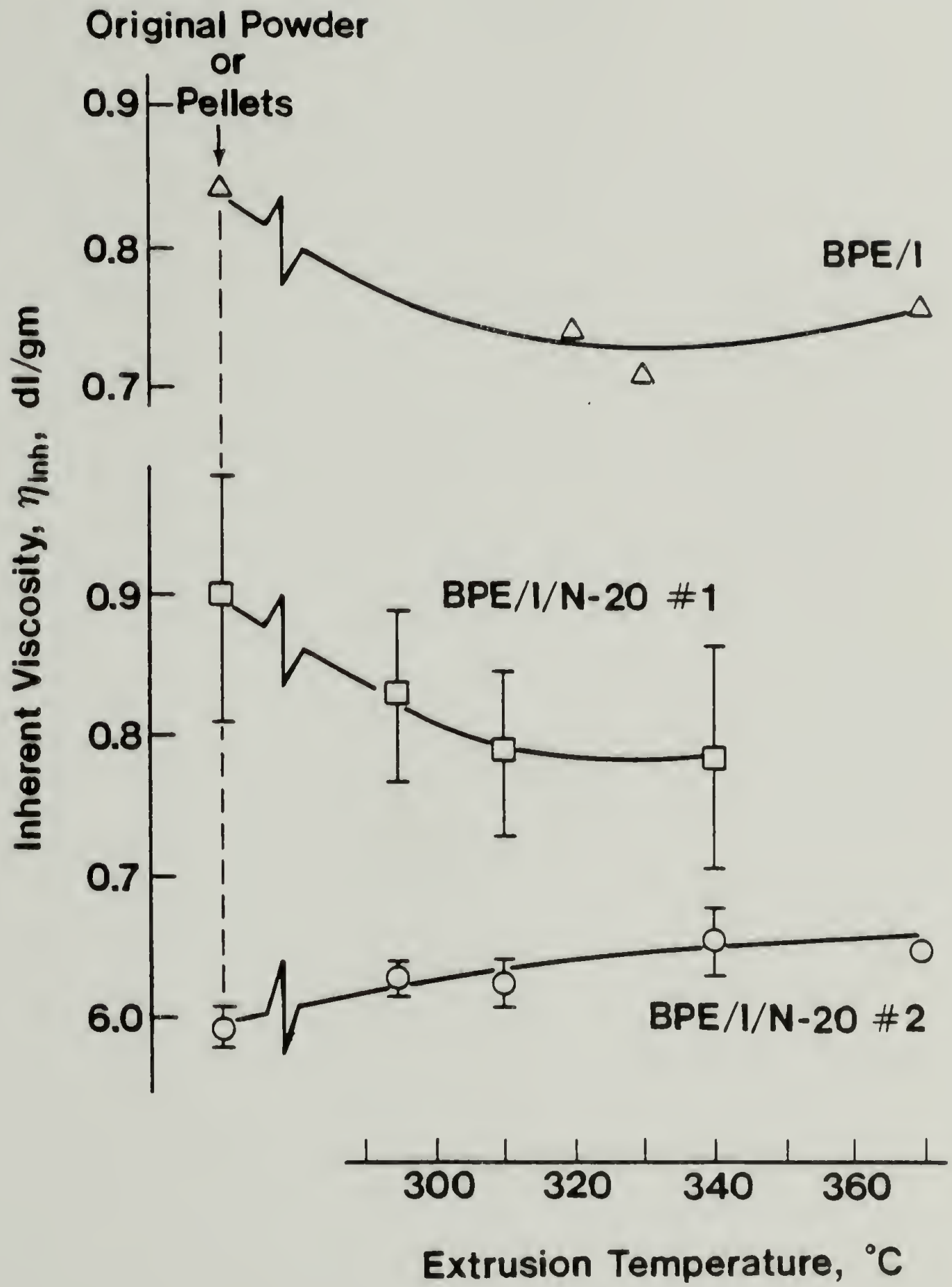

Fig. 28. Inherent viscosities of rheometer extrudates as a function of extrusion temperature.

experience at Monsanto has shown that a fairly consistent pattern of degradation can be expected from that polymer, with inherent viscosity decreasing during extrusion (34,35).

Discussion by Copolymer

Behavior of the three polyesters will be discussed separately. The BPE/I non-liquid crystalline homopolymer is examined first, to provide a reference for comparison of the BPE/I/N-20 liquid crystalline copolymers. The two copolymers are discussed individually, since differences in molecular weight and/or composition resulted in substantial differences in rheology.

Poly(Bisphenol E isophthalate). The BPE/I non-liquid crystalline homopolyester exhibited conventional behavior for thermoplastic polymer melts, and was consistent with the rheology of other BPE/I samples characterized previously by R.A. Mendelson at Monsanto (37). Mendelson has reported viscosity-molecular weight-temperature-shear rate relationships for BPE/I, and has compared BPE/I behavior to that of poly(ethylene terephthalate), polycarbonate, polysulfone, and other polyarylates. The BPE/I sample which was used in this thesis as a reference for the BPE/I/N-20 polymers had an η_{inh} = 0.85 dl/gm. Mendelson has studied BPE/I samples within the range η_{inh} = 0.22 - 1.09 dl/gm, thus permitting comparison of the BPE/I/N-20 polymers to BPE/I over a range of molecular weights. His study also permits comparisons with the other more familiar high-temperature thermoplastics.

Most of the BPE/I curves in Figures 15 and 21 show Newtonian behavior at low shear rates ($\dot{\gamma} < \sim 10\ s^{-1}$). This is evidenced by viscosities tending toward plateau values and n (= dlog τ_w/dlog $\dot{\gamma}_{app}$) approaching 1 as shear rate was decreased toward zero.

One BPE/I curve which does not show Newtonian behavior at low shear rates is that at 310°C, where a yield stress is inferred. A yield stress is to be expected at this temperature, due to the proximity of the extrusion temperature to the melting range for BPE/I. At 310°C, residual high-melting crystallites are present in the polymer during extrusion. These act as junctions in a mechanically "cross-linked" network. Resistance of the network to deformation gives rise to the yield behavior upon shearing.

Shear thinning is observed for the BPE/I at shear rates above ~10 s^{-1}, as manifested by viscosities decreasing with increasing shear rate (Fig. 21) and by n becoming less than 1 (Fig. 15). Shear thinning is characteristic for polymers which exceed a critical entanglement molecular weight (M_c). Mendelson's study suggests that M_c for BPE/I occurs near a viscosity - average molecular weight, $\bar{M}_v$, of ~30,000 - which corresponds to an inherent viscosity $\eta_{inh} \sim 0.60$ dl/gm (37). Since the BPE/I studied here had $\eta_{inh} \sim 0.85$ dl/gm, it was expected to display shear thinning in the regions observed.

A characteristic relaxation time, λ, for a polymer is often defined as the reciprocal of the shear rate where deviation from Newtonian behavior first occurs (32). From the data of Figures 15 and 21, λ for this BPE/I sample at temperatures greater than 312°C

was in the range 0.1-0.7 s. This agrees well with λ = 0.56 s predicted from equations provided by Mendelson (37) for BPE/I with η_{inh} = 0.85 dl/gm at 316°C.

At shear rates near ~1000 s^{-1} power-law dependence is approached by the BPE/I, with n ($d\log \tau_w / d\log \dot{\gamma}_{app}$) becoming nearly constant at ~0.4. This value of n in the power-law region is greater than the value ~0.3 predicted by the Graessley theory (38) for a polymer having the most-probable molecular weight distribution (MWD) of 2. Since BPE/I is a condensation polymer it is expected to have an MWD of ~2, and should thus display a power-law slope of ~0.3. Possible reasons for the higher observed value of n include: 1) power-law dependence has not been reached in Figure 15, and the slope n will continue to decrease to the expected 0.3 limit; 2) the BPE/I has an MWD greater than the expected value of 2; 3) the Graessley theory is in error, predicting a slope which is too low. The value of n ≃ 0.4 in the power-law region appears valid for BPE/I, since it is consistent with the value n = 0.42 reported in empirical models by Mendelson (37).

The temperature dependence of viscosity for BPE/I (Fig. 24) shows a conventional monotonic decrease in viscosity with temperature. A sharp drop in viscosity occurs through the melting range, 300-320°C. Above 320°C, the data fit an Arrhenius relationship:

$$\eta \ (\text{const } \tau_w) = k \exp(E_a/RT) \qquad \text{--- 7}$$

The activation energy for viscous flow, E_a, found for BPE/I was ~ 8-11

kcal/g mole. This value for E_a is lower than that of ~15 kcal/g mole estimated by Mendelson (37). However, the value 15 for E_a was generated using temperatures as low as 316°C, which may have been too close to the melting point for BPE/I to exhibit fully Arrhenius behavior. (See Chapters II and VII for DSC thermograms of the BPE/I melt transition).

In summary, the BPE/I sample in this thesis followed closely the empirical rheological models developed by Mendelson, with a minor descrepancy in the value of the activation energy for viscous flow. Viscosity-temperature-shear rate data were consistent with a sample having η_{inh} = 0.85 dl/gm. The BPE/I data appear reasonable and consistent with that from Mendelson's study, and are considered to be a suitable reference for comparison of the BPE/I/N-20 copolyesters.

Poly(Bisphenol E isophthalate-co-naphthalate) #1. This copolyester exhibits a number of differences in viscosity behavior as compared to the BPE/I. First, at the same temperatures and shear rates, BPE/I/N-20 #1 shows lower viscosities (and shear stresses) than BPE/I - lower by more than an order of magnitude! The lower viscosities are believed to be due to the liquid crystalline nature of the copolyester. As mentioned in Chapter I, an almost universal characteristic of any substance which exhibits a nematic state is the manifestation of lower viscosity in the nematic state vs. the corresponding isotropic state. This has been observed whether the transition between isotropic and nematic is brought about by changes in temperature or changes in

mesogen concentration. For the nematic BPE/I/N-20 #1, at a given temperature, the BPE/I represents such a "corresponding isotropic state." The transition from one "state" to the other is accomplished by changing mesogen concentration (via changes in naphthalate content). Analogous behavior has been observed with copolyesters of PET and p-hydroxybenzoic acid (PHB), where nematic copolyesters containing 60/40 to 80/20 ratios of PHB/PET displayed lower melt viscosities than a comparable isotropic PET homopolymer (3,4).

An alternative explanation for the low melt viscosities of BPE/I/N-20 #1 is that it may have lower molecular weight than the BPE/I. This possibility is not obvious from comparison of inherent viscosities: η_{inh} = 0.90 dl/gm for BPE/I/N-20 #1; η_{inh} = 0.85 dl/gm for BPE/I. The Mark-Houwink coefficients, which provide the relationship between inherent viscosity and molecular weight, have not been measured for BPE/I/N-20. However, the copolyester is expected to have a higher Mark-Houwink exponent than the homopolymer, due to the chain-extending tendency of the naphthalate groups. Thus, at similar inherent viscosities, the BPE/I/N-20 would tend to have lower molecular weight. Without the Mark-Houwink coefficients, it is difficult to know whether the BPE/I/N-20 #1 molecular weight is actually higher or lower than that of the BPE/I.

One argument against attributing the lower melt viscosity of BPE/I/N-20 #1 simply to lower molecular weight is the extent of shear thinning. BPE/I/N-20 #1 exhibits shear thinning over the entire 1-1000 s^{-1} range studied, whereas BPE/I displays Newtonian plateaus

near 1-10 s^{-1}. The absence of Newtonian plateaus for the BPE/I/N-20 #1 in this range indicates a longer relaxation time vs BPE/I, and longer relaxation times are generally associated with higher molecular weight. If the lower melt viscosity of BPE/I/N-20 #1 vs BPE/I were attributable solely to lower molecular weight, more Newtonian behavior should have been observed, with a delay in the onset of shear thinning until higher shear rates.

In addition to shear thinning over a wider range, the viscosity (shear stress) of BPE/I/N-20 #1 shows a more rapid decrease with increasing shear rate than that of the BPE/I. In the power-law region, n (= dlog τ_w/dlog $\dot{\gamma}$) for BPE/I/N-20 #1 is in the range 0.28-0.40, as compared to n ~ 0.4+ for BPE/I. The value of n for the thermotropic BPE/I/N-20 #1 is closer to the value n ~ 0.3 predicted by the Graessley theory for a polymer having the most probable MWD of 2.

The steeper shear thinning of BPE/I/N-20 #1 may be a result of its liquid crystalline nature. Strong shear thinning has been observed in other nematic polymers - both lyotropic and thermotropic (eg.,15,39). The reason for the pronounced shear thinning in these systems is not fully understood. It has been suggested that the shear thinning is associated with yield-like behavior, involving the breakdown of some kind of aggregated structure. Another hypothesis suggests the formation of a boundary layer during capillary flow of anisotropic fluids. The boundary layer would have a lubricating effect, resulting in slip at the wall, and causing dlog τ_w/dlog $\dot{\gamma}_{app}$ to approach zero. A third reason is that rods orient differently than

flexible chains. Any of these three mechanisms might explain the steeper shear thinning (lower power-law index) observed for BPE/I/N-20 #1 vs BPE/I, although a yield stress is not clearly indicated by the data. To establish whether BPE/I/N-20 #1 will exhibit a true yield stress at low shear rates would require a more sensitive instrument than the Sieglaff-McKelvey capillary rheometer.

Perhaps the most unusual aspect of BPE/I/N-20 #1 behavior is its dependence of viscosity upon temperature (Fig. 25). Above ~ 310°C, viscosity does not decrease monotonically with temperature as for conventional thermoplastics. In fact, it increases slightly. The possibility that degradative cross-linking could be possible for the viscosity increase has been ruled out. The viscosity increase is consequently believed to result from the thermotropic character of the BPE/I/N/20 #1, and to correspond to a gradual transition from nematic to isotropic structure over the range of viscosity measurement.

Although a nematic-isotropic transition is not observed for BPE/I/N-20 #1 at temperatures up to 400°C (Chapter II), a low molecular weight (n_{inh} = 0.38 dl/gm) prepolymer having the same composition did show a nematic-isotropic clearing temperature at ~380°C (See Chapter X). This suggests that shorter polymer chains become disordered more readily than longer ones. A decrease in $T_{N \rightarrow I}$ with decreasing molecular weight has been documented for other nematic polymers (36). Assuming that a distribution of molecular weights (and/or of mesogen sequence lengths) exists in the BPE/I/N-20 #1, disorder could occur over a range of temperature - resulting in a broadened nematic-isotropic transition. A gradual decrease in

structural order could account for the increase in viscosity with temperature.

It was noted in Chapter I that an increase in viscosity with temperature near the nematic-isotropic transition is characteristic of low molecular weight liquid crystals, and is also observed for many lyotropic systems. The same mechanism is believed to operate for BPE/I/N-20 #1. Such behavior was not expected for the BPE/I/N-20 copolyesters, since - at the time the experiments were conducted - the most widely studied thermotropic polymers (copolymers of PET and PHB) had not exhibited any unusual temperature dependence of viscosity (4,7-11). Recently, however, several researchers have documented increases (or plateaus) in viscosity with temperature for a number of rod-like thermotropic polymers (12-18). These were described in Chapter I.

Degradative cross-linking does not appear to play a role in the viscosity increase for BPE/I/N-20 #1, based upon two pieces of evidence. First, a re-examination of all strip chart recordings from the capillary rheometry of BPE/I/N-20 #1 has confirmed that extrusion pressures had reached steady-state values at all temperatures and shear rates tested. If thermal degradation were responsible for the viscosity increase, the viscosity should have continued to change with time during the experiment. Secondly, the inherent viscosities of BPE/I/N-20 #1 rheometer extrudates, which were monitored as a function of extrusion temperature, did not show signs of cross-linking (Fig. 28). Cross-linking would be expected to increase the polymer molecular

weight, and hence increase inherent viscosity. The opposite was observed: inherent viscosity decreased somewhat with extrusion temperature. An equivalent drop in inherent viscosity was also observed for the BPE/I reference polymer, and was not unexpected. Polyesters commonly undergo molecular weight reduction at these temperatures, since the ester bonds are readily broken by hydrolysis or free radical-initiated reactions.

The temperature where viscosity passes through a minimum for BPE/I/N-20 #1 (and #2) is ~310°C. This appears to correspond to the peak melting point for BPE/I homopolymer (See DSC studies, Chapters II and VII), and suggests that residual unmelted crystallites of the BPE/I homopolymer are likely to be present in the BPE/I/N-20 when extruding at T < 310°C. Evidence for such high-melting crystallites has been observed in extrudates of BPE/I/N-20 #1 (and #2) collected at temperatures lower than 310°C (See Chapter VII). No residual crystallites are observed for samples extruded above 310°C. The reason that the minimum in viscosity with temperature should occur precisely at 310°C is as yet unclear.

In conclusion, the BPE/I/N-20 #1 has exhibited a number of differences in melt rheology vs BPE/I which are attributed to its thermotropic liquid crystalline nature. The most unusual finding is the viscosity plateau and even an increase with temperature. Other differences include the order-of-magnitude lower melt viscosity vs BPE/I, a steeper shear-thinning curve, longer relaxation times, and the absence of a low shear Newtonian plateau over the shear rate range

studied.

Poly(Bisphenol E isophthalate-co-naphthalate) #2. The BPE/I/N-20 #2 copolyester exhibited rheology similar to that of BPE/I/N-20 #1 in many respects. It also displayed some rather puzzling differences.

Similarities to BPE/I/N-20 #1 included an increase in melt viscosity with temperature above ~310°C, the absence of Newtonian behavior over the range 1-1000 s^{-1}, steeper shear-thinning than the BPE/I reference homopolymer, and lower viscosity than the BPE/I by roughly an order of magnitude. However, for the BPE/I/N-20 #2 the lower melt viscosity was attributable simply to lower molecular weight. The inherent viscosity of BPE/I/N-20 #2 was ~0.60 dl/gm as compared to ~0.85 dl/gm for the BPE/I. Mendelson's study of BPE/I rheology (37) predicts a 14-fold drop in Newtonian melt viscosity for a change in η_{inh} from 0.85 to 0.60 dl/gm, and this is roughly the difference observed between BPE/I and BPE/I/N-20 #2. Hence, the liquid crystalline structure of BPE/I/N-20 #2 did not contribute to a reduction in melt viscosity versus BPE/I of the same inherent viscosity.

The BPE/I/N-20 #2 melt viscosity is, in fact, greater than that of BPE/I/N-20 #1 - surprising, since BPE/I/N-20 #2 has an apparently lower molecular weight than BPE/I/N-20 #1 (η_{inh} = 0.60 dl/gm vs η_{inh} = 0.90 dl/gm, respectively). Conventional behavior dictates that, for polymers having the same composition, melt viscosity should increase with solution viscosity. The reversal of behavior between the two BPE/I/N-20 copolyesters is not yet understood.

The possibility that the two copolyesters could have different compositions which would affect their melt viscosities was investigated (Chapter V), but only small, if any, differences were detected. DSC thermograms do suggest that the two polymer samples may differ in chemical homogeneity (Chapter VII), though it is unclear in what way the heterogeneity would affect melt viscosity.

It is conceivable that the inverse dependence of melt viscosity upon molecular weight for the BPE/I/N-20 copolyesters is a unique result of their thermotropic liquid crystalline nature. Studies of additional BPE/I/N-20 copolyesters in Chapter X indicate a possible maximum in melt viscosity with molecular weight. Such a maximum has also been noted for lyotropic PBA solutions (33), as shown in Chapter I.

The reason for the decrease in melt viscosity at higher molecular weights is not understood, but seems to be analogous to the effects of concentration and temperature on liquid crystalline order. Perhaps, at high molecular weights, the lower concentration of end groups results in less disruption of the mesogenic order. Another possibility is that chain entanglements at high molecular weights prevent phase-separation of isotropic and nematic regions, somehow resulting in lower viscosity. A greater tendency for phase-separation at lower molecular weights is noted for the BPE/I/N-20 copolyesters in DSC studies (Chapters VII, X).

C H A P T E R IV

EXTRUDATE SWELL MEASUREMENTS

Very low, and perhaps even negative, extrudate swell ("die swell") has been observed in previous studies of rod-like liquid crystalline polymers (9-13,17,18,39). It has been suggested that this may be a general characteristic of polymer liquid crystals (13). Such behavior is not usually seen in conventional thermoplastics without the presence of added filler particles.

This unusual phenomenon was investigated for the Bisphenol E isophthalate-co-naphthalate liquid crystalline polyesters. Their behavior is compared here to that of the non-liquid crystalline Bisphenol E isophthalate reference polymer.

Unannealed Extrudate Swell

Extrudate swell was determined for polymer strands which had been collected during the capillary flow studies described in Chapter III. Extrudates were collected at shear rates of 7.7-800 s^{-1} and temperatures of 288-340°C. Swelling was computed as the ratio of extrudate diameter to capillary diameter, D_e/D_o, where extrudate diameters were measured via micrometer on solidified, unannealed extrudates. Diameter measurements were compared at a point 4 mm from the leading ends of the extrudates, to avoid error due to gravitational draw.

Extrudate swell ratios, D_e/D_o, as a function of extrusion temperature are shown for the BPE/I, BPE/I/N-20 #1, and BPE/I/N-20 #2 polyesters in Figs. 29-31. Data for the BPE/I/N-20 polyesters are plotted at discreet shear rates of 7.7, 30, 150, and 800 s^{-1} (Figs. 30,31). For the BPE/I polymer, no significant change in D_e/D_o with shear rate ws observed, so that Fig. 29 incorporates BPE/I data at all shear rates from 7.7 to 800 s^{-1}. The vertical bars in Fig. 29 represent the ranges of observed swelling for the BPE/I polymer. Swelling for all three polymers as a function of extrusion temperature is compared at a shear rate of 30 s^{-1} in Fig. 32.

The horizontal lines in the figures at $D_e/D_o = 1$ indicate the point where no change is observed in the diameter of the extrudates relative to the diameter of the capillary. Above these lines, extrudate swell is referred to as being "positive"; below the lines extrudate swell is "negative".

In general, the extrudate swell measured for the BPE/I/N-20 polymers was much lower than for the BPE/I reference polymer. In fact, below ~330°C swelling for the BPE/I/N-20 polymers appeared to be negative as measured by this technique. BPE/I/N-20 #2 exhibited a definite decrease and minimum in extrudate swell between 300°C and 330°C.

Above 330°C the extrudate swell for the BPE/I/N-20 polymers increased and became positive. This increase in extrudate swell paralleled an increase in viscosity with temperature (Chapter III). It is possible that both phenomena are a result of a decrease in

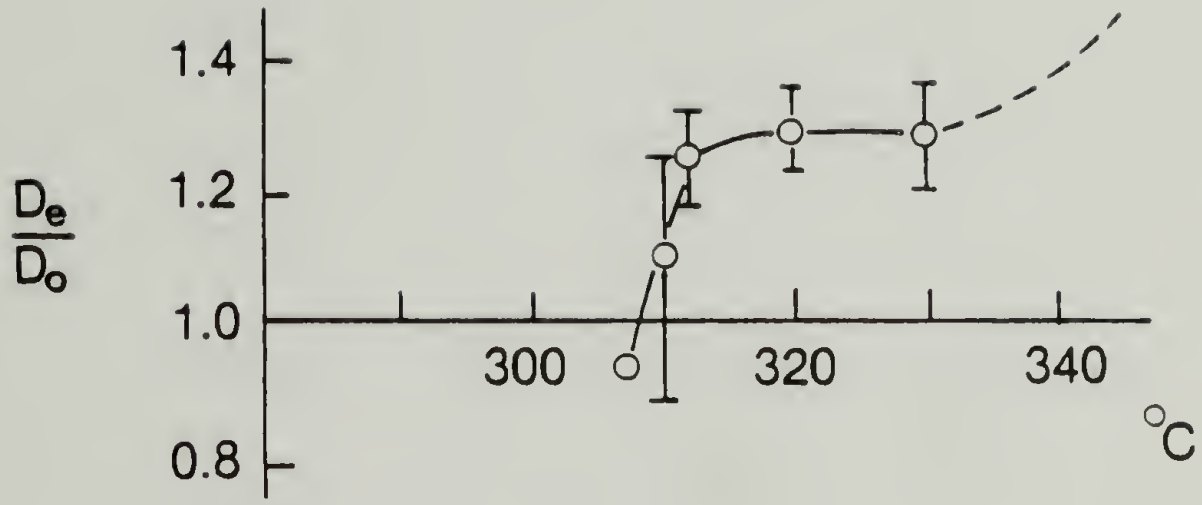

Fig. 29. Extrudate swell ratio as a function of extrusion temperature for BPE/I.

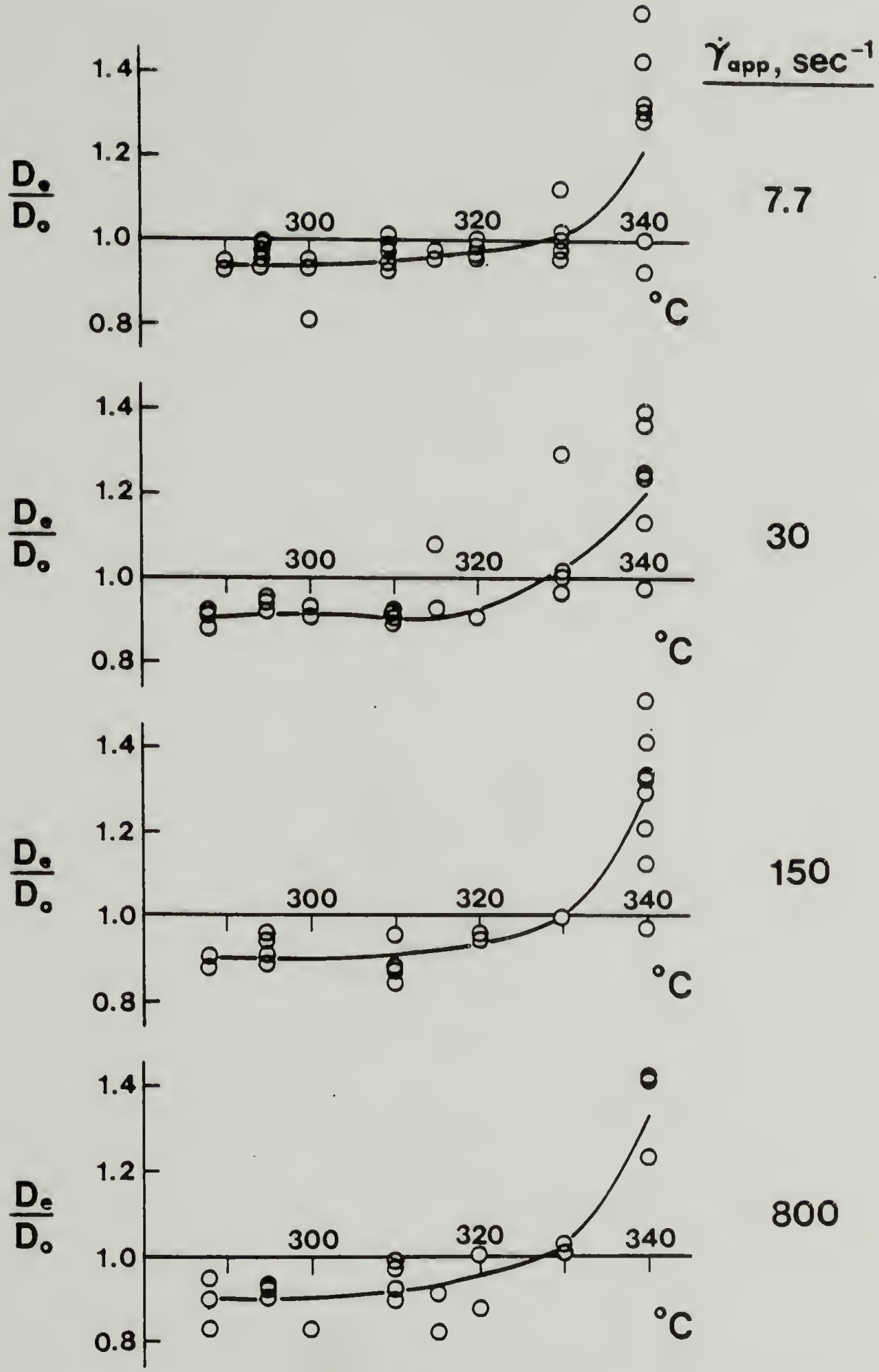

Fig. 30. Extrudate swell ratio as a function of extrusion temperature for BPE/I/N-20 #1.

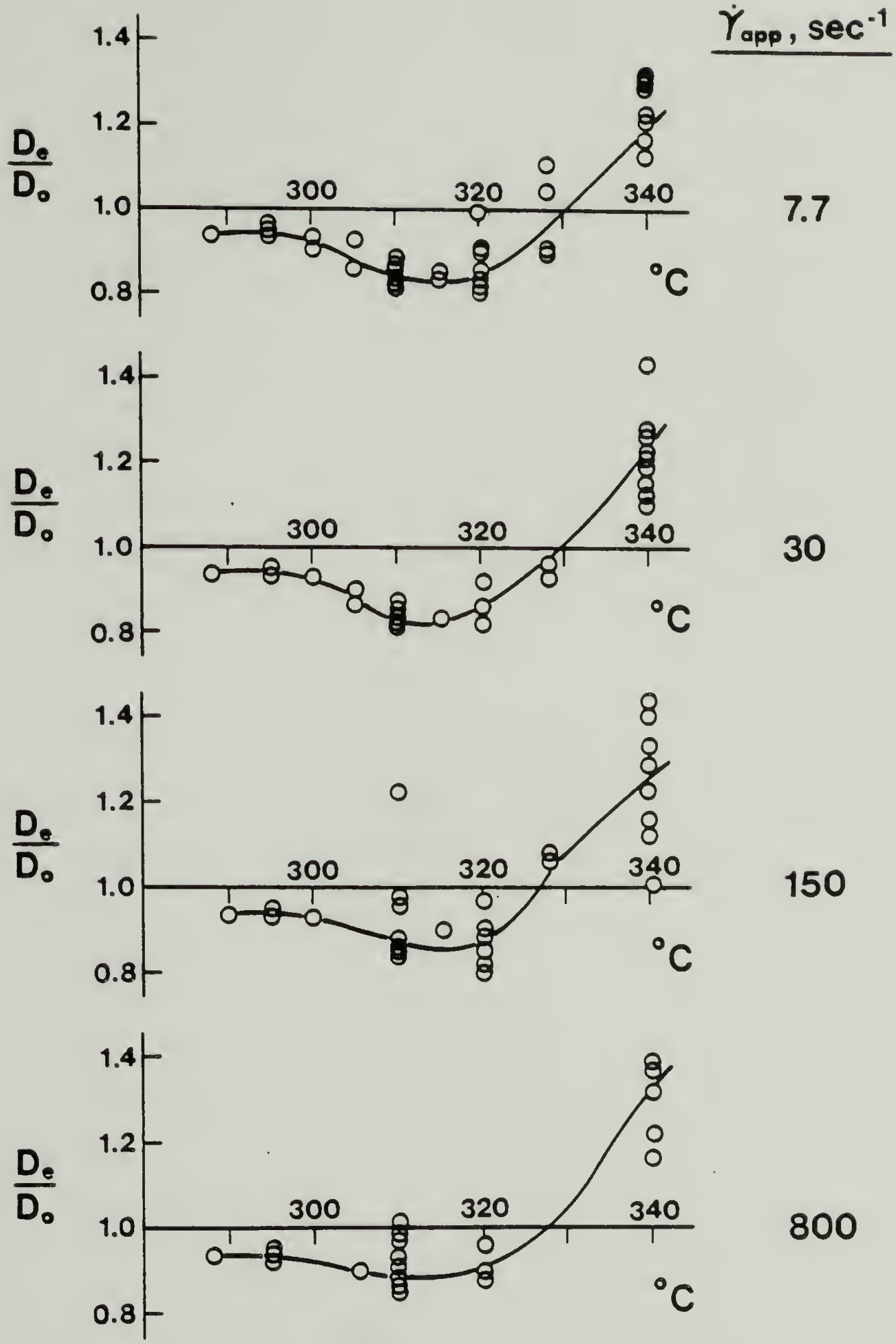

Fig. 31. Extrudate swell ratio as a function of extrusion temperature for BPE/I/N-20 #2.

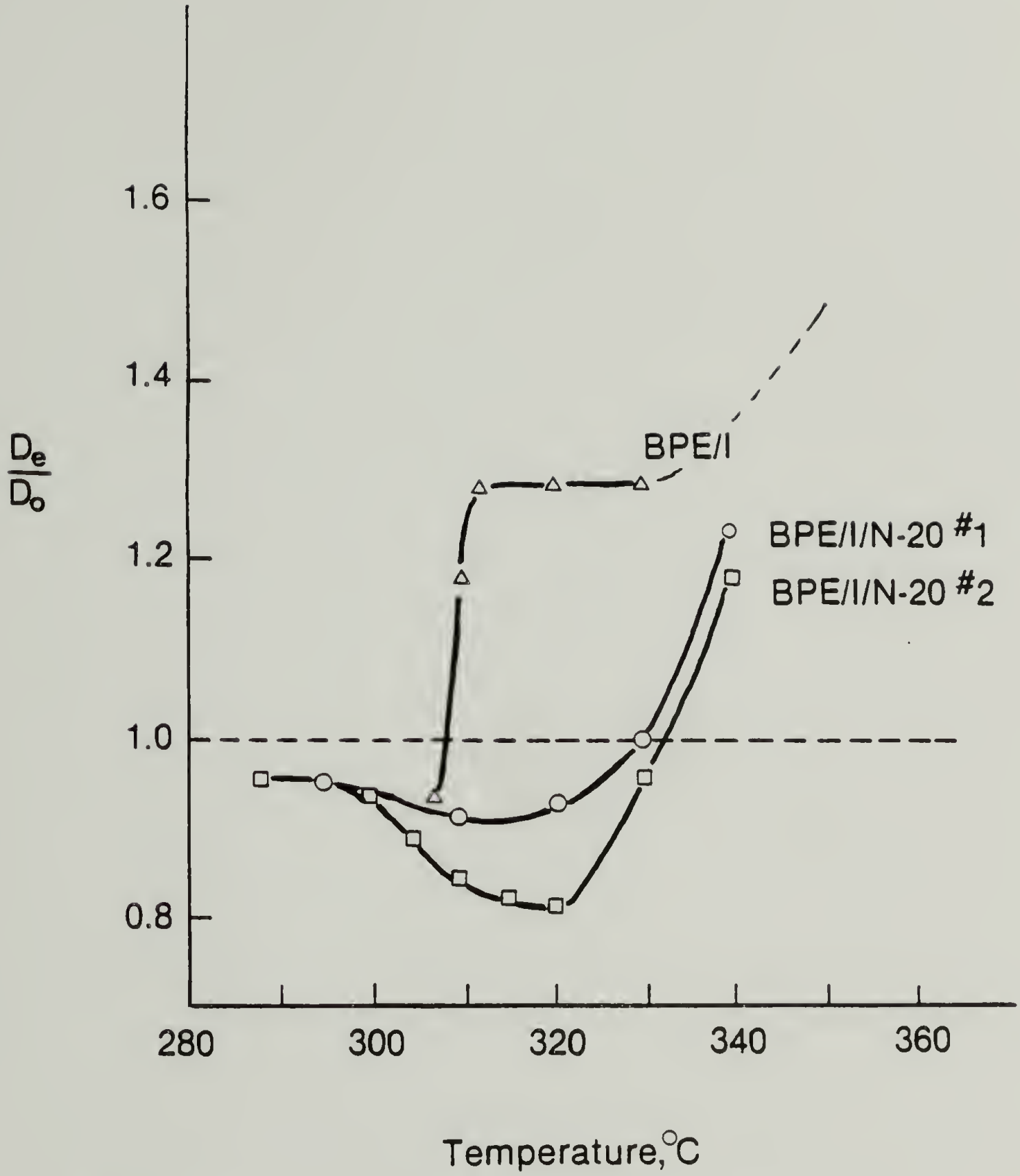

Fig. 32. Comparison of extrudate swell for BPE/I, BPE/I/N-20 #1, and BPE/I/N-20 #2 as a function of extrusion temperature ($\dot{\gamma}=30s^{-1}$).

liquid crystalline order with increasing temperature. However, at these higher temperatures thermal degradation also begins to occur, accompanied by generation of bubbles in the extrudates. The bubbles have the effect of increasing the extrudate diameter, thus contributing to the observed increase in D_e/D_o. The relative contributions of the bubble formation and the decrease in liquid crystallinity to increased extrudate swell have not yet been determined.

For the BPE/I reference polymer, extrudate swell was positive over nearly the entire range studied. From 312 to 330°C swelling was essentially constant at D_e/D_o ~1.28. Above 330°C, the BPE/I polymer exhibited an increase in swelling with temperature similar to that observed for the BPE/I/N-20 polymers - again due, at least partially, to bubble formation.

Below 312°C, extrudate swell for BPE/I decreased - dropping to a "negative" value (D_e/D_o ~0.93) at 307°C. This temperature was very near the peak melting point for BPE/I, and corresponded essentially to solid-state extrusion. Under these conditions, a yield stress was shown to exist in the BPE/I (Chapter III) which could have inhibited elastic recovery, and probably accounts for the negligible swelling.

As noted earlier, very low (perhaps negative) extrudate swell has been observed for other liquid crystalline polymers (9-13,17,18,39) and has been suggested to be a general characteristic of these systems (13). Negligible swelling implies a lack of elastic recoil by the polymer chains after being sheared. Proposed explanations for the negligible swelling include: 1.) these polymers may have inherently

low elasticity; ie., they "like" the conformations in which they are placed during shearing, 2.) negative normal forces may exist, or 3.) their tendency for elastic recoil may be inhibited by a yield stress (9).

Annealed Extrudate Swell

There was some concern that the BPE/I/N-20 polymers displayed low extrudate swell because elastic recoil did not have time to occur before the extrudates crystallized. To test for residual elastic recovery, selected extrudates were annealed in silicone oil (Dow 210H) above their peak transition temperatures (T_m or $T_{c \rightarrow n}$) for varying lengths of time. Specifically, strands of BPE/I/N-20 #2 which had been extruded at 295, 310, and 340°C and 7.7 s^{-1} were annealed under the following conditions: 280°C for 20 min.; 290°C for 2 min.; 310°C for 2 min. Under these annealling conditions, no additional swelling was observed. Since these strands were among those having the least swell initially, and might have been expected to exhibit the greatest residual recovery, tests were not conducted on strands produced under less severe conditions.

Correction to Extrudate Swell for Volume Change upon Cooling

It is possible that the "negative" extrudate swell (contraction) exhibited by the BPE/I/N-20 polymers is a result of negative normal forces. This would imply spontaneous extension of the extrudate at the capillary exit, rather than recoil. Alternatively, the contraction of

the extrudates may have resulted solely from a decrease in volume (increase in density) during cooling, since measurements were made on solidified extrudates. Ideally, this question should have been answered by measuring extrudate swell at the die exit, eg., photographically. Since this was not done, attempts were made to correct the extrudate swell measurements for possible density changes following extrusion.

Corrections to the swell ratio for the volume change during solidification were estimated as follows. A cylindrical material element was considered having a length L_i, diameter D_i, mass M_i, and density ρ_i in the initial (heated) state (Fig. 33). Similarly, parameters in the final (room temp.) state were L_f, D_f, M_f, and ρ_f. By the definition of density,

$$\rho_i = \frac{M_i}{V_i} = \frac{M_i}{\pi D_i^2 L_i/4} \qquad \text{---8}$$

and

$$\rho_f = \frac{M_f}{V_f} = \frac{M_f}{\pi D_f^2 L_f/4} \, . \qquad \text{---9}$$

By conservation of mass, $M_i = M_f$ for the cylindrical material element. If, additionally, one assumes that $L_i = L_f$ (no axial contraction) in order to calculate the <u>maximum</u> possible radial contraction due to densification, one finds:

$$\frac{D_i}{D_f} = \frac{(\rho_f)^{1/2}}{\rho_i} \qquad \text{--10}$$

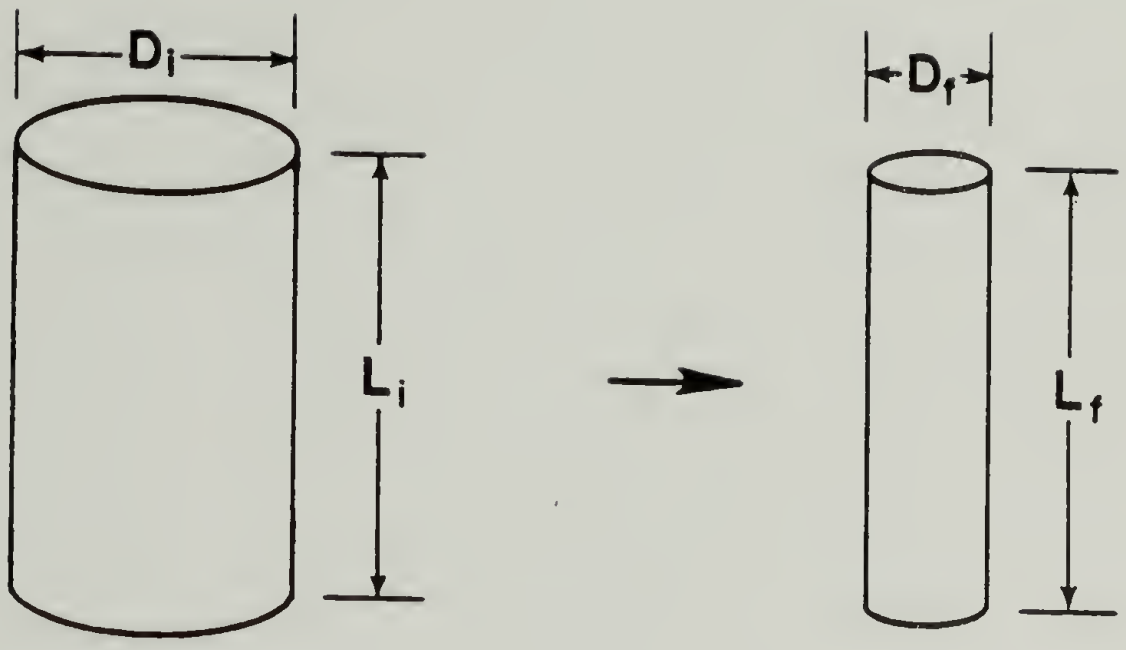

Fig. 33. Cylindrical material elements for computing the volume change upon cooling for rheometer extrudates.

The corrected extrudate swell ratio then is

$$\left(\frac{D_e}{D_o}\right)_{corrected} = \frac{D_i}{D_o} = \frac{D_f}{D_o}\,\frac{(\rho_f)^{1/2}}{\rho_i} \qquad \text{--11}$$

Thus, volume change upon cooling may be accounted for if both solid and melt densities are known.

The melt densities which were used to estimate the correction to extrudate swell ratio for the volume change on cooling were determined using the Sieglaff-McKelvey rheometer. The rheometer was heated to a selected temperature, fitted with a capillary, and loaded with sample in the manner used to make viscosity measurements. A known volume of melt was extruded (determined by displacement of the piston in the barrel). The extrudate was then cooled and weighed upon a micro-analytical balance. Melt density, ρ_{melt}, was calculated as:

$$\rho_{melt}(gm/ml) = \frac{\text{weight of extrudate}}{\text{volume of melt extruded}}\ \frac{(gm)}{(ml)} \cdot \qquad \text{---12}$$

Densities of the solidified extrudates were measured in a density gradient column (heptane/carbon tetrachloride at 25°C) which had been prepared by another researcher. Only crude measurements could be made, since the extrudates were less dense than the lowest-density calibration bead (1.32 gm/ml), and values were extrapolated. However, the column calibration was extremely linear, and the extrapolation is considered to be valid. In any case, the densities of the solidified extrudates are known to be less than 1.32 gm/ml.

Estimated corrections to the extrudate swell of BPE/I/N-20 #1

and BPE/I/N-20 #2 for the volume change upon cooling are shown in Table 3. The corrections were estimated for extrudates produced at 310°C and 30 s^{-1}, since these were among those having the least swelling.

As can be seen, the "true" extrudate swell for the BPE/I/N-20 polyesters is probably 6-9% greater than the value measured on solidified strands. What is interesting from this exercise is that, particularly for BPE/I/N-20 #2, the volume change upon cooling does not appear to completely account for the negative extrudate swell. The data suggest that either 1.) the polymers truly exhibit negative extrudate swell at the capillary exit under these conditions, or 2.) that the extrudates must undergo axial extension, rather than recoil, during their cooling (crystallization) process. Either of these possibilities would represent a departure from conventional polymer behavior.

Table 3

Estimated Corrections to Extrudate Swell Ratio for the Volume Change Upon Cooling

	BPE/I/N-20 #1	BPE/I/N-20 #2
D_e/D_o, extruded at 310°C and 30 s^{-1}; uncorrected	0.90 - 0.93	0.83 - 0.85
Density at 310°C, ρ_{melt}, gm/ml	1.10 - 1.14	1.10 - 1.14
Density at 25°C, ρ_{solid}, gm/ml	1.29 - 1.31	1.29 - 1.31
$(\rho_{solid}/\rho_{melt})^{1/2}$	1.06 - 1.09	1.06 - 1.09
D_e/D_o extruded at 310°C and 30 s^{-1}; corrected for the volume change upon cooling, assuming no axial contraction	0.95 - 1.01	0.88 - 0.93

CHAPTER V

COMPOSITIONAL ANALYSES

Justification

Theoretically, the composition of each polyester studied was fixed by its starting monomer ratio. However, slight differences in the structure of BPE/I/N-20 #1 and #2 were suggested by observed differences in rheology. In contrast to conventional polymer behavior, the sample with higher molecular weight exhibited a lower melt viscosity. Since differences in composition might explain the unusual finding, copolymer compositions were investigated using infrared spectroscopy, carbon-hydrogen-oxygen elemental analyses, and ^{1}H nuclear magnetic resonance. Results of these three methods will be discussed individually, followed by a synopsis of the conclusions.

Infrared Spectroscopy

Polymer films for infrared (IR) analyses were prepared by compression molding of vacuum-dried powder or pellets between sheets of teflon-coated aluminum foil[a] at 315°C. Spectra were obtained using a Perkin-Elmer Model 283 Infrared Spectrophotometer operated in the % transmittance mode using recommended settings for normal operation.

a. Penfoil, Penetone Corporation, 74 Hudson Avenue, Tenafly, NJ 07670.

The objective of the infrared studies was to identify compositional differences, if any, between BPE/I/N-20 #1 and #2. In order to establish which frequencies were most likely to manifest such differences, the copolyester spectra (Figures 34,35) were first compared with that of the BPE/I homopolymer (Figure 36). Significant differences between the homopolymer and the copolymers were observed for at least thirteen frequencies. These differences are indicated with arrows in the figures, and the corresponding frequencies are listed in Table 4.

Spectral differences between the homopolyester and the copolyesters are further highlighted in Figure 37, in which the BPE/I spectrum has been subtracted from the BPE/I/N-20 #1 spectrum by placing the BPE/I film in the reference beam while the BPE/I/N-20 #1 was scanned in the sample beam. Although this technique was not used quantitatively, it served to emphasize and confirm the location of spectral differences. Similar subtractions of the BPE/I spectrum from that of BPE/I/N-20 #2, and of one copolyester spectrum from the other, were less successful due to imprecisely-matched film thicknesses, and were not pursued.

Semi-quantitative comparisons of the compositions of the two BPE/I/N-20 copolyesters were made by considering relative intensities of the thirteen peaks mentioned above. No significant differences in the ratios of intensities were evident between the two spectra, and the two copolyesters appeared indistinguishable by these methods.

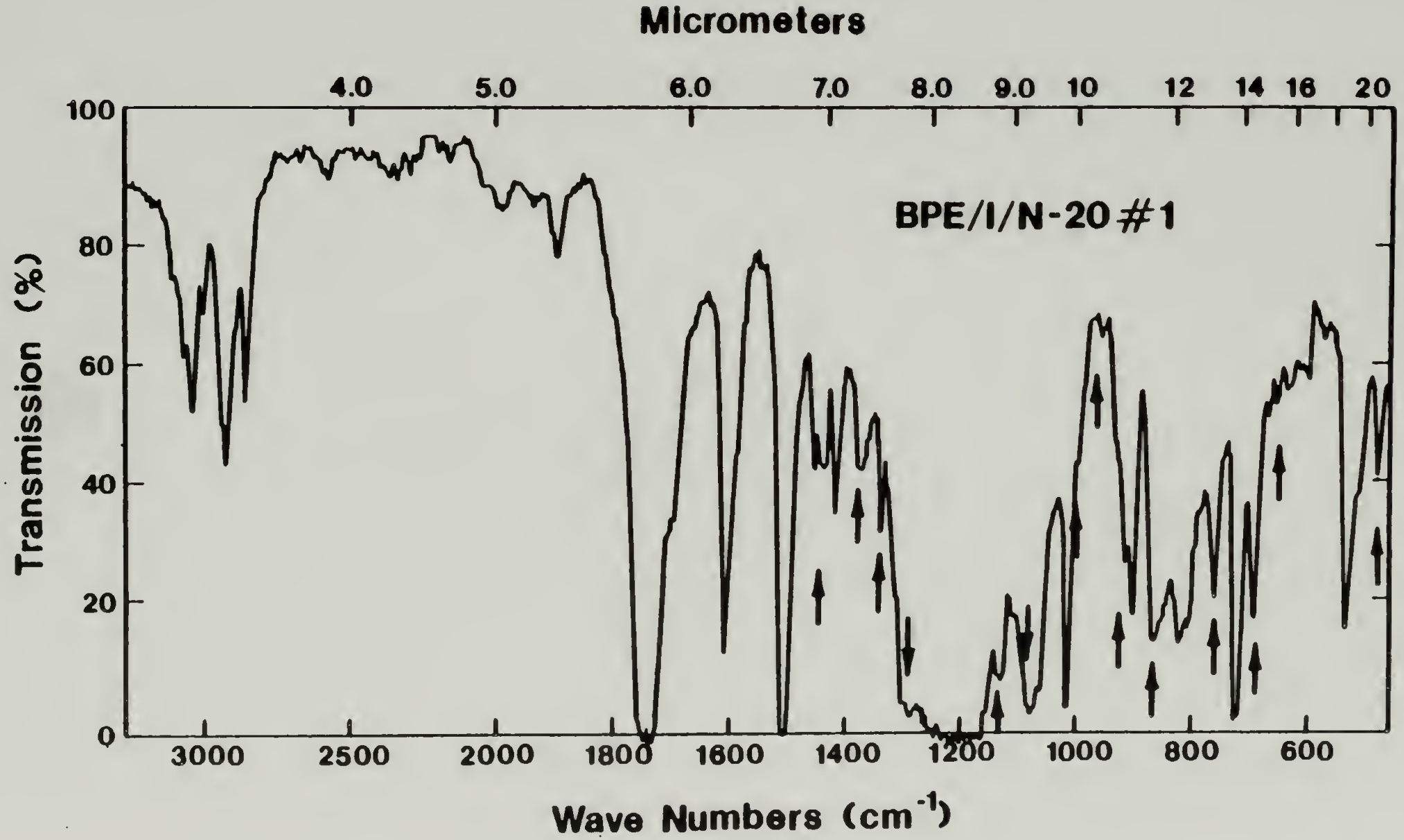

Fig. 34. Infrared spectrum for BPE/I/N-20 #1 compression molded film.

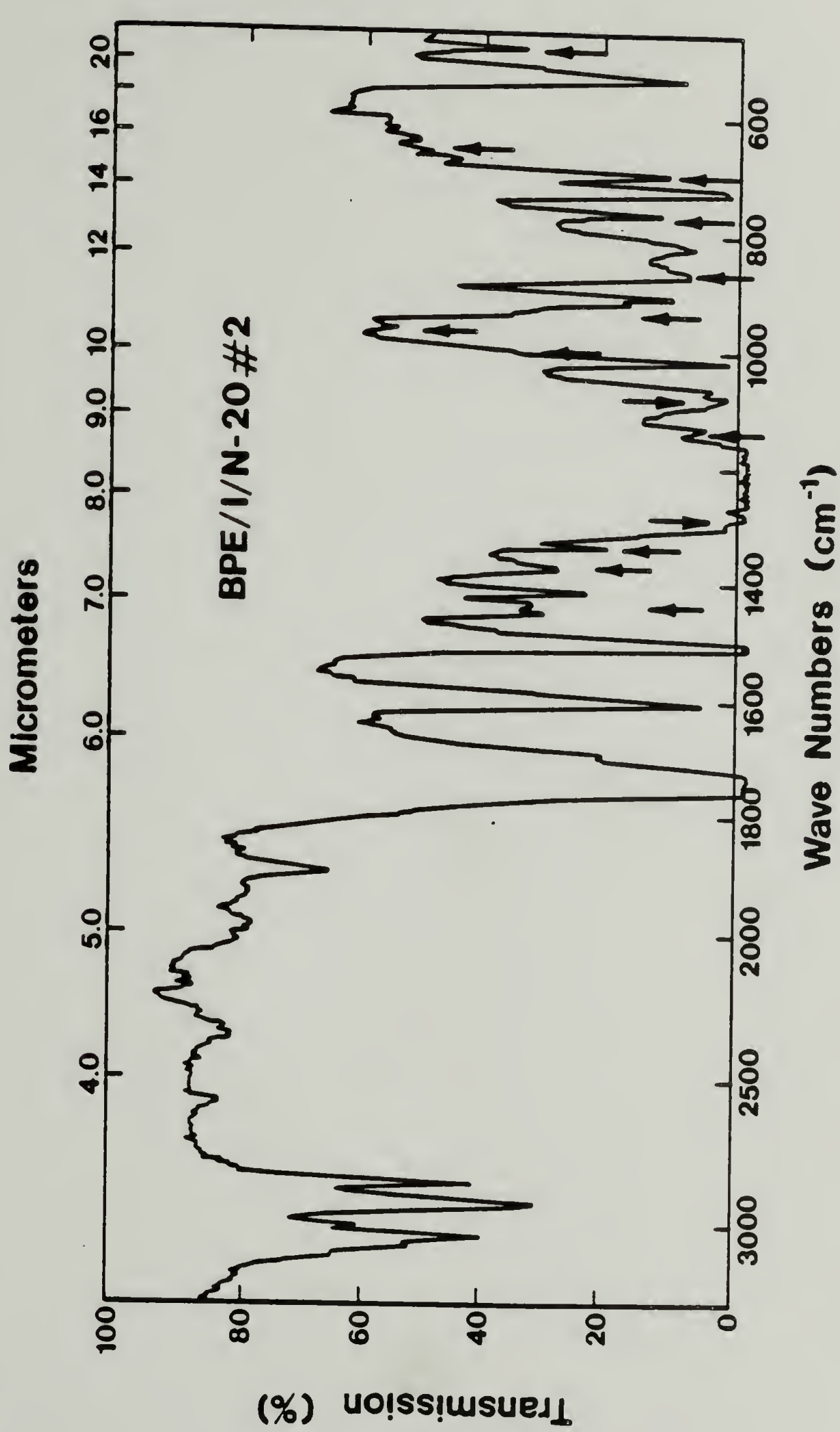

Fig. 35. Infrared spectrum for BPE/I/N-20 #2 compression molded film.

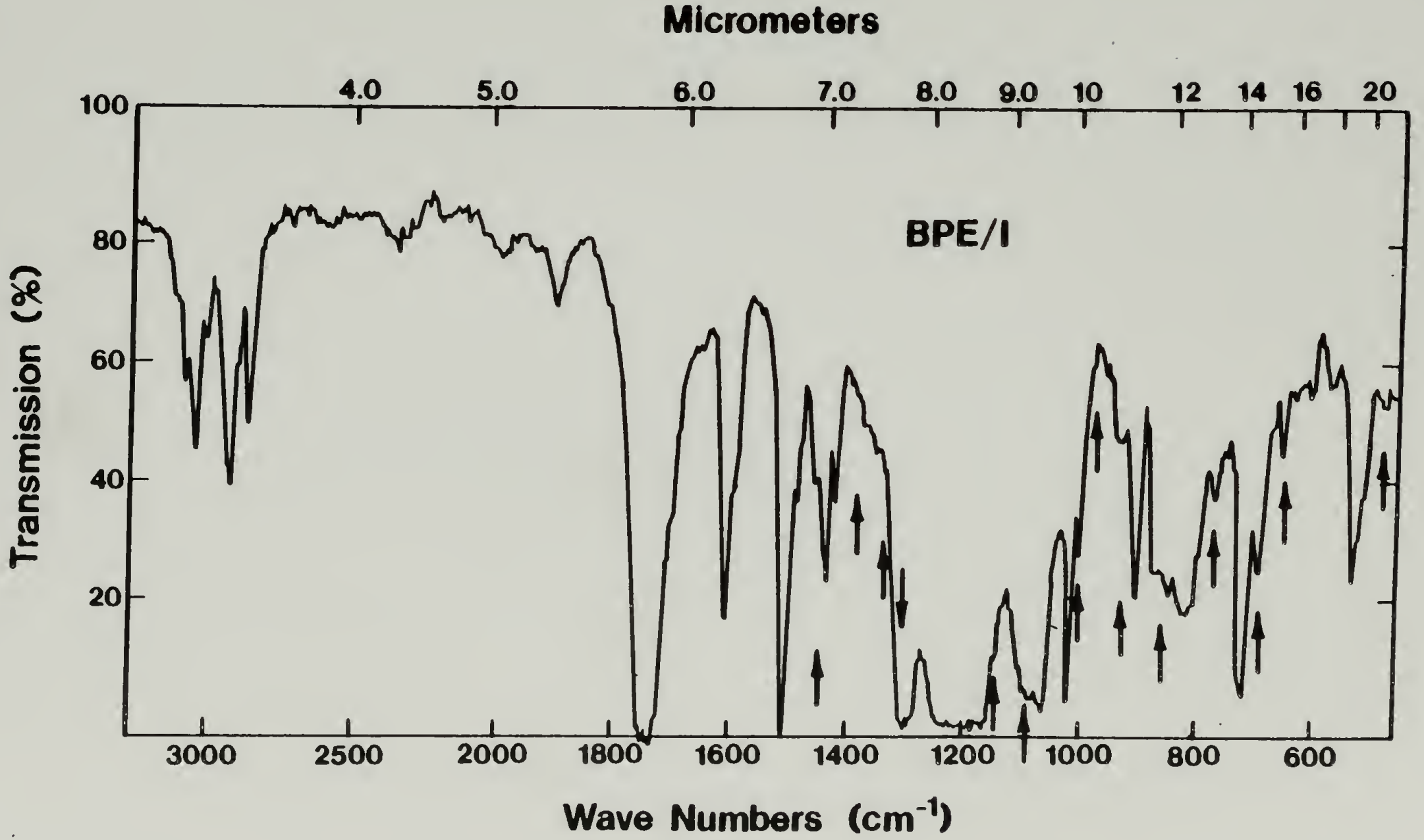

Fig. 36. Infrared spectrum for BPE/I compression molded film.

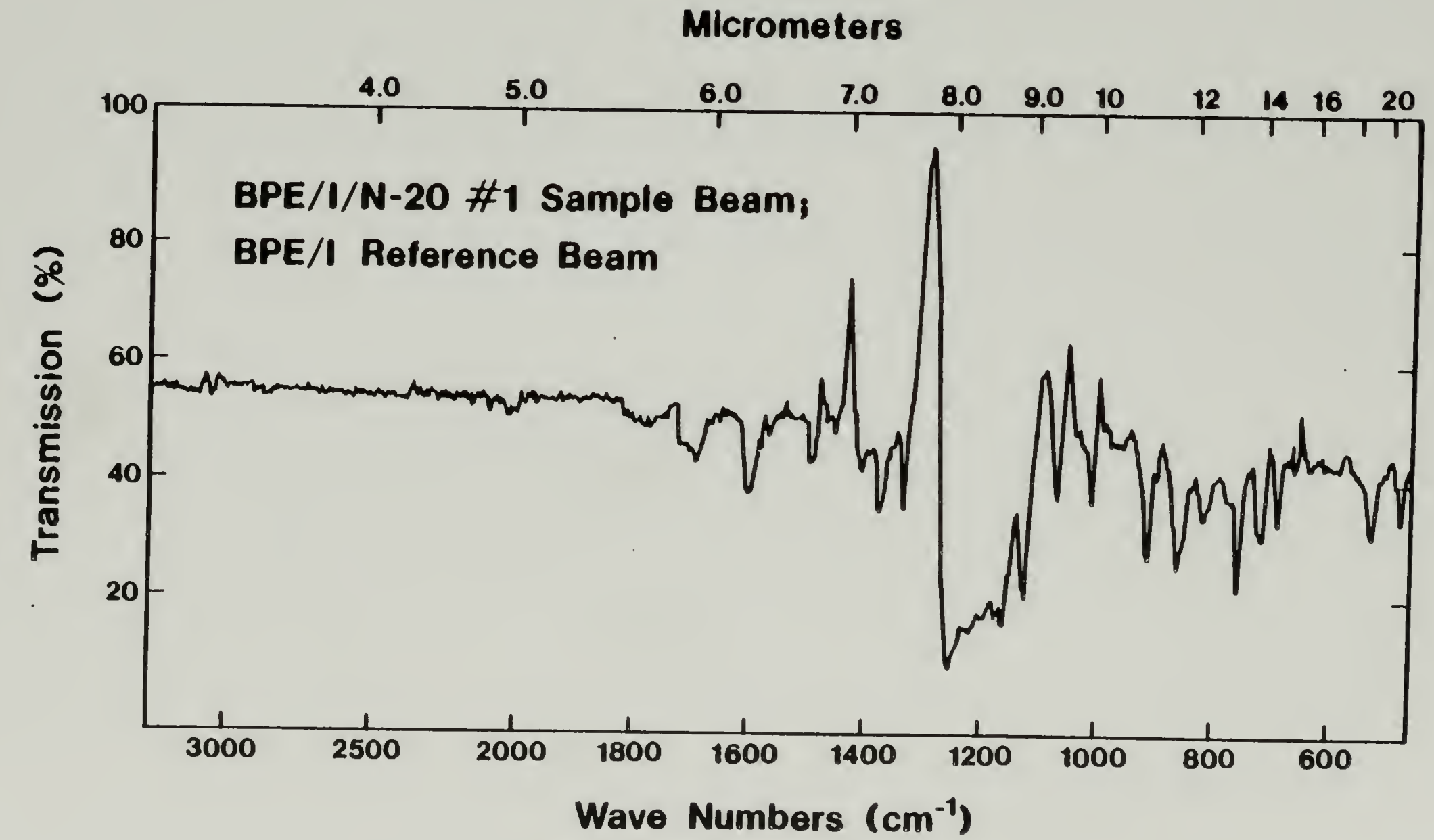

Fig. 37. Subtraction of the infrared spectrum of BPE/I from that of BPE/I/N-20 #1.

Table 4

Comparison of BPE/I and BPE/I/N-20
Infrared Absorbance Bands

Wavenumber cm^{-1}	BPE/I	BPE/I/N-20 #1 and #2
1435	Stronger	Weaker
1375	Absent	Present
1340	Absent	Present
1300	Stronger	Weaker
1130	Absent	Present
1100	Weaker	Stronger
1000	Present	Absent
960	Absent	Present
930	Weaker	Stronger
865	Weaker	Stronger
760	Weaker	Stronger
700	Weaker	Stronger
650	Present	Absent
475	Absent	Present

Further differentiation by IR would require a more refined approach, such as the use of model compounds to establish absorption coefficients for quantitation. Alternatively, the spectral subtraction approach could be facilitated through use of a computer-equipped FTIR capable of normalizing spectra from samples of different thickness. However, these avenues are more involved and did not appear to be justifiable for this project.

Carbon-Hydrogen-Oxygen Elemental Analyses

Polyester samples were submitted in the as-received conditions (powder or pellets) to the University of Massachusetts Microanalytical Laboratory for carbon, hydrogen, and oxygen (CHO) elemental analyses. Analytical methods consisted of sample pyrolysis, followed by quantitative analysis of gaseous products. The carbon and hydrogen analyses were performed in triplicate; the oxygen analyses were performed only once per sample. Results were compared with theoretical percentages of C,H, and O calculated from monomer repeat units, neglecting end groups (Table 5).

As expected, the BPE/I/N-20 copolyesters showed greater carbon content and lesser hydrogen content than the BPE/I homopolyester. Beyond this, the data are largely inconclusive. The compositions of the two copolyesters were thus indistinguishable, but this may be more a reflection of the limitation in experimental precision rather than a statement that the compositions are truly identical.

Table 5

Carbon-Hydrogen-Oxygen Elemental Analysis

	BPE/I		BPE/I/N-20 #1		BPE/I/N-20 #2	
	Theoretical	Experimental	Theoretical	Experimental	Theoretical	Experimental
Carbon, Wt %	76.73	76.69 ± 0.06	77.28	76.94 ± 0.20	77.28	76.93 ± 0.12
Hydrogen, Wt %	4.68	4.57 ± 0.04	4.66	4.53 ± 0.01	4.66	4.49 ± 0.01
Oxygen, Wt %	18.58	16.56	18.06	16.93	18.06	16.77
Total, Wt %	100.00	97.82	100.00	98.30	100.00	98.19

The CHO analyses appeared to be hampered by incomplete pyrolysis of the polyesters, as evidenced by the fact that measured elemental percentages were less than predicted. Poor combustibility for these polyesters should not be surprising, since the Monsanto patent claims excellent flame resistance as a key property (5). The data are presented here as a caution to future workers that the technique is limited with these polyesters.

^{1}H Nuclear Magnetic Resonance

Of the techniques chosen to study copolymer composition, ^{1}H nuclear magnetic resonance (NMR) proved to be the most successful for quantitation. Polyester samples were dissolved in 1,1,1,3,3,3-hexafluoro-2-propanol (HFIP) at concentrations of ~8% (wt./vol.). Due to the poor solubility of the highly crystalline as-received polyester powders and pellets, solutions were prepared from rheometer extrudates which were less crystalline. The extrudates had been collected at ~310-312°C and ~8 s^{-1}. NMR spectra for the neat HFIP solvent and the BPE/I, BPE/I/N-20 #1, and BPE/I/N-20 #2 solutions were recorded using a Varian T-60 instrument, as presented in Figures 38-41. Recordings were obtained using a sweep offset of 100 Hz relative to tetramethylsilane (TMS); that is, TMS resonates at a frequency of -100 Hz relative to the recorded spectra.

Peaks were assigned to the various protons in the polyesters using conventional methods for estimating chemical shifts, peak

intensities, and signal splitting. The assignments were later confirmed by comparison of the spectra with those of model compounds in the literature (40,41). Identification of the naphthalate and isophthalate peaks was simplified by contrasting the BPE/I and BPE/I/N-20 spectra. Peak assignments are identified in Table 6.

Mole fractions of the BPE, I, and N comonomer units in the polyesters were determined from integrated intensities of selected peaks. The peak labelled "a" (Figures 39-41) was used to quantify isophthalate content; peak "i" (Figures 40 and 41) was used for naphthalate; the multiplet of "d" plus "e" (Figures 39-41) was used for Bisphenol E. The ratios of peak areas a:i and a:(d+e) for the polyesters are compared with theoretical values in Table 6. These ratios were in turn used to compute the mole fractions of comonomers (X_I, X_N, X_{BPE}) by solving the following three equations in three unknowns:

$$\frac{X_I}{X_N} = 2\,\frac{(\text{Area of a})}{(\text{Area of i})} \qquad \text{---13}$$

$$\frac{X_I}{X_{BPE}} = 8\,\frac{(\text{Area of a})}{(\text{Area of d+e})} \qquad \text{---14}$$

$$X_I + X_N + X_{BPE} = 1 \qquad \text{---15}$$

Computed mole fractions are compared with the targeted polyester compositions in the three-component diagram of Figure 42.

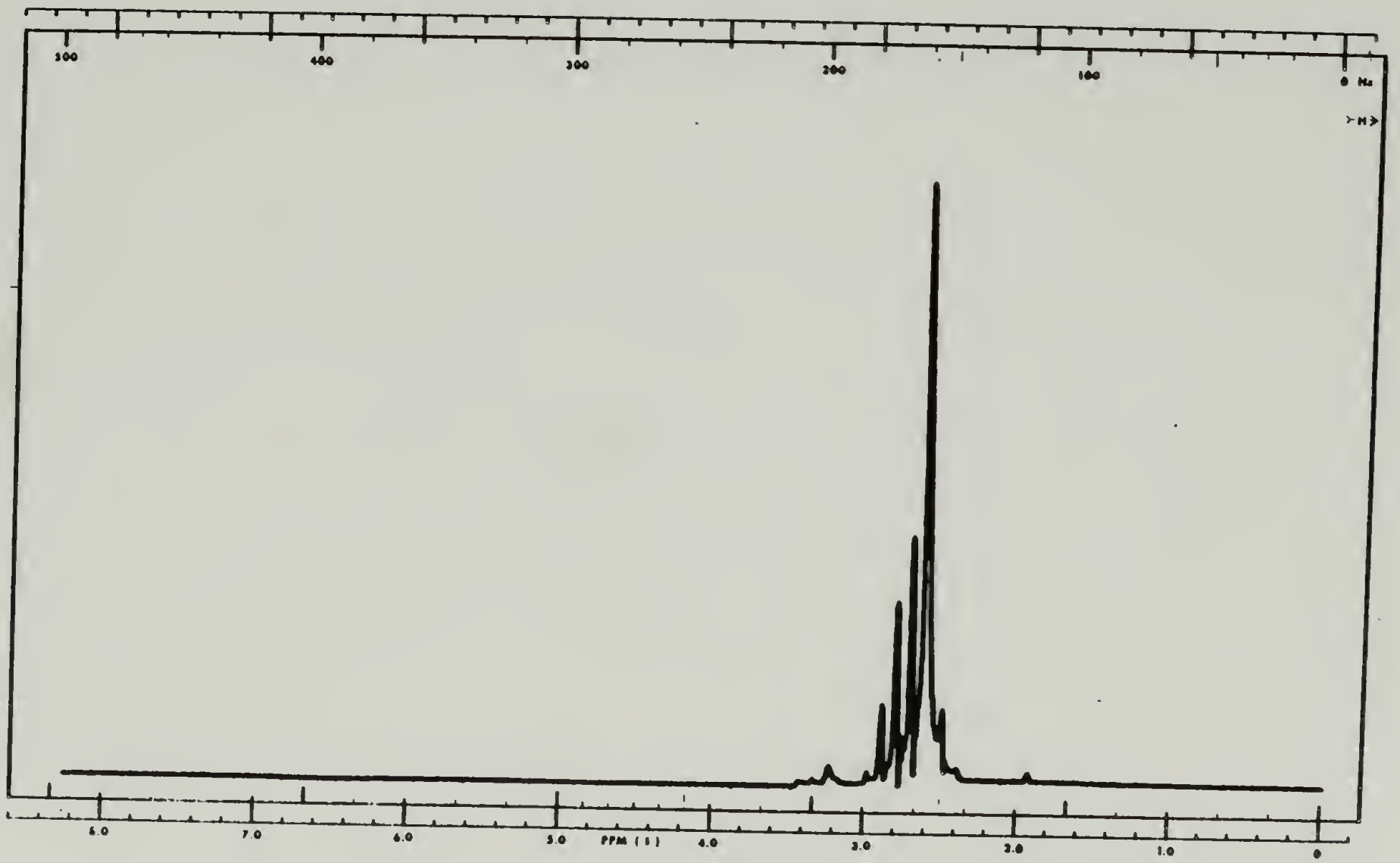

Fig. 38. ^{1}H NMR spectrum for 1,1,1,3,3,3-hexafluoroisopropanol (HFIP).

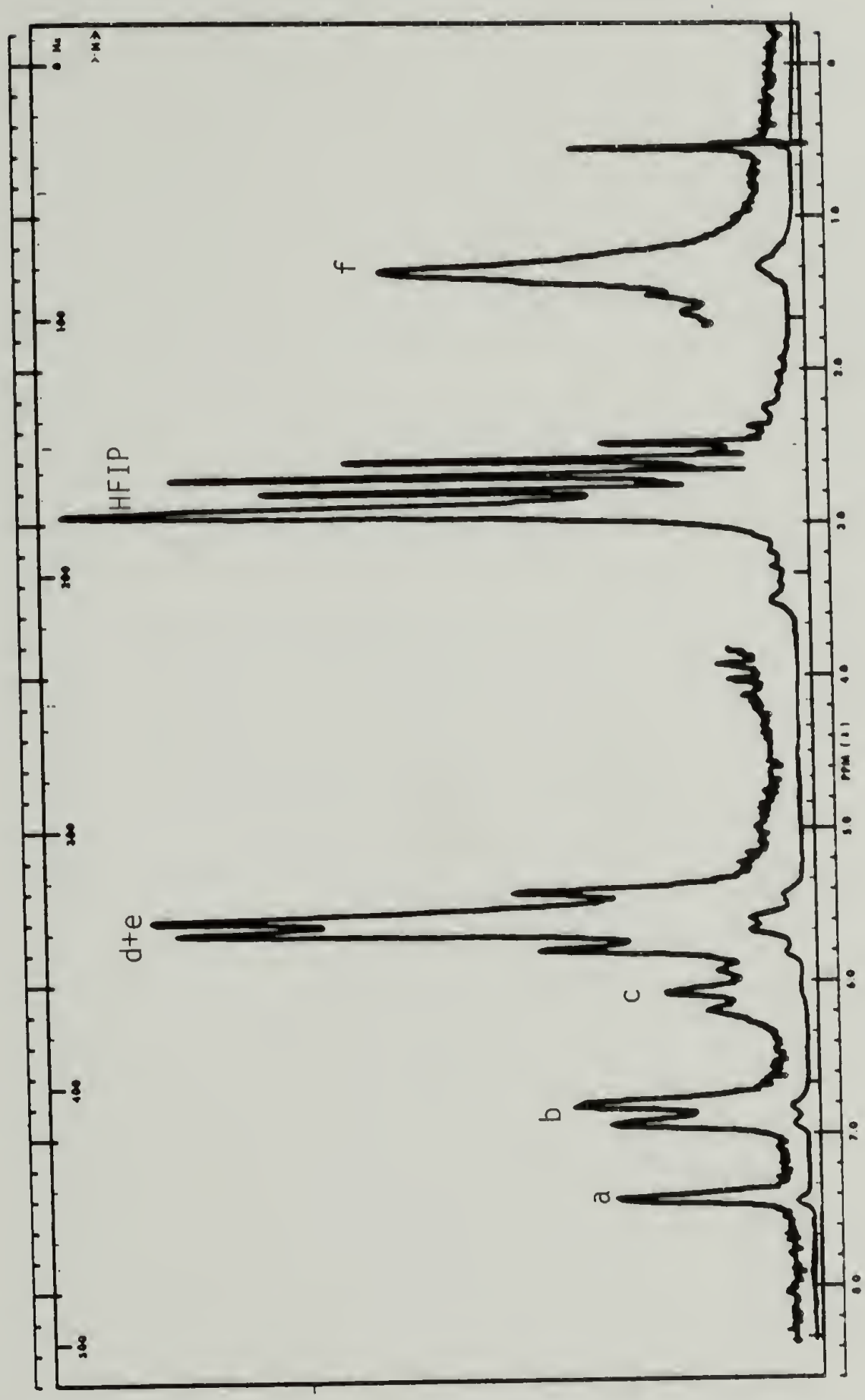

Fig. 39. ^1H NMR spectrum for BPE/I in HFIP.

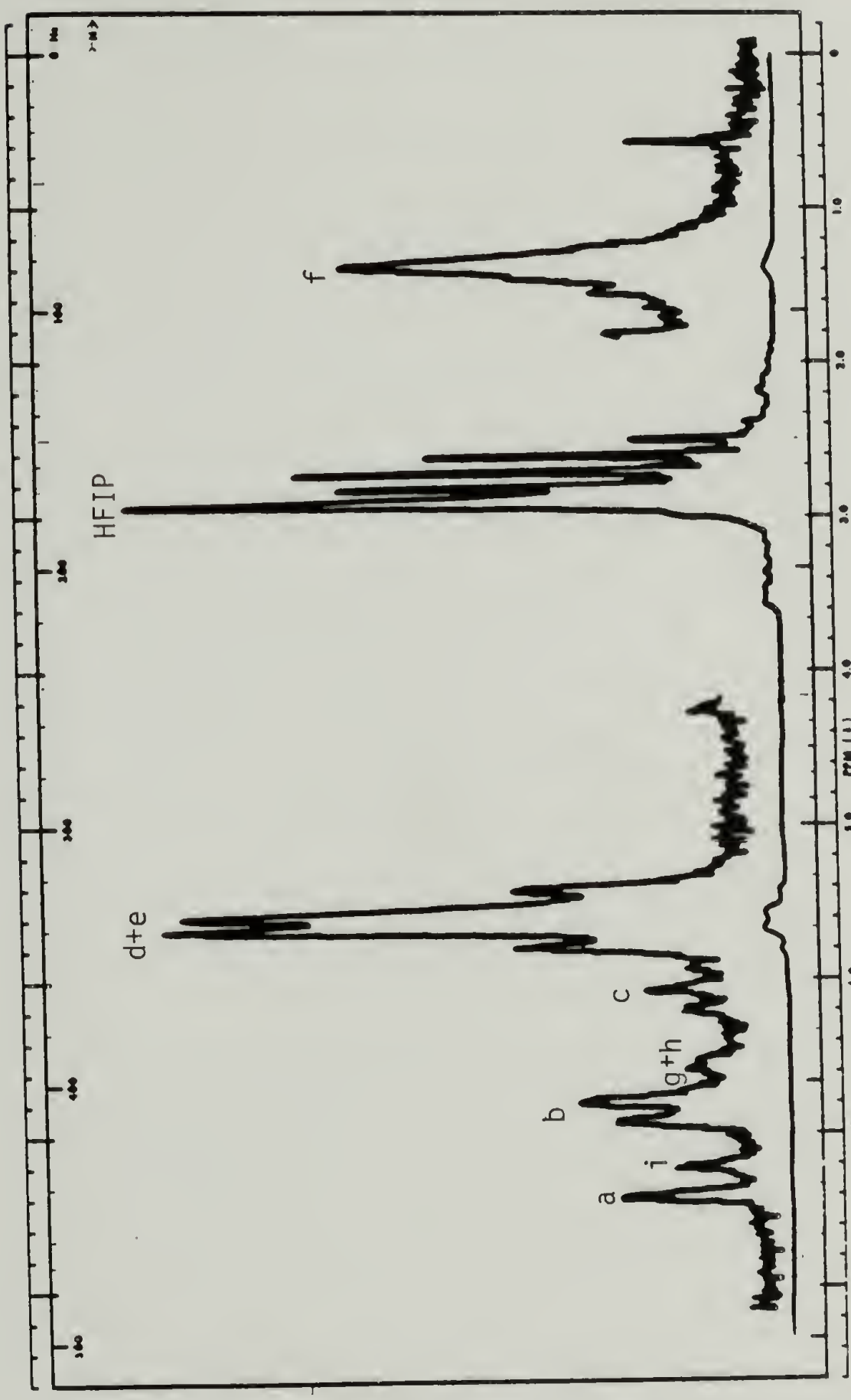

Fig. 40. ^{1}H NMR spectrum for BPE/I/N-20 #1 in HFIP.

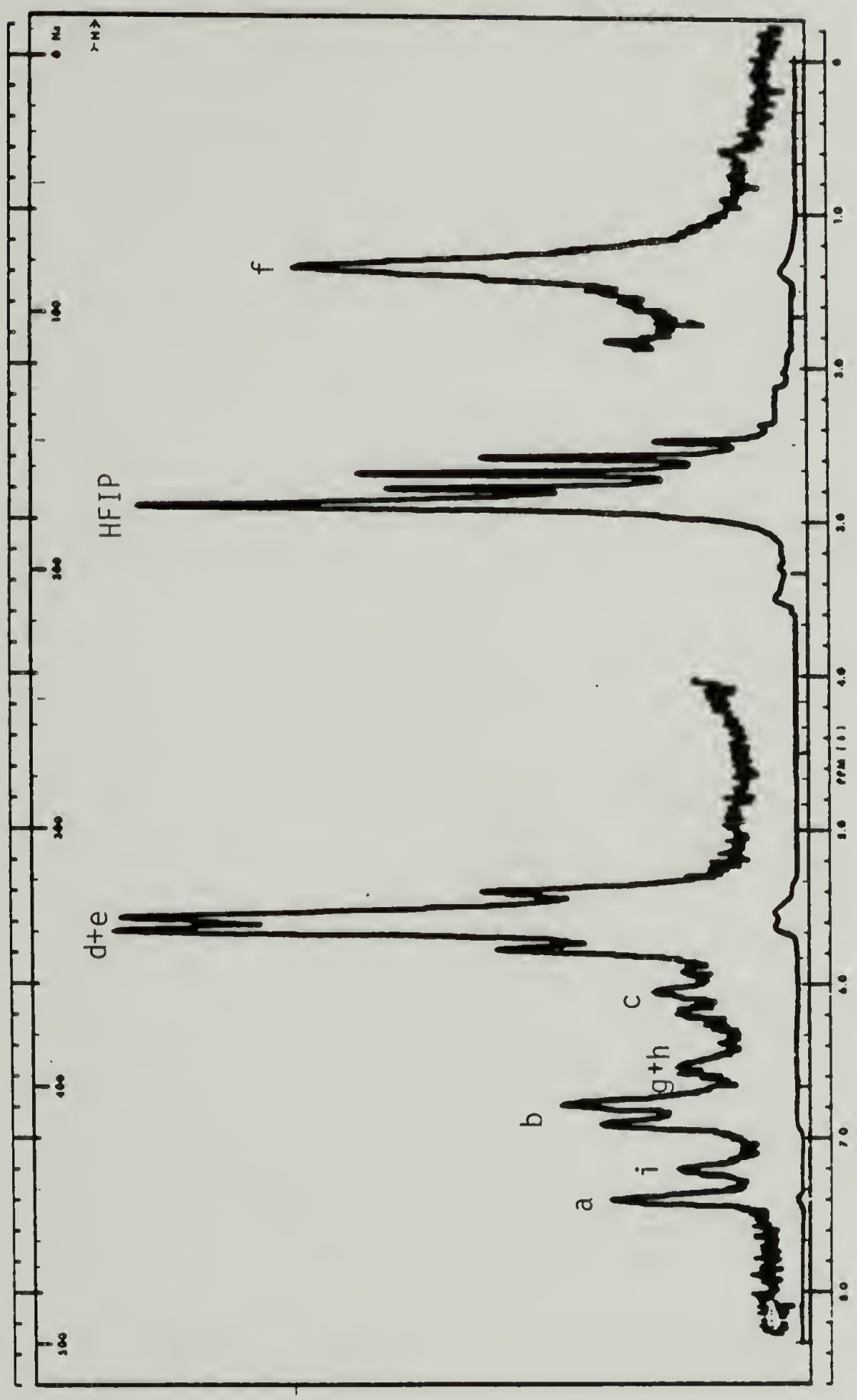

Fig. 41. ^{1}H NMR spectrum for BPE/I/N-20 #2 in HFIP.

Table 6

Relative Peak Intensities from NMR Quantitative Analysis of

Monomer Mole Fractions in the Polyesters

60 Hz ^1H

Ratios of Integrated* Peak Areas	BPE/I		BPE/I/N-20 #1		BPE/I/N-20 #2	
	Theoretical	Experimental	Theoretical	Experimental	Theoretical	Experimental
a : i	———	———	2.0	1.6 - 1.9	2.0	1.8 - 2.2
a : (d+e)	0.125	0.11	0.10	0.088-0.108	0.10	0.076-0.100
(a+b+c+g+h+i): (d+e)	0.50	0.43	0.55	0.51 - 0.56	0.55	0.52 - 0.55

*Peak assignments:

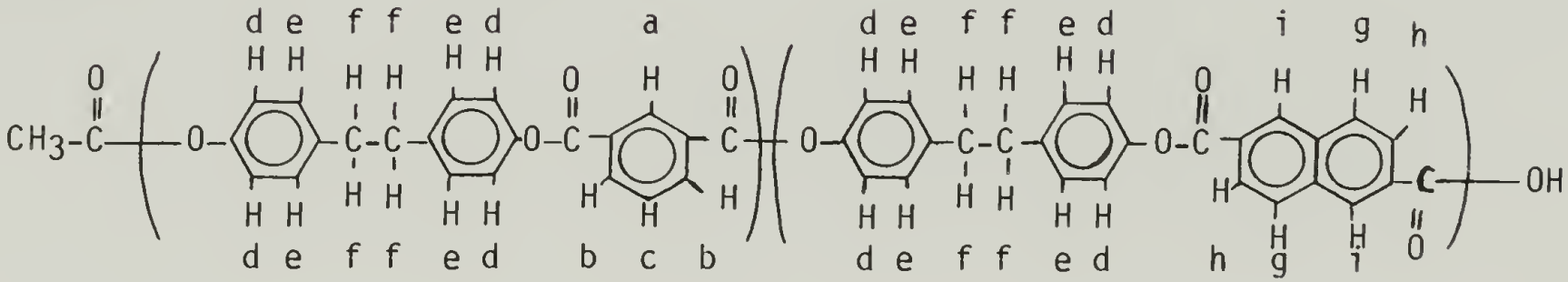

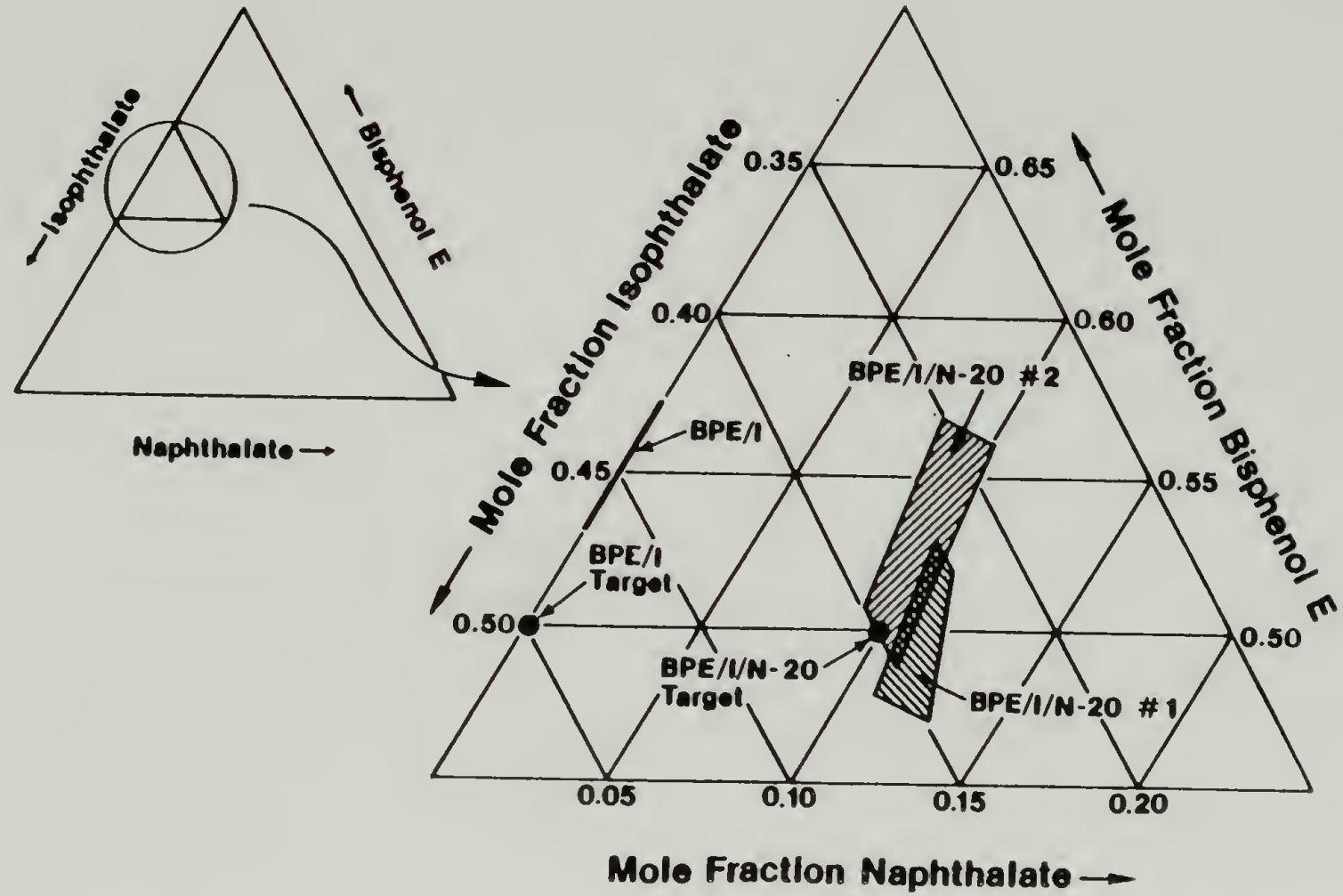

Fig. 42. Three-component compositional diagram for BPE/I, BPE/I/N-20 #1, and BPE/I/N-20 #2 (based upon ^{1}H NMR analyses).

Now, to answer the question: do the two BPE/I/N-20 copolyesters differ in composition? Within the uncertainty of the NMR measurements, they appear to be nearly identical, and very close to their targeted 50:40:10 molar ratio of BPE:I:N. Yet, there is an indication that sample #2 may contain slightly less naphthalate and slightly more Bisphenol E than sample #1. A reduced naphthalate content in sample #2 would be consistent with its observed higher viscosity vs sample #1. In addition, an elevated Bisphenol E content would explain the unexpectedly low inherent viscosity (η_{inh}) found for sample #2. That is, if the initial monomer mole fraction of BPE had differed from 0.50, there would not have been an exact molar equivalence of acid and alcohol groups during polymerization, and the potential degree of polymerization (η_{inh}) would have been limited. Hence, it is feasible that the BPE/I/N-20 polyesters do differ slightly in composition, with sample #2 having less naphthalate and more Bisphenol E than sample #1.

Conclusions

The two BPE/I/N-20 copolyesters appeared to be virtually indistinguishable in composition using the methods described here, though there was some indication via ^1H NMR that sample #2 could contain slightly more Bisphenol E and slightly less naphthalate than sample #1. If so, these compositional differences would be in a direction consistent with the observed differences in DSC, rheology, and η_{inh} between the two samples. Whether or not the magnitude of the differences would be sufficient to account for the DSC and rheological behavior is, however, questionable.

C H A P T E R VI

CRYSTALLINITY MEASUREMENTS BY WIDE-ANGLE X-RAY SCATTERING (WAXS)

Wide-angle x-ray scattering (WAXS) was used to determine the degree of crystallinity in selected polymer samples. Since the x-ray technique can, in principle, give an absolute measure of crystallinity, these samples could then be used as standards for subsequent determination of crystallinity in other samples by differential scanning calorimetry, a reference method.

Samples

Three samples were examined for crystallinity via WAXS: 1.) as-received BPE/I pellets, 2.) as-received BPE/I/N-20 #1 powder, and 3.) a BPE/I rheometer extrudate prepared at 320°C and 30 s^{-1} shear rate. The rheometer extrudate was used to clarify the position of amorphous scattering ("amorphous halo") for BPE/I, since the extrudate was less crystalline than the as-received pellets. The amorphous scattering for BPE/I/N-20 #1 was approximated by comparison with that from the BPE/I samples, since scattering patterns for the two polymers were similar.

Oriented samples could not be analyzed via the available WAXS techniques. The BPE/I extrudate did not appear to be significantly oriented, judging by flat-film photographs of the x-ray scattering

using a Statton camera (Chapter VIII). However, most (if not all) of the BPE/I/N-20 #1 extrudates exhibited significant axial orientation, and could not be examined for crystallinity via WAXS.

Special sample holders were required to support the powder and pellet samples, since the available holder was designed to accommodate films. The powder and pellets were contained in thin-walled glass capillaries[a] (0.01 mm wall thickness x 1.5 mm diameter x 8 cm length) which were, in turn, fastened to rectangular cardboard windows before mounting in the test apparatus. The BPE/I rheometer extrudate did not require a glass capillary, but was supported on a cardboard holder.

The BPE/I/N-20 #2 polymer was not examined via WAXS, since it was presumed that its crystal structure would be similar to that of the BPE/I/N-20 #1, and that the crystallinity of BPE/I/N-20 #2 could be calculated later by comparison of the enthalpies-of-transition for the two copolymers from differential scanning calorimetry.

Experimental

The intensity of x-ray scattering as a function of 2Θ scattering angle was detected using a Siemens D-500 wide-angle x-ray diffractometer. Samples were mounted vertically and probed in the transmission mode using a slit beam geometry. Data scans were obtained for both the sample and background using a Siemac V microprocessor. Subsequent analyses were facilitated by computer software available

a. Purchased from Charles Supper Company, 15 Tech Circle, Natick, MA 01760.

within Prof. R.S. Stein's area of the Materials Research Laboratory, University of Massachusetts. The computer programs corrected for polarization, absorption, Lorentz, background, and incoherent scattering, and provided tabulated data in the form of Ruland-corrected intensity (42,43), Is^2, as a function of scattering vector, s.

Plots of Is^2 vs s were obtained by computer. The location of crystalline and amorphous peaks were estimated visually. The weight fraction of crystals, x_c, in each sample was computed from the area fraction under the crystalline peaks using the conventional expression for a simple two-phase model (43):

$$x_C = \frac{\int_0^\infty Is^2 \, ds \text{ (crystal)}}{\int_0^\infty Is^2 \, ds \text{ (total)}} \qquad \text{---16}$$

$$= \frac{\text{area under crystalline peaks}}{\text{area under total scattering curve}}$$

Results

Data from WAXS scans of the three samples have been plotted in two forms: 1.) uncorrected intensities as a function of scattering angle (Figures 43-45), and 2.) Ruland-corrected intensities, Is^2, as a function of scattering vector, s (Figures 46-48). The dashed lines in Figures 43-45 designate the intensities of measured background scattering, while the dashed lines in Figures 46-48 give subjective estimates of the locations of the amorphous scattering from the

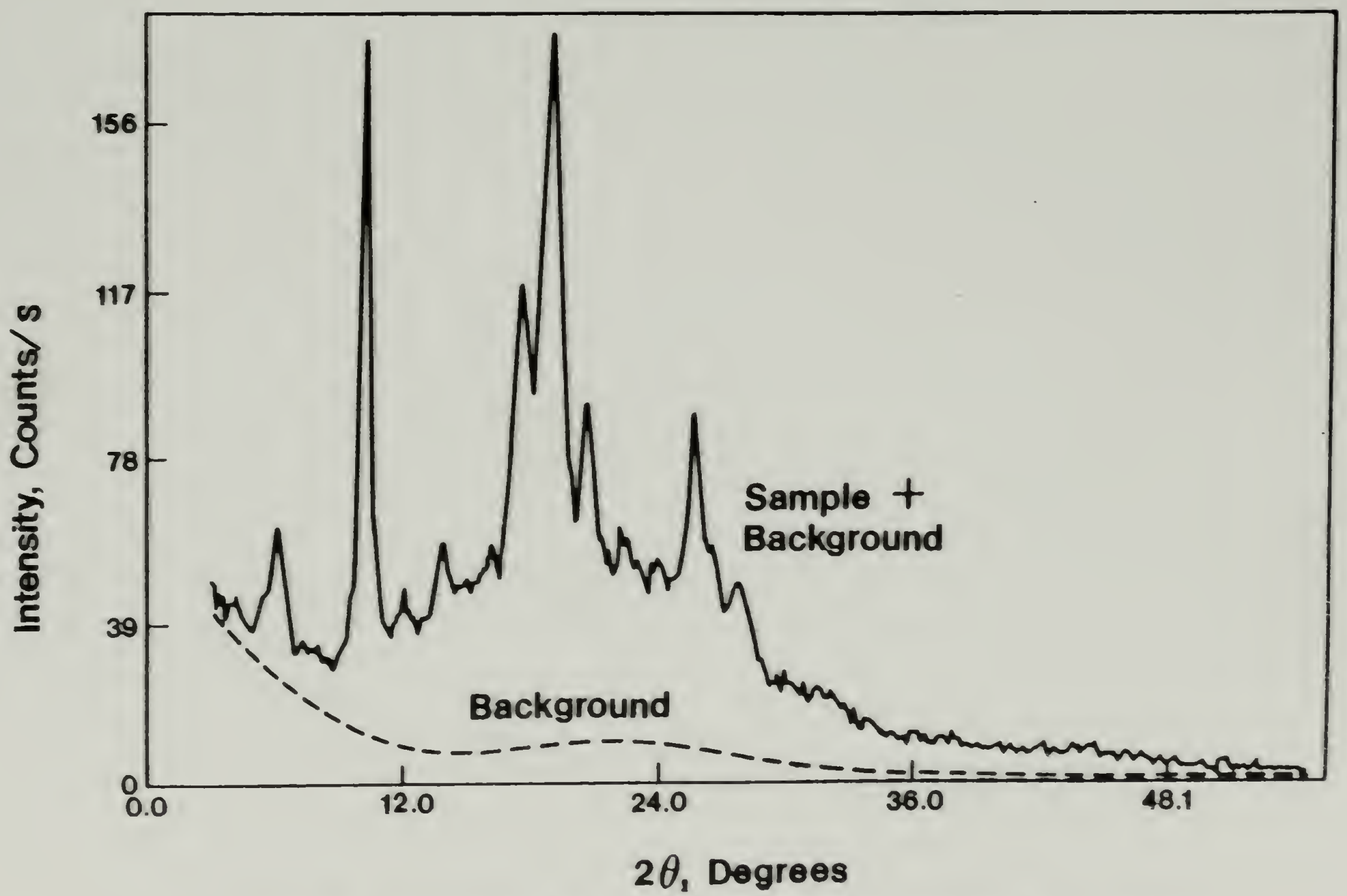

Fig. 43. Uncorrected WAXS intensities for as-received BPE/I pellets.

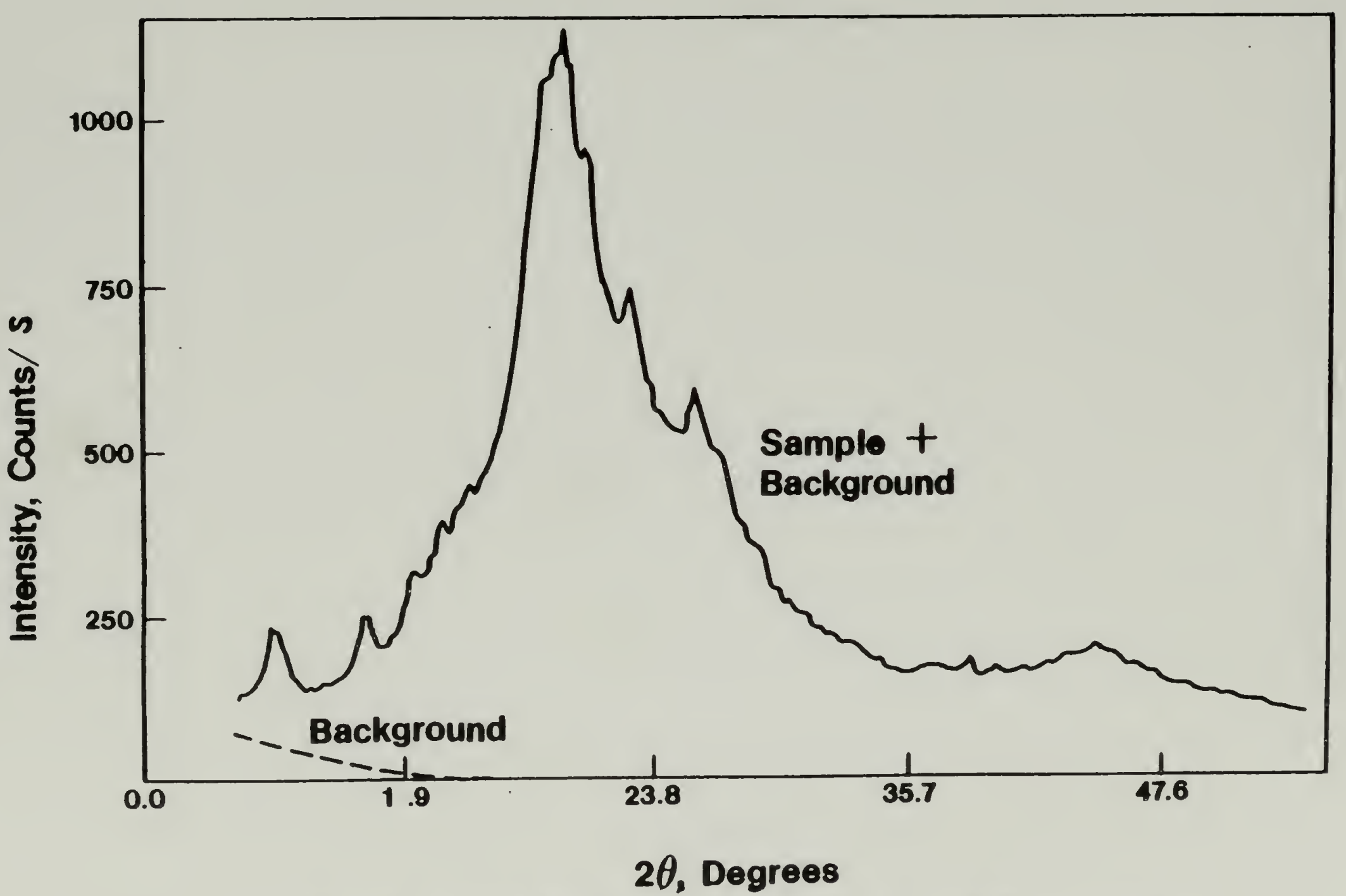

Fig. 44. Uncorrected WAXS intensities for a BPE/I rheometer extrudate.

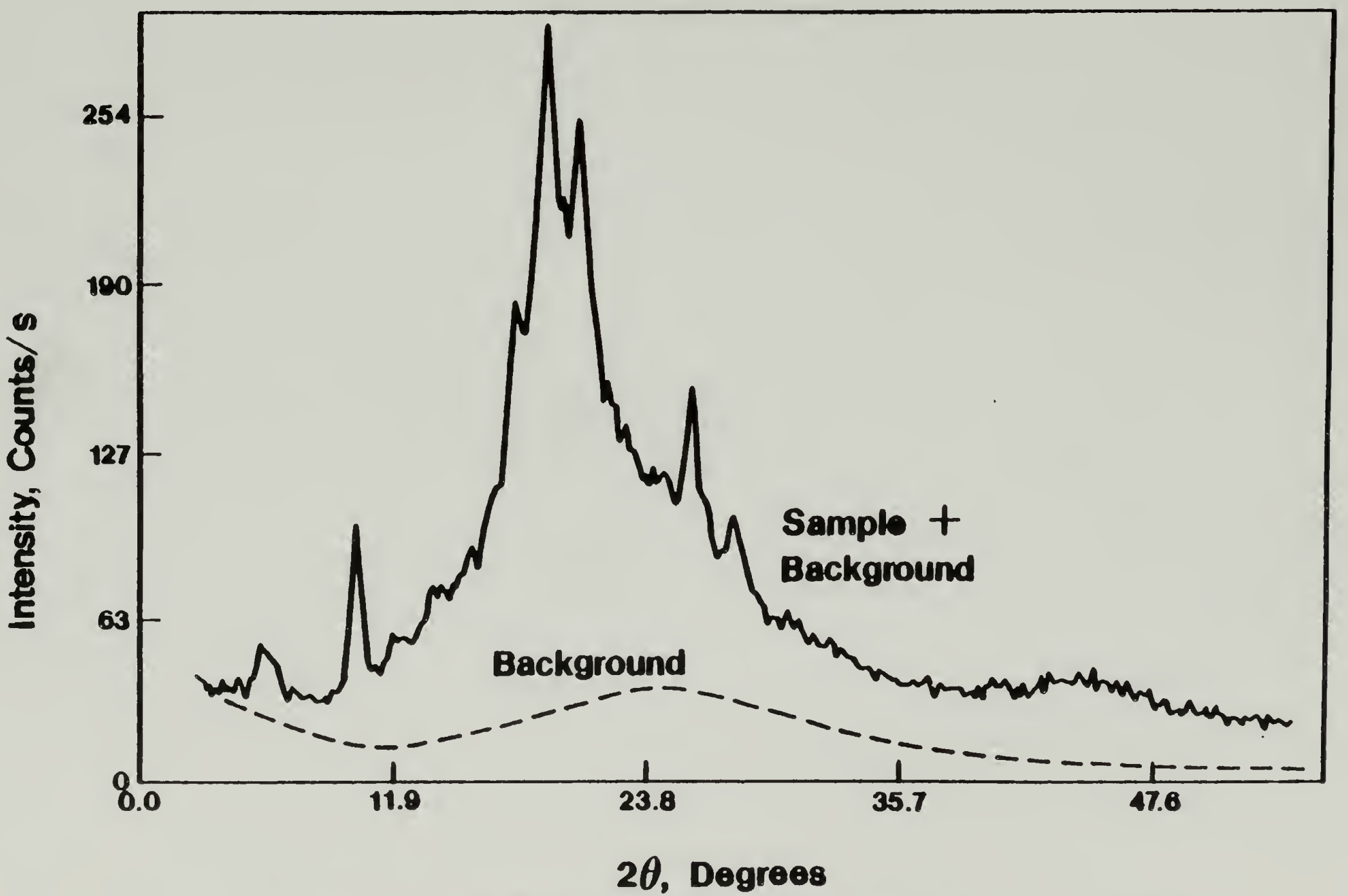

Fig. 45. Uncorrected WAXS intensities for as-received BPE/I/N-20 #1 powder.

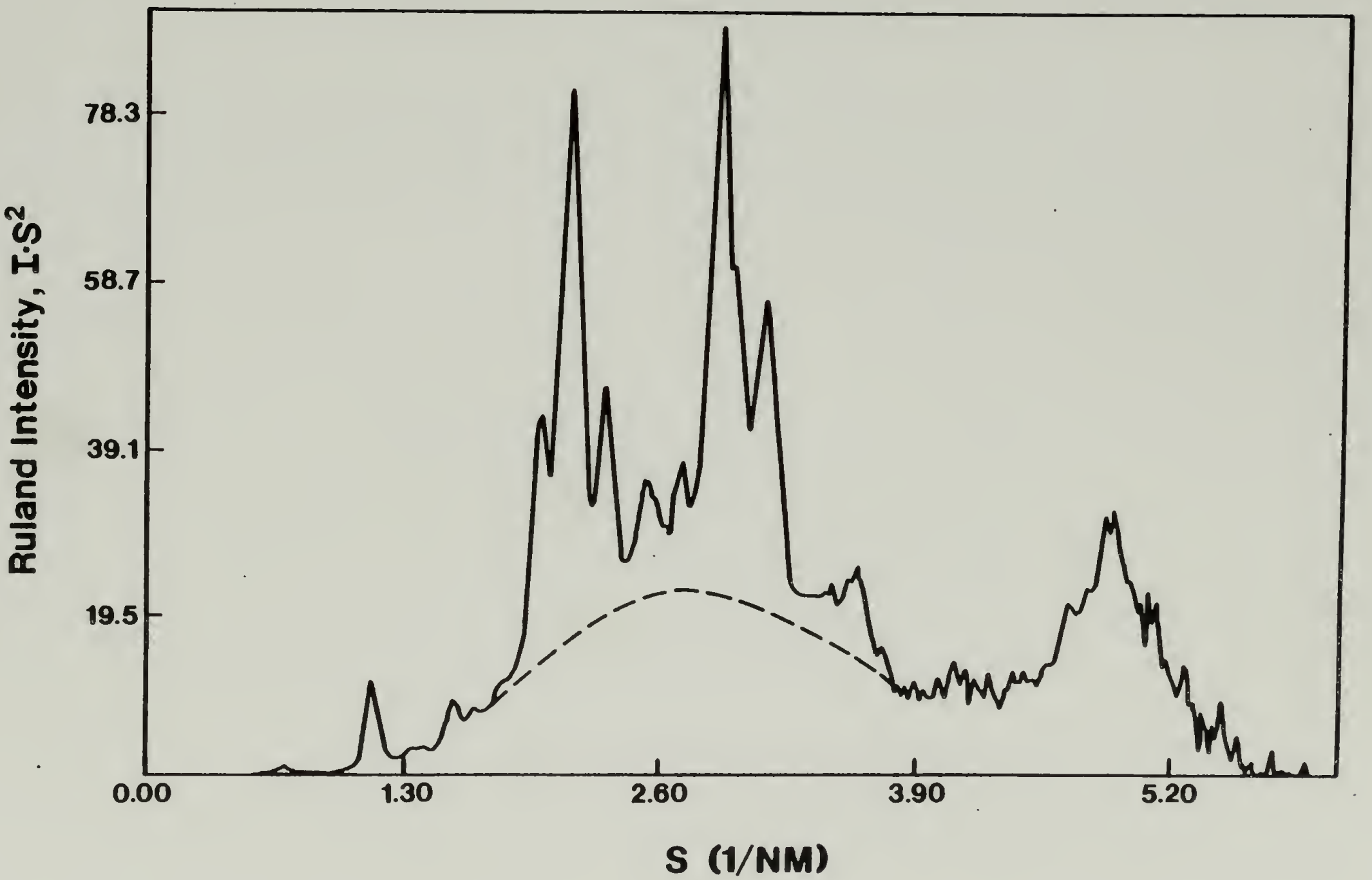

Fig. 46. Ruland-corrected WAXS intensities for as-received BPE/I pellets.

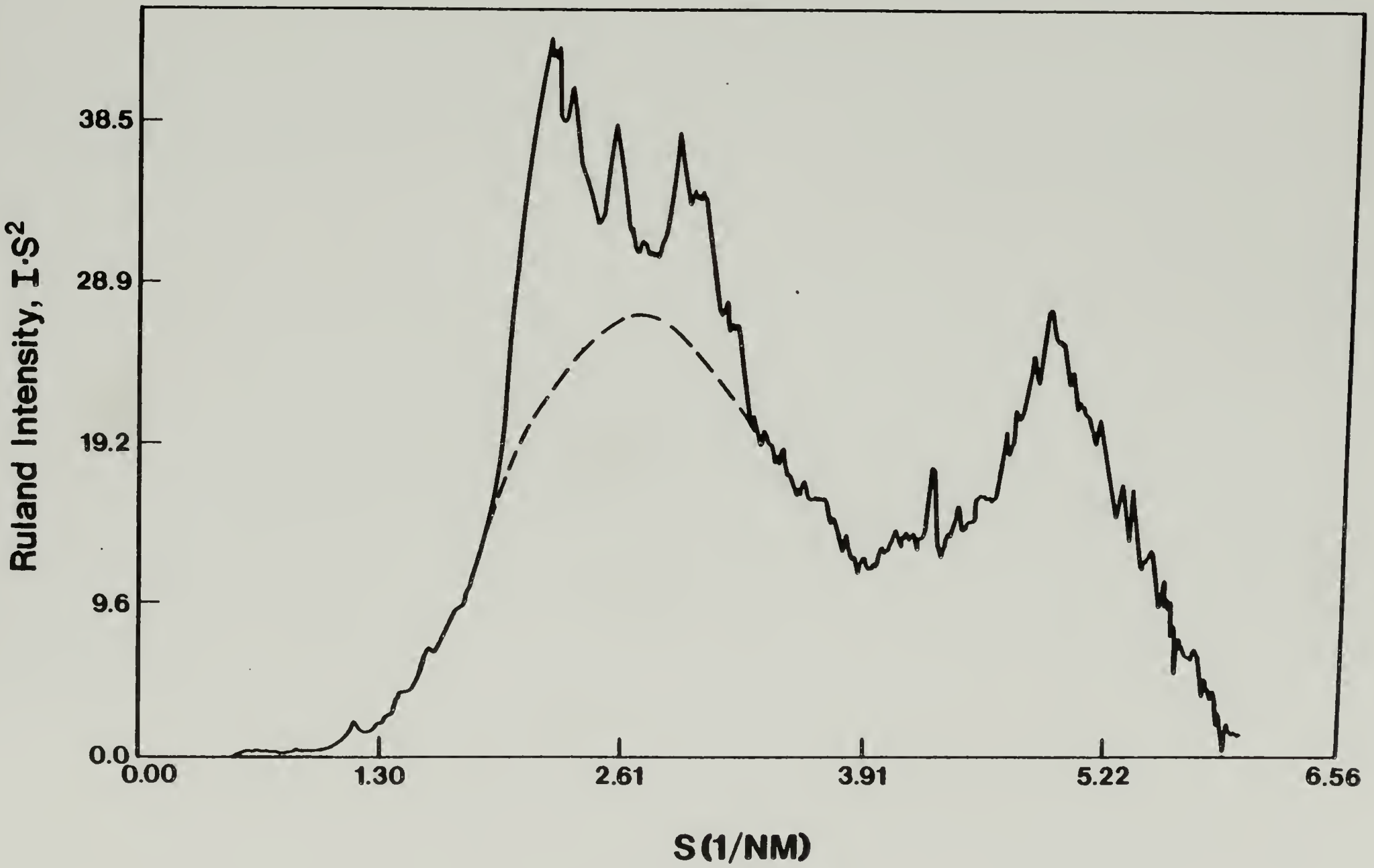

Fig. 47. Ruland-corrected WAXS intensities for a BPE/I rheometer extrudate.

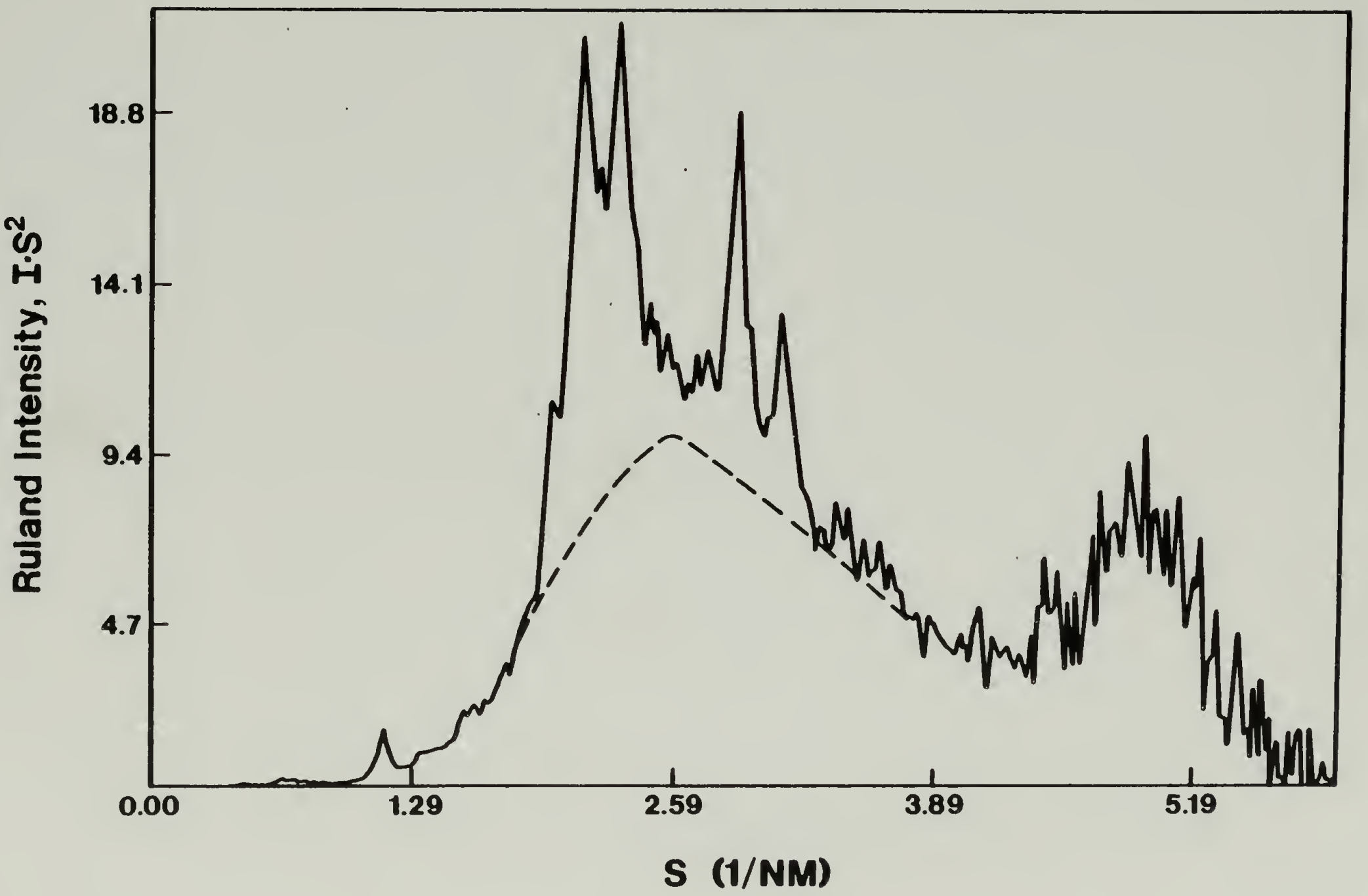

Fig. 48. Ruland-corrected WAXS intensities for as-received BPE/I/N-20 #1 powder.

polyesters. The areas above the dashed lines, but below the solid lines, in Figures 46-48 have been assigned to scattering from the crystalline regions in the polymers.

The relative areas under the crystalline and total scattering were measured by the cutting-and-weighing technique. The weight fraction of crystals, x_c, in each of the three samples was then computed using Equation 16. Results are listed in Table 7.

Clearly, the as-received BPE/I pellets were the most crystalline of the three samples. The pellets possessed a rather high degree of crystallinity as a result of the annealing which accompanies solid-state polymerization. Note that the BPE/I rheometer extrudate reached a degree-of-crystallinity less than half that of the original BPE/I pellets.

The BPE/I/N-20 #1 powder was less crystalline than the BPE/I pellets by ~37%, although the two polyesters had been subjected to similar heat histories by solid-state polymerization. This suggests that BPE/I/N-20 #1 may not crystallize as readily as BPE/I.

No attempts were made to elucidate crystal structures or sizes from the WAXS data, although the location of peaks in the scattering patterns suggest that the type(s) of crystals in the BPE/I and BPE/I/N-20 #1 may be the same. This would not be surprising, since 90 mole % of the BPE/I/N-20 #1 has the same chemical composition as BPE/I.

No unusual peaks were detected in the BPE/I/N-20 #1 vs BPE/I which might have pin-pointed scattering from the naphthyl groups.

Table 7

Results of X-ray Crystallinity Measurements

Sample	Weight Fraction of Crystals, x_c, (gm crystal/gm polymer)
BPE/I pellets, as-received	38
BPE/I rheometer extrudate	15
BPE/I/N-20 #1 powder, as-received	24
BPE/I/N-20 #1 rheometer extrudate	Not measured, due to anisotropic scattering

CHAPTER VII

DIFFERENTIAL SCANNING CALORIMETRY

Experimental

Instrumentation. Thermal analyses of the polyesters were accomplished using a Perkin-Elmer DSC-2 differential scanning calorimeter equipped with a Thermal Analysis Data Station (TADS). The TADS is a microprocessor which facilitates collection and analysis of DSC data, and provides for storage on floppy discs. Special features of the TADS which were used included 1.) automatic subtraction of a pre-recorded baseline, 2.) normalization of data on a per-unit-weight basis, 3.) adjustment of slope, when necessary, 4.) expansion of the temperature scale, as desired, 5.) expansion or contraction of the y scale, as desired, and 6.) integration of peak areas for enthalpies-of-transition.

For each test, ~10 mg of sample were weighed to ± 0.02 mg, placed in an aluminum DSC sample pan, fitted with a cover, and crimped. Tests were performed with a purge of nitrogen gas through the sample cell, and with an empty pan-plus-cover in the reference side of the cell. The temperatures and transition enthalpies were calibrated with indium and lead standards.

Heating Studies. Thermograms were obtained at heating rates of 5, 10, 20, (40), and 80°C/min over the range 40-400°C for BPE/I,

BPE/I/N-20 #1, and BPE/I/N-20 #2 as received polyesters (pellets and powders). These are shown in Figures 49-51.

The magnitudes of all curves within a given figure may be directly compared, since the data were normalized on a per-unit-weight basis. However, the BPE/I/N-20 figures were plotted at a higher sensitivity than the BPE/I, so the magnitudes of peaks in different figures should not be visually compared.

Transition temperatures and enthalpies as a function of heating rate are listed in Table 8. Also included are values extrapolated to a heating rate of 0° C/min.

Transition Enthalpies for Pure Crystals. Unless the transition enthalpy for a pure crystal is known, differential scanning calorimetry, by itself, gives only the relative degree of crystallinity among samples having the same crystalline composition. However, if the crystallinity of a given sample has been determined by an absolute method (such as x-ray), then the absolute crystallinities of other samples may be found by comparison:

$$X_c = \Delta H \, (X_{c,Ref}/\Delta H_{Ref})$$
$$= \Delta H/\Delta H_{crystal} \qquad \text{---17}$$

X_c and $X_{c,Ref}$ represent the weight fractions of crystal in the sample of interest and the reference, gm crystal/gm polymer; ΔH and ΔH_{Ref} are the enthalpies for the crystalline transitions in the sample and

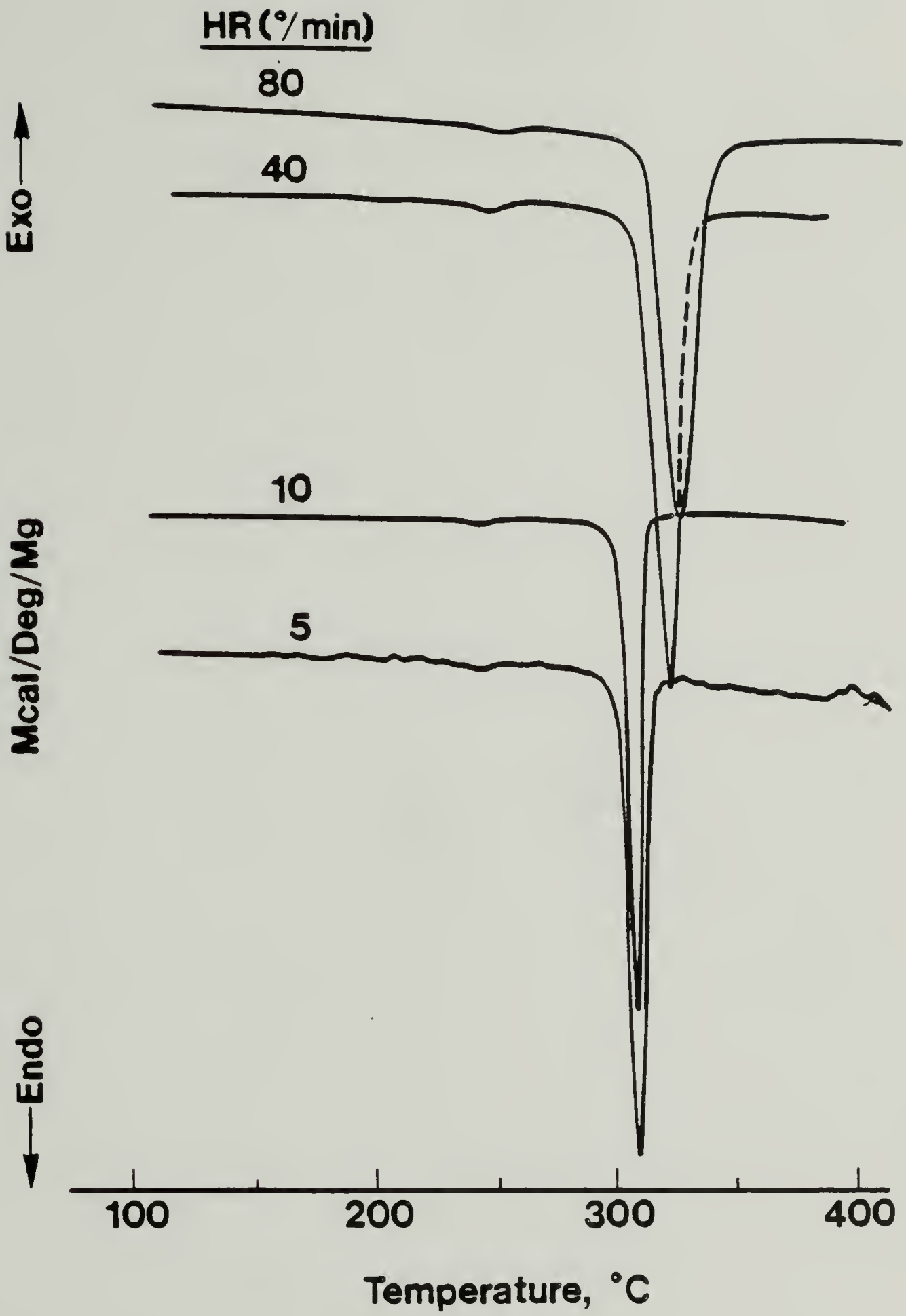

Fig. 49. DSC temperature scans for BPE/I at various heating rates.

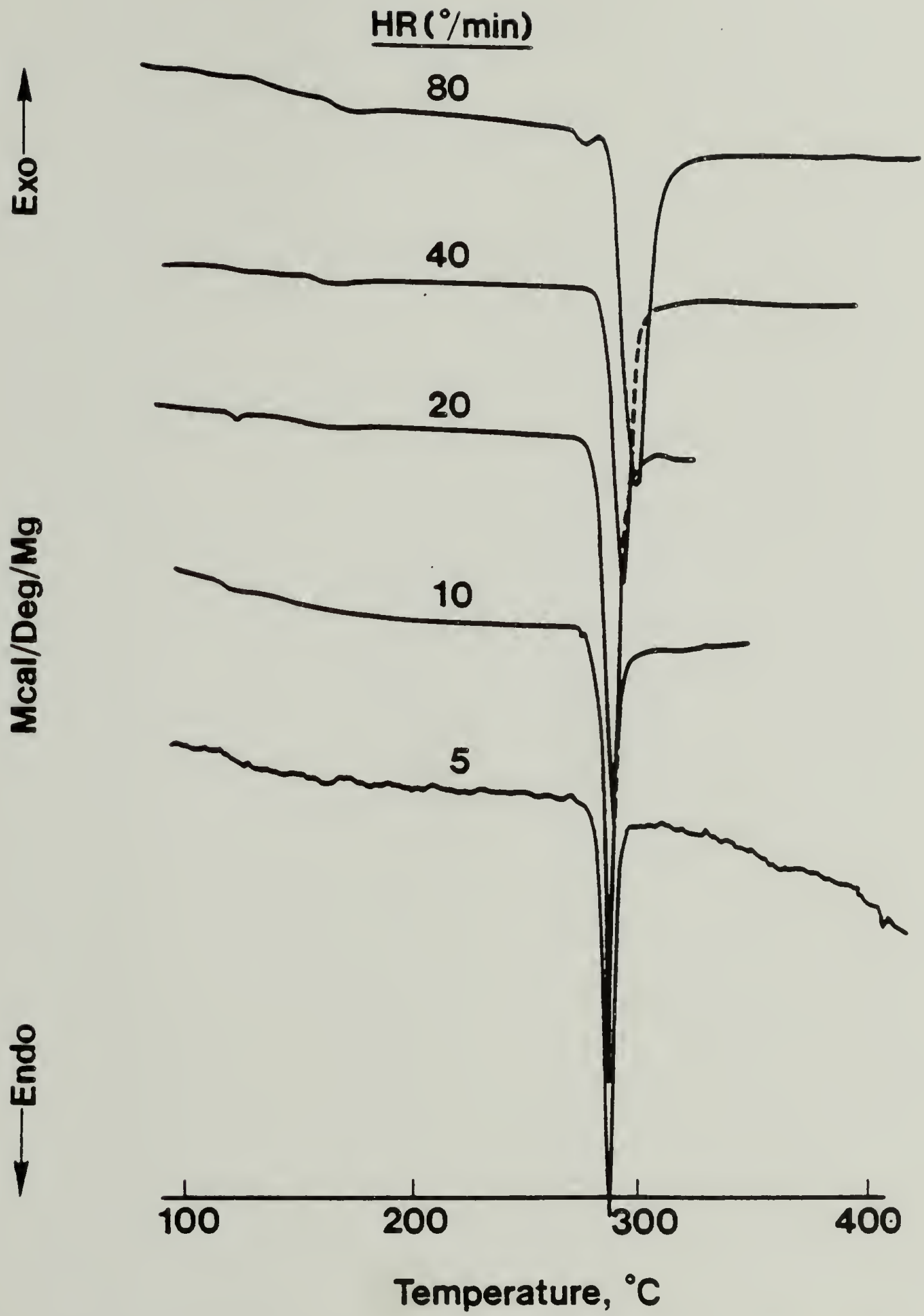

Fig. 50. DSC temperature scans for BPE/I/N-20 #1 at various heating rates.

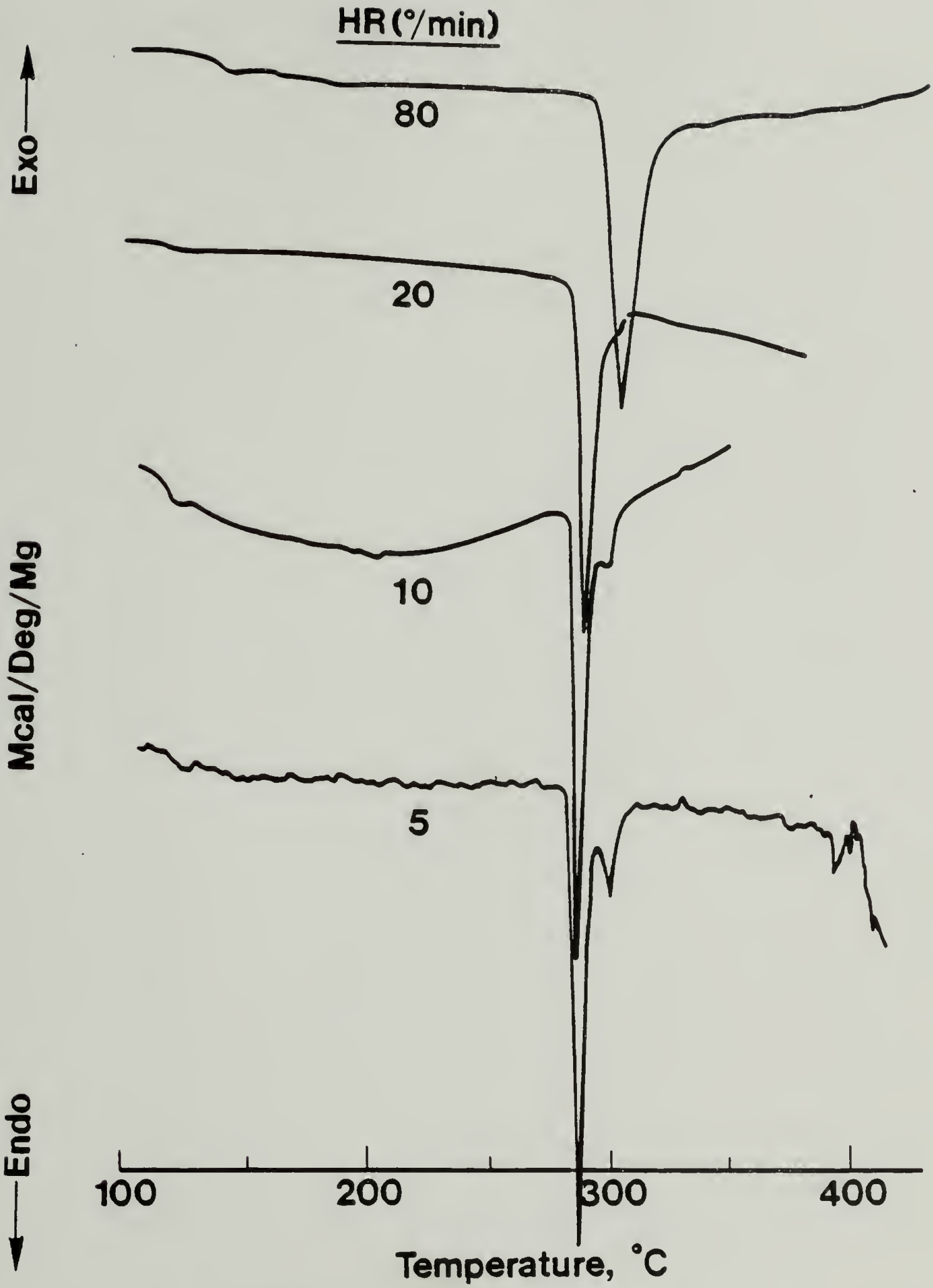

Fig. 51. DSC temperature scans for BPE/I/N-20 #2 at various heating rates.

Table 8

Results of DSC Heating Rate Studies

	BPE/I	BPE/I/N-20 #1	BPE/I/N-20 #2
T_g onset, °C			
Heating rate, °C/min:			
80	240	127,167	118,178
40	227	119,157	117,174
20	---	110,(147?)	111,(187?)
10	220	114	115,(187?)
5	210	117	110
0 (extrapolated)	~214	~110-120	~111
T_M or $T_{C\rightarrow N}$ peaks, °C			
Heating rate, °C/min:			
80	331	301	302
40	326	294	294
20	---	287	288,(300)
10	310	287	286,300
5	310	286	286,305
0 (extrapolated)	310	286	286,310
ΔH_m or $\Delta H_{C\rightarrow N}$ cal/gm polymer			
Heating rate, °C/min:			
80	17.8	7.9	7.7
40	16.8	6.6	7.4
20	----	6.1	5.0
10	17.2	6.4	5.4
5	17.1	5.0	5.3
0 (extrapolated)	~17.	~5.3	~5.3

reference, cal/gm polymer; $\Delta H_{crystal}$ is the enthalpy for the crystalline transition of a pure crystal, cal/gm crystal.

As described in Chapter VI, wide-angle x-ray scattering was used to determine the weight percent crystallinity for three polyester samples. These were: 38% for BPE/I pellets (as-received), 24% for BPE/I/N-20 #1 powder (as-received), and 15% for a BPE/I rheometer extrudate. DSC transition enthalpies (ΔH_m or $\Delta H_{C \rightarrow N}$) were determined for these samples, as ΔH_m = 17 cal/gm polymer, $\Delta H_{C \rightarrow N}$ = 5.3 cal/gm polymer, and ΔH_m = 7.1 cal/gm polymer, respectively. In Figure 52, these enthalpies have been plotted versus weight fraction crystallinity, X_c. The slopes of the lines extrapolated to the origin give the transition enthalpies per gram of pure crystal, $\Delta H_{crystal}$. The data suggest that $\Delta H_{crystal} \simeq 46$ cal/gm crystal for BPE/I and $\Delta H_{crystal} \simeq 22$ cal/gm crystal for BPE/I/N-20 #1. If one assumes that BPE/I/N-20 #2 has similar crystalline structure and composition to BPE/I/N-20 #1, then a value of $\Delta H_{crystal} \simeq 22$ cal/gm crystal may also be assigned to BPE/I/N-20 #2.

Melting, Cooling, Reheating. The effect of melting, followed by cooling at different rates, on thermal properties was examined via the following procedure. Samples of as-received polyesters were first heated rapidly to 610K (~337°C) and held isothermally for 5 min. Each sample was then cooled at a preselected rate (5, 10, 20, or 80°C/min), followed by reheating at 20°C/min. The resulting thermograms are shown in Figures 53-55. Again, curves within each figure are normalized. The transition

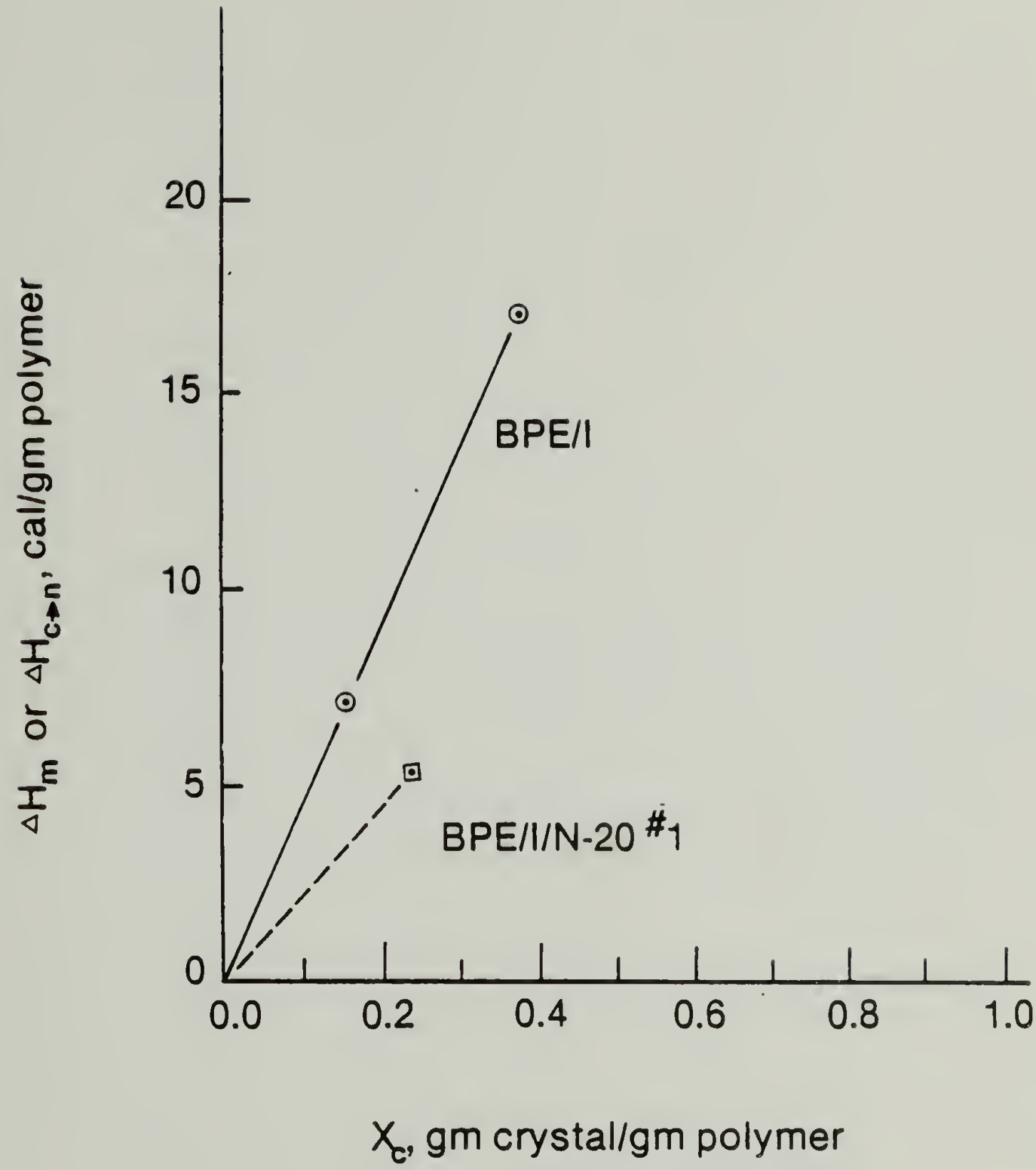

Fig. 52. DSC transition enthalpies vs crystalline weight fraction from wide-angle x-ray scattering.

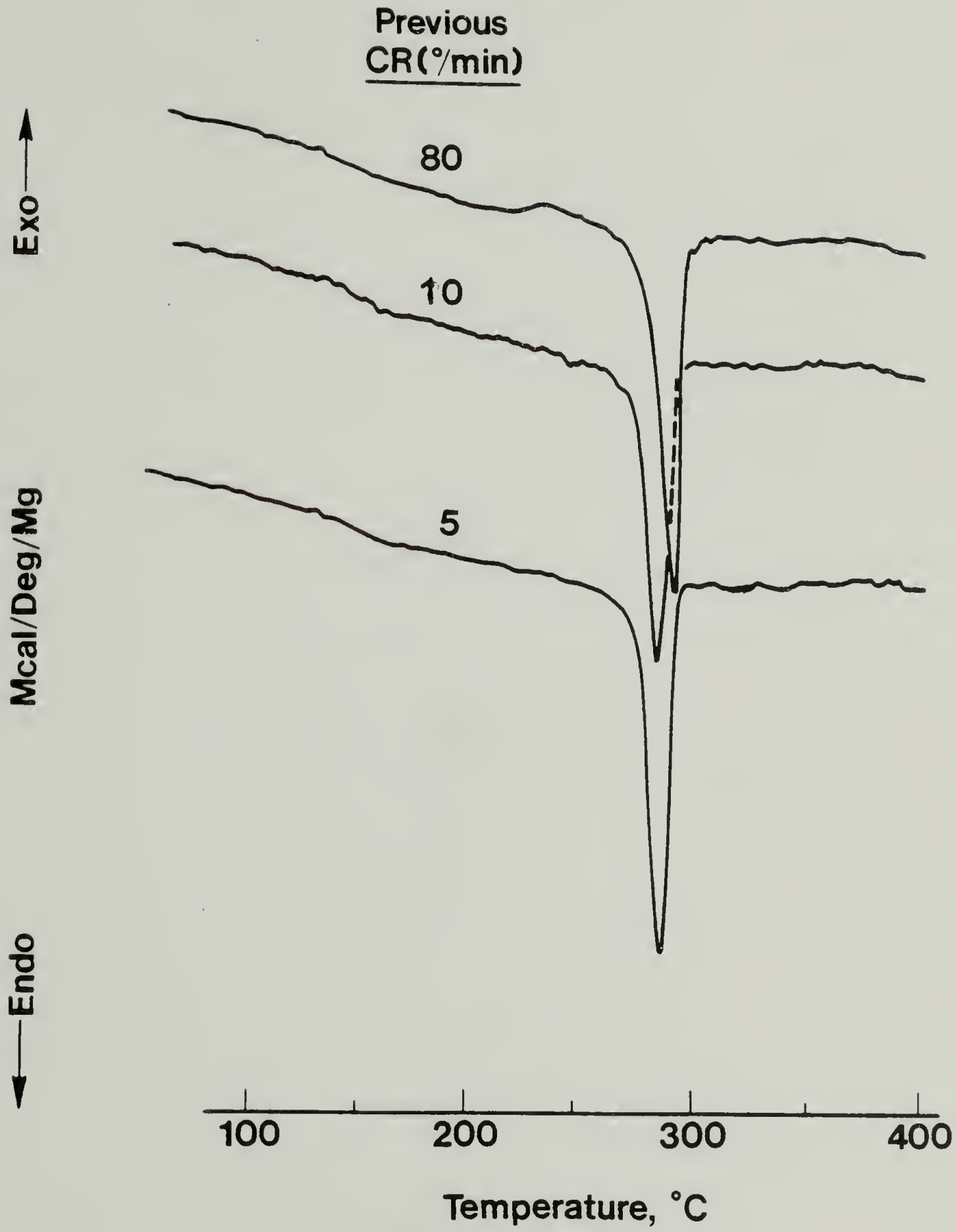

Fig. 53. DSC temperature scans of BPE/I after cooling from the melt at various rates (Heating rate 20^{o}C/min.).

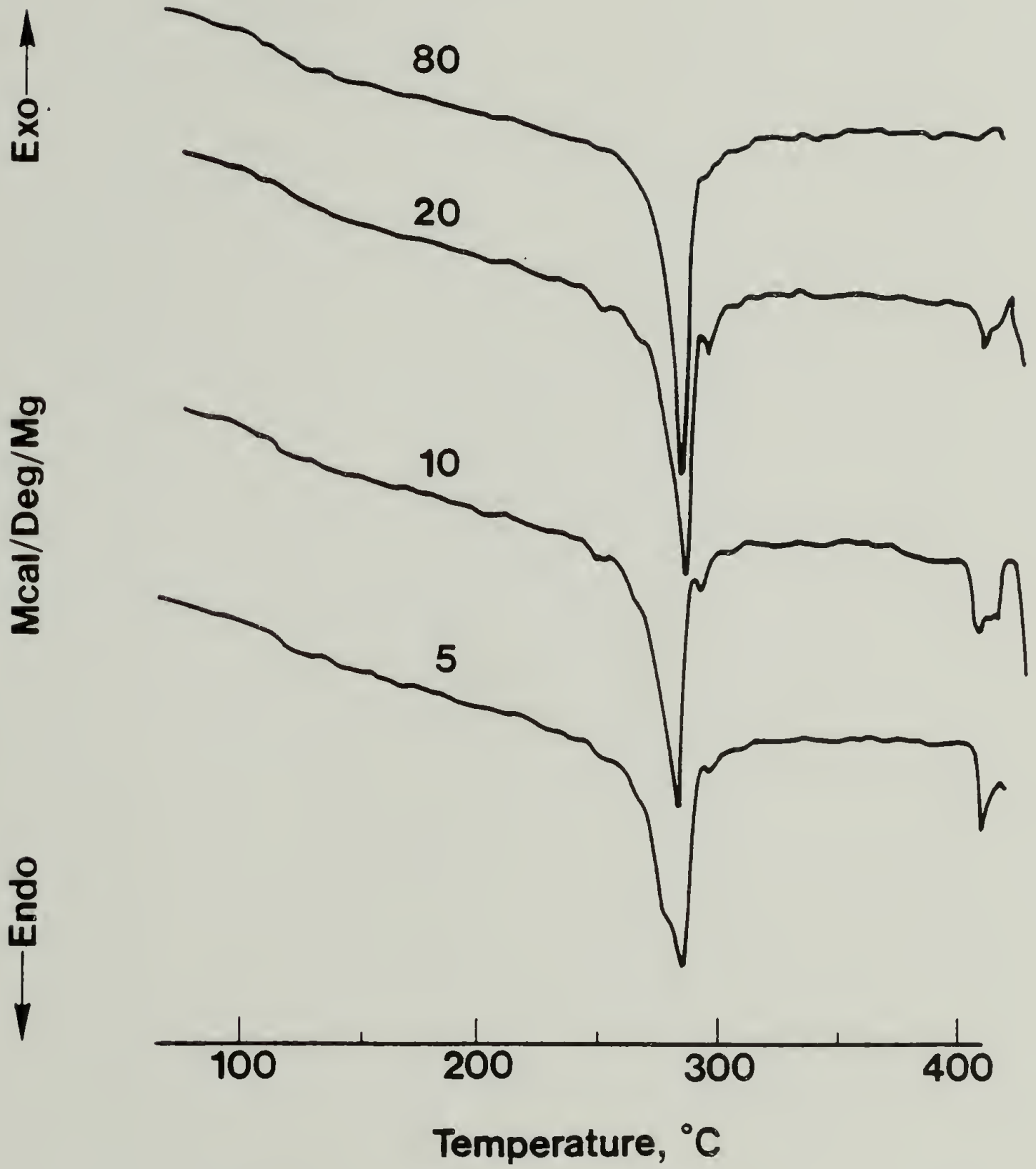

Fig. 54. DSC temperature scans of BPE/I/N-20 #1 after cooling from the melt at various rates (Heating rate 20°C/min.).

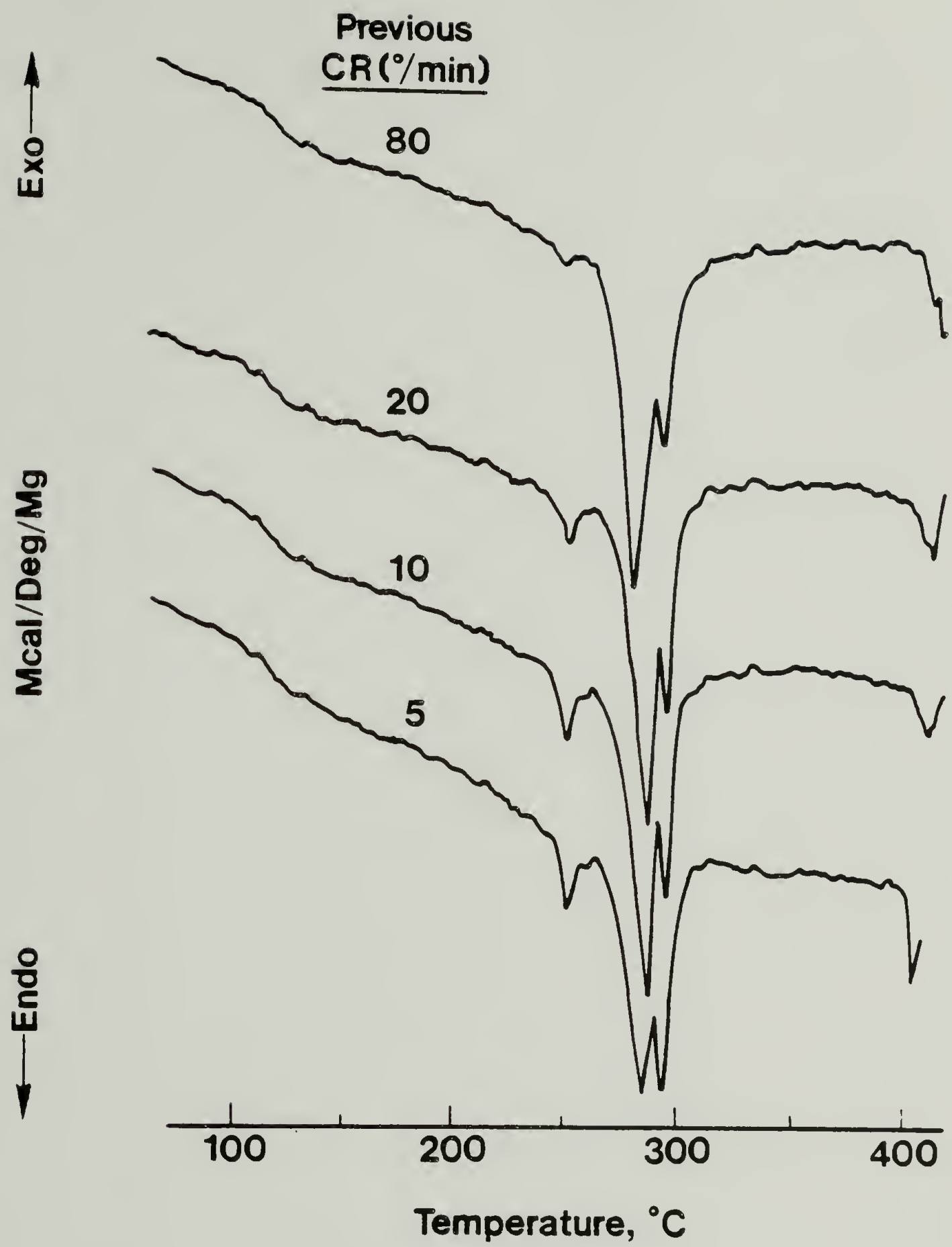

Fig. 55. DSC temperature scans of BPE/I/N-20 #2 after cooling from the melt at various rates (Heating rate 20°C/min.).

Table 9

The Effect of Previous Cooling Rate on DSC Properties*

	BPE/I	BPE/I/N-20 #1	BPE/I/N-20 #2
Tg onset, °C			
Previous cooling rate °C/min:			
80	130	102	110
20	137	106	110
10	136	110	110
5	137	113	110
Tm and $T_{C\rightarrow N}$ peaks, °C			
Previous cooling rate °C/min:			
80	294	284	247,280,292
20	290	(245),284,(293)	249,286,292
10	286	(249),284,(293)	250 286,295
5	289,(324)	(250),284,(295)	249,284,293
ΔH_m and $\Delta H_{C\rightarrow N}$, cal/gm polymer			
Previous cooling rate °C/min:			
80	7.2	4.3	4.0
20	6.5	4.0	3.7
10	6.9	4.0	3.6
5	7.5,(0.2)	4.0	3.3
Crystallinity, Wt%			
Previous cooling rate °C/min:			
80	16	20	18
20	14	18	17
10	15	18	16
5	17	18	15

*Heating rate 20 °C/min.

temperature, enthalpies, and estimated % crystallinities are recorded in Table 9.

Rheometer Extrudates. DSC heating scans of selected rheometer extrudates were performed to examine the effect of extrusion upon the crystallinity and the transition temperatures of the polyesters. Scans were obtained at a heating rate of 10 °C/min. The extrudates were all collected at $\dot{\gamma}$ = 30 s^{-1}, and at different extrusion temperatures. The resulting thermograms are compared to those of the original pellets/powders in Figures 56-58. The location of the extrusion temperature for each extrudate has been marked with an arrow, and curves within each figure have again been normalized on a per-unit-weight basis. The corresponding transition temperatures, enthalpies, and estimated % crystallinities are listed in Table 10.

Interpretation

Heating and Cooling Studies. Upon first heating the as-received polyesters, the BPE/I exhibited a higher glass transition temperature (T_g), higher melting point (T_m), larger enthalpy of fusion (ΔH_m), and greater weight fraction crystallinity (X_c) than the corresponding properties of the BPE/I/N-20 copolyesters (Figs. 49-51 and Table 8). However, these differences appear to have been largely artifacts of solid-state polymerization. After melting, cooling, and reheating, the characteristics of the three polyesters were much more similar (Figs. 53-55 and Table 9). The main endothermic peaks occurred at

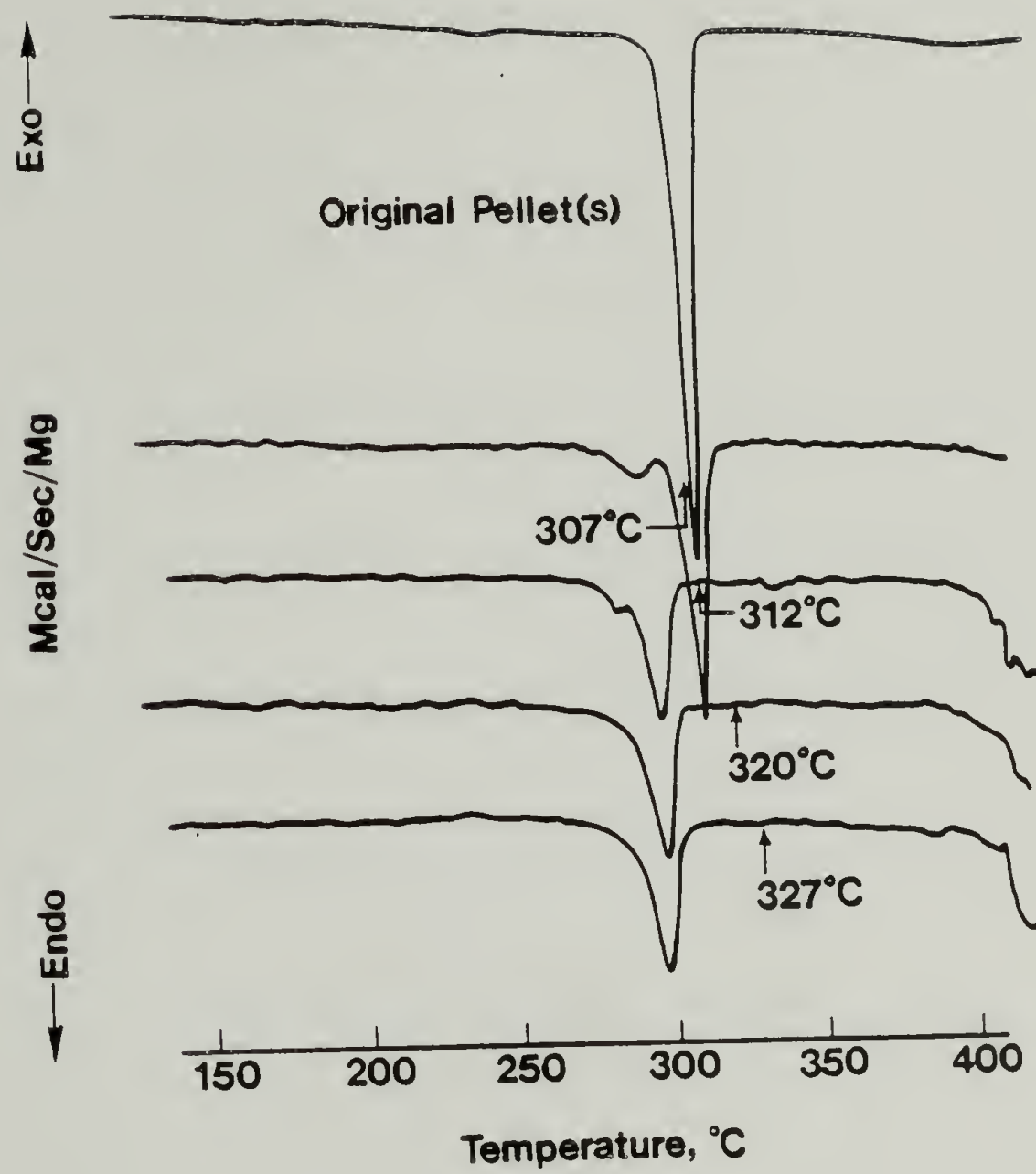

Fig. 56. DSC temperature scans of BPE/I rheometer extrudates.

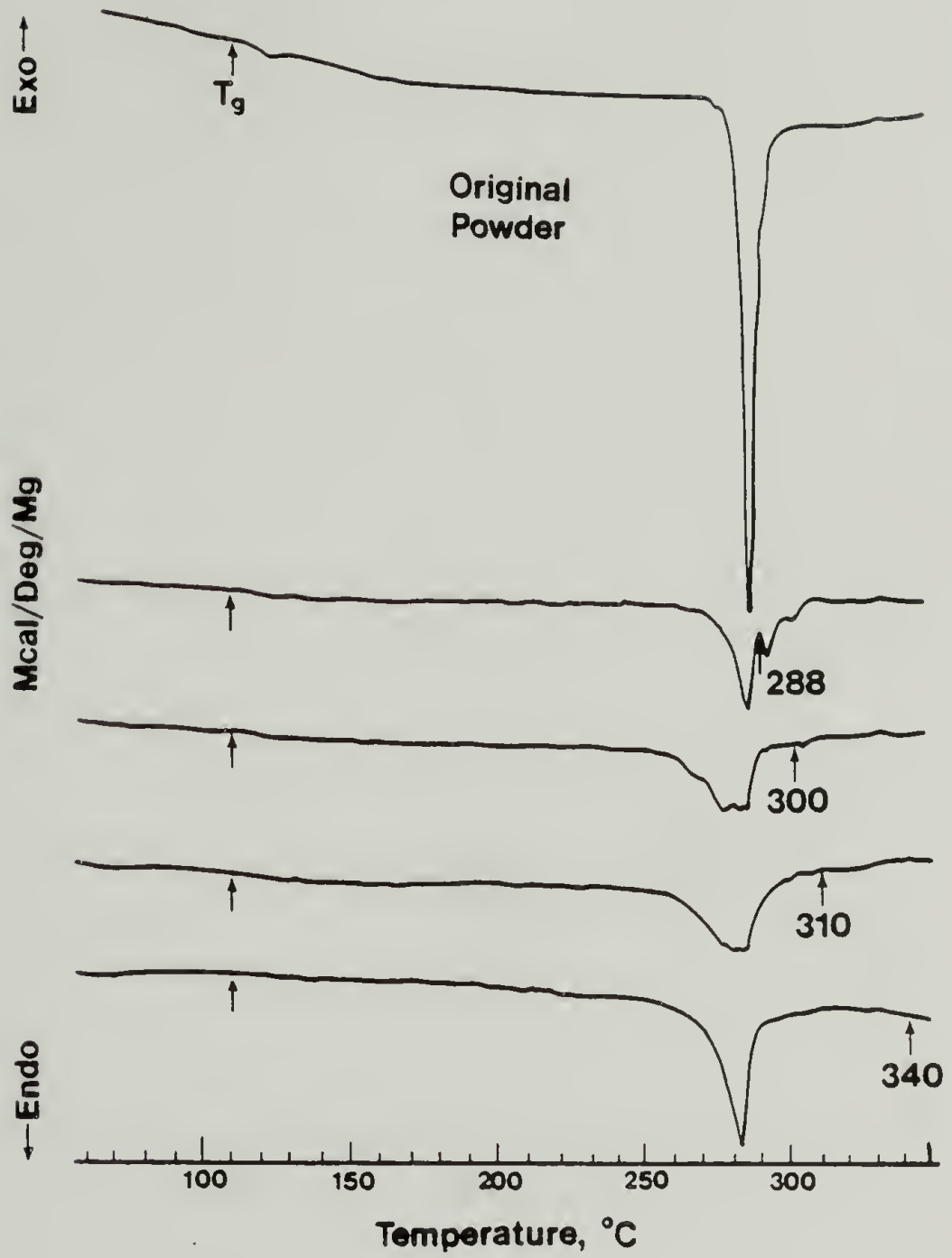

Fig. 57. DSC temperature scans of BPE/I/N-20 #1 rheometer extrudates.

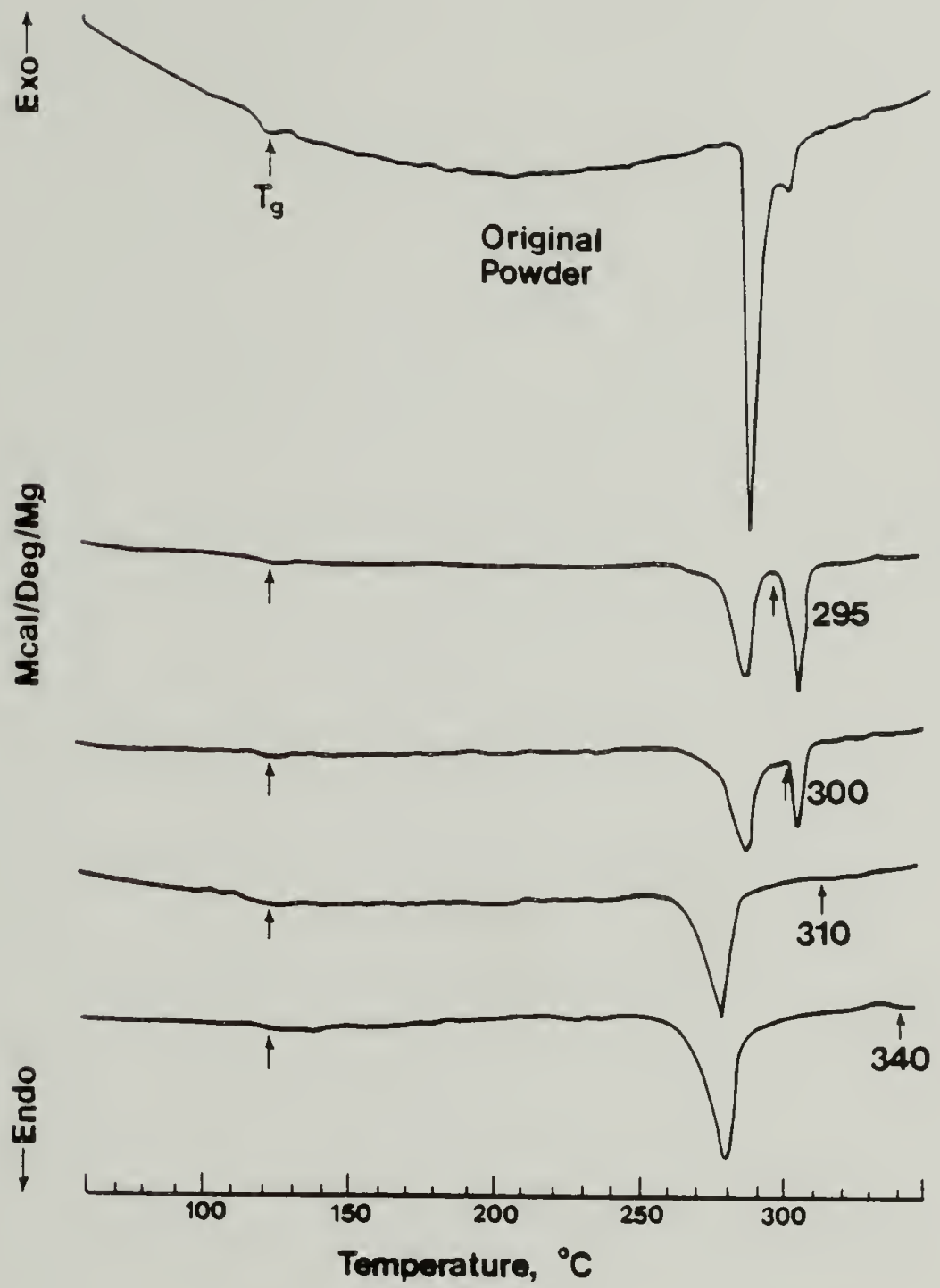

Fig. 58. DSC temperature scans of BPE/I/N-20 #2 rheometer extrudates.

Table 10

The Effect of Extrusion Upon Subsequent Thermal Properties*

Polymer	Extrusion Temperature °C	T_m or $T_{C\rightarrow N}$ °C	ΔH_m or $\Delta H_{C\rightarrow N}$ cal/gm polymer	Crystallinity Weight %
BPE/I	Unextruded	310	17.2	37
	307	293,311	12.9	28
	312	282,297,(332)	7.5,(0.2)	16,(0.5)
	320	298	7.1	15
	327	297	6.6	14
BPE/I/N-20#1	Unextruded	287	6.4(?)	29(?)
	288	286,292,301	3.0	14
	300	277,284,304	2.9	13
	310	280	3.7	17
	340	284	3.7	17
BPE/I/N-20#2	Unextruded	286,300	5.4	25
	295	287,304	3.9	18
	300	286,304	3.5	16
	310	277	3.1	14
	340	279	3.9	18

*DSC heating rate 10 °C/min.

roughly the same temperature, and the degrees of crystallinity became nearly identical.

The data suggest that the principal endotherm exhibited by the BPE/I/N-20 copolyesters is due to melting of the same kind of crystals found in BPE/I, rather than arising from the mesogenic units. Wide-angle x-ray scattering patterns (Chapters VI, VIII) also indicated that the predominant crystal species in BPE/I/N-20 is the same as that in BPE/I. This would not be surprising, since 90 mole % of the two polyester compositions is identical.

There are other features of the BPE/I/N-20 thermograms which seem attributable to the presence of the naphthalate comonomers, since these features were not observed for BPE/I. Both BPE/I/N-20 #1 and BPE/I/N-20 #2 displayed two glass transitions - one at ~ 110-127 °C and another at ~ 147-187 °C. These were most evident during heating of the as-received polyesters at fast rates (20, 40, 80 °C/min). The Tgs are somewhat difficult to discern in Figures 50 and 51, but were clearly evident in the original thermograms.

The occurrence of two glass transitions in the BPE/I/N-20 copolyesters is indicative of separate amorphous phases which were not completely compatible. Presumably, one phase would be richer in naphthalate groups, and the other one richer in isophthalate groups. The higher Tg should be associated with the isophthalate-rich phase, since its temperature is closer to the Tg of the BPE/I homopolyester.

There are other indications that the naphthalate and isophthalate units of the copolyesters may not be completely compatible. Evidence

of possible phase-separation was observed after cooling of the BPE/I/N-20 polyesters from the melt (nematic state). This was manifested by a broadening of the main endotherm in BPE/I/N-20 #1 upon reheating and by the appearance of three distinct endotherms in BPE/I/N-20 #2 (Figs. 54,55). The polymers appeared to become increasingly more heterogeneous when cooled at slower rates.

In examining the BPE/I/N-20 #2 behavior upon reheating, three distinct endotherms were observed (Fig. 55). The main endotherm was postulated earlier to correspond to melting of BPE/I-type crystals, due to its proximity to the melting point for BPE/I homopolyester. Similar logic suggests that the lowest-temperature endotherm may be associated with naphthalate-containing crystals, since that transition is displaced significantly from the peak melting point for BPE/I. If so, this could be the true "crystal→nematic transition" for the BPE/I/N-20 mesogenic units. The transition may not have been observed under other conditions because the naphthalate groups were unable to aggregate sufficiently to crystallize.

The origin of the third endotherm (~ 293°C) for BPE/I/N-20 #2 (Fig. 55) is less clear. Its location suggests that it corresponds to melting of BPE/I-type crystals, but ones which are more perfect than those which melt at the main peak (~ 286°C). A similar high-temperature peak was observed in the as-received BPE/I/N-20 #2 (Fig. 51), but did not appear in the as-received BPE/I/N-20 #1 (Fig. 50).

The greater tendency of BPE/I/N-20 #2 to exhibit multiple endotherms versus BPE/I/N-20 #1 implies a stronger tendency toward

phase-separation. It is possible that phase-separation occurs more easily in BPE/I/N-20 #2 because of its lower molecular weight. With lower molecular weight, fewer chain entanglements are likely to exist, thus permitting diffusion of like comonomers toward each other.

Greater homogeneity with increasing molecular weight has been observed in a separate BPE/I/N-20 molecular weight study (Chapter X). However, it is not yet known whether the increased homogeniety is a direct result of increased molecular weight, or a result of exposure to the higher SSP temperatures used to achieve higher molecular weight.

Additional small endotherms are present in the BPE/I/N-20 thermograms at ~ 390-420 °C. These coincide with the onset of rapid degradation, and are followed by a strong endothermic response with increasing temperature. Similar degradation is seen for the BPE/I homopolyester in DSC scans of the BPE/I rheomoter extrudates (Fig. 56).

It has not yet been determined whether the small BPE/I/N-20 peaks at ~ 390-420 °C are themselves associated with degradation, or whether they represent nematic→isotropic transitons which happen to coincide with the onset of severe degradation. An apparent nematic→isotropic transition at ~ 380 °C has been noted for a lower-molecular weight BPE/I/N-20 polymer (η_{inh} ~ 0.38 dl/gm) via melt turbidity investigations (Chapter II, X). However, the apparatus could not be heated beyond 400 °C, and thus did not permit the study of possible transitions in the other BPE/I/N-20 samples at higher temperatures.

Rheometer Extrudates. DSC thermograms are shown for the rheometer extrudates in Figures 56-58. After extrusion, the transition enthalpies and peak transition temperatures consistently decreased relative to the as-received polymers. This indicated a lower degree of crytallinity and lesser crystal perfection than was achieved during the solid-state polymerization process.

In Chapter III it was noted that certain extrusions were performed at temperatures too close to the melting points for all of the original crystals to have been melted. This is apparent from Figs. 56-58, where some of the crystals in the extrudates exhibit melting point maxima above their extrusion temperature. Thus higher-melting crystals are likely to have existed, and perhaps even became larger through annealing, during the course of the extrusion.

The extrusion temperatures at which all of the original crystals appear to be melted are: ~ 310 °C for BPE/I/N-20 #1 and BPE/I/N-20 #2; ~ 312-320 °C for the BPE/I homopolyester. For the BPE/I/N-20 copolyesters, the completion of melting corresponds to their minima in viscosity as a function of temperature (Figs. 25, 26). For BPE/I, the completion of melting corresponds to the beginning of the Arrhenius region in its viscosity-temperature relationship (Fig. 24).

C H A P T E R VIII

ORIENTATION EVALUATION OF SELECTED EXTRUDATES

One of the most striking characteristics of nematic liquid crystals is their tendency to orient readily in flow fields, and to retain their orientation for relatively long times after any external stresses have been removed. It is this characteristic which provides low viscosity during processing, and permits the attainment of high tensile modulus after processing. In this chapter, scanning electron microscopy (SEM) and wide-angle x-ray scattering (WAXS) are used to illustrate the greater degree of orientation developed by the liquid crystalline BPE/I/N-20 #1 as compared to the BPE/I homopolymer in rheometer extrudates produced under similar conditions.

Scanning Electron Microscopy

Specimen Preparation. Two rheometer extrudates - one BPE/I/N-20 #1 and one BPE/I - were examined via SEM. The rheometer extrudates were prepared at identical shear rates (30 s^{-1}) and nearly the same extrusion temperatures (310°C for BPE/I/N-20 #1 and 320°C for BPE/I), using the same 20/1 L/D capillary which was used to measure melt viscosity (Chapter III). The internal morphologies of the two extrudates were exposed for viewing using two different sample preparation techniques: the BPE/I/N-20 #1 extrudate was slit down the center with a razor at one end, then peeled apart by hand; the BPE/I extrudate (which would not peel apart) was cooled in liquid nitrogen

for a few minutes, then flexed gently by hand until it fractured.

Both extrudates were mounted upon sample holders using silver paint as an adhesive. They were then sputter-coated with gold (350 Å) in a Polaron Type E5100 sputter-coater for four minutes to render their surfaces conductive.

SEM instrumentation. Micrographs were obtained using a U1 Autoscan scanning electron microscope manufactured by ETEC Corporation. A tungsten hairpin filament was used as an electron probe source. Accelerating voltage was 20 kev; beam current was 175 μA; the working distance for focal length was 25 mm. Images were photographed using Polaroid Type 55 positive/negative film.

Results. Scanning electron micrographs of the BPE/I/N-20 #1 and BPE/I rheometer extrudates are presented in Figures 59 and 60, respectively.

The BPE/I/N-20 #1 extrudate appeared to be more highly oriented in the axial direction than the BPE/I, judging from its unique fibrillar morphology. The fibrillar morphology was observed in all BPE/I/N-20 extrudates which were obtained above ~305°C, both for BPE/I/N-20 #1 and BPE/I/N-20 #2, although the content of fibrils was noticeably lower above ~360°C. At temperatures below ~305°C the extrudates would not peel apart, but exhibited brittle fracture when flexed.

The BPE/I extrudates, in contrast, did not exhibit fibrillar morphologies under any extrusion conditions, and appeared to be much less oriented than the BPE/I/N-20 #1. The micrograph in Figure 60

Fig. 59. Scanning electron micrograph of BPE/I/N-20 #1 rheometer extrudate. (66x).

Fig. 60. Scanning electron micrograph of BPE/I rheometer extrudate (66x).

shows that the BPE/I had a relatively continuous structure.

Wide-Angle X-Ray Scattering

Specimens. As with SEM, two rheometer extrudates - one BPE/I/N-20 #1 and one BPE/I - were selected for examination of orientation via WAXS. The extrudates were prepared at identical shear rates (30 s^{-1}) and similar temperatures (310°C for BPE/I/N-20 #1 and 312°C for BPE/I), using a 20/1 L/D capillary.

Technique. Scattering patterns were photographed using a Statton camera and nickel-filtered copper K_α radiation. Kodak XAR-5 film was used, with exposure times of 17 hours. Extrudate samples were mounted with their axes parallel to the length-wise direction of the film. The sample-to-film distance was 54.1 mm, which was calibrated using Al_2O_3.

Results. The WAXS patterns for the BPE/I/N-20 #1 and BPE/I extrudates are presented in Figures 61 and 62, respectively. The BPE/I/N-20 #1 clearly shows greater orientation than the BPE/I - manifested by the diffraction rings tending to appear as arcs, rather than being circularly symmetric.

The BPE/I pattern exhibits essentially no orientation. Evidently, at 30 s^{-1} and 312°C, the BPE/I was able to relax out most of the orientation which was induced by extrusion. Other indications for such relaxation were given by significant extrudate recovery (Chapter IV) and relatively short characteristic times, λ, associated with the

Fig. 61. Wide-angle x-ray scattering from BPE/I/N-20 #1 rheometer extrudate.

Fig. 62. Wide-angle x-ray scattering from BPE/I rheometer extrudate.

onset of shear thinning in the viscosity-shear rate curves (Chapter III).

In contrast, the BPE/I/N-20 #1 showed 1.) a more oriented WAXS pattern, 2.) negligible extrudate recovery (Chapter IV), and 3.) much longer characteristic relaxation times than BPE/I (Chapter III). All three points support the earlier observation that liquid crystals tend to retain their orientation for relatively long times once they have been subjected to a flow field.

Other Comments. The number and location of the diffraction rings were observed to correspond precisely to the peaks in x-ray intensity as measured by the Siemens D-500 (Chapter VI), especially if one compares the BPE/I WAXS photograph in Figure 62 with the BPE/I intensity scan in Figure 43. It is reassuring to see that the two WAXS techniques agree. The angular locations of the rings may be correlated with their locations in the photographs by:

$$2\Theta = \tan^{-1}(0.5\ y/x) \qquad \text{---18}$$

where y is the diameter of the rings, as measured in the photographs of Figures 61 and 62; x is the sample-to-film distance (54.1 mm); 0.5 is a factor correcting for the enlargement of the photograph as compared to the original negative.

C H A P T E R IX

MECHANICAL PROPERTIES

The primary reason for the current high interest in rod-like liquid crystalline polymers (LCP's) is their potential for forming materials having ultra-high strength and ultra-high modulus. These properties are more readily achieved with rod-like LCP's than with conventional polymers because of the greater ease with which LCP's can be oriented.

One of the original goals of this thesis investigation was to compare the tensile strengths and moduli of BPE/I/N-20 and BPE/I rheometer extrudates produced under various extrusion conditions. Difficulties were encountered, however, due to irregularities in extrudate dimensions resulting from gravitational drawing, voids, and occasional flow instabilities. Measurements were, therefore, limited to a comparison of BPE/I extrudates produced at a single extrusion condition to those of a single BPE/I/N-20 polymer - BPE/I/N-20 #1. BPE/I/N-20 #1 was chosen over the other BPE/I/N-20 polymers because its η_{inh} (0.90 dl/gm) most closely matched that of the available BPE/I reference polymer (0.85 dl/gm).

The extrusion temperature chosen for the comparison was 320°C, just above the point at which the BPE/I/N-20 polymers exhibit minima in viscosity and extrudate swell (Chapters III, IV). This temperature

was selected because it was sufficiently high to ensure that all crystals in the polymers would melt prior to extrusion, yet was otherwise low in order to maximize liquid crystalline order in the BPE/I/N-20 #1 and minimize thermal degradation. The polymers were extruded at a moderate shear rate of 30 s^{-1}.

Tensile measurements were made on an Instron Model 1321 servo-hydraulic testing system using the grip separation technique. The extrudates were clamped in grips designed by a previous researcher to accommodate cylindrical samples (44). Sample gage lengths were ~3-6 cm. Longer samples would have been preferred for increased accuracy of strain measurements, but were difficult to obtain due to gravitational drawing during extrusion. The drawing caused a steady decrease in extrudate diameter with increasing length.

Ultimate tensile strengths and elongation-at-break were not measurable, since the exrudates began to slip from the grips at strains of ~3 %. However, tensile moduli were measurable. These were: 2.5 ± 0.2 GPa for BPE/I/N-20 #1 and 1.3 ± 0.2 GPa for BPE/I.

Certainly, neither of these modulus values could be described as ultra-high. They are, in fact, somewhat lower than the values 2.8-4.1 GPa reported for injection-molded poly(ethylene terephthalate) (45), and much lower than the 124 GPa listed for Kevlar 49 fibers in Table 1 (2). This demonstrates that the BPE/I/N-20 #1 does not inherently have a high modulus, and implies a discontinuous crystal structure. The BPE/I/N-20 #1 did, however, exhibit a modulus nearly twice that of BPE/I for extrudates produced under identical extrusion

conditions. Based upon comparisons with other rod-like aromatic polyesters (1), there is reason to believe that BPE/I/N-20 #1 could provide a high-strength, high-modulus fiber if processed under optimum conditions.

C H A P T E R X

MOLECULAR WEIGHT EFFECTS

In capillary flow studies (Chapter III), BPE/I/N-20 #1 exhibited a higher melt viscosity than BPE/I/N-20 #2 - despite having higher apparent molecular weight (η_{inh}). This is contrary to expected behavior. The possibility that compositional differences might account for the viscosity anomaly was investigated (Chapter V), but no significant compositional difference was found. To better understand the role of molecular weight in determining melt viscosity, an additional four samples of BPE/I/N-20 copolyester were obtained from Monsanto - each having a different molecular weight.

Polymerization

These copolyesters were prepared from a single prepolymer batch (η_{inh} ~0.38 dl/gm), thus ensuring that they contained the same ratios of comonomers. The prepolymer was made with the same composition as BPE/I/N-20 #1 and BPE/I/N-20 #2, i.e., 50:40:10 BPE:I:N. Four different molecular weight polymers were obtained by first dividing the prepolymer into four equal portions, then solid-state polymerizing each at a different temperature for a different length of time. Solid state polymerization conditions are given in Table 11.

The polymers have been labelled BPE/I/N-20 #3 - "X," where "X" denotes the η_{inh} of the particular aliquot. The η_{inh} measured were 0.38, 0.52, 0.55, and 0.76 dl/gm.

Table 11

Properties of BPE/I/N-20 #3 Copolyesters*

	BPE/I/N-20 #3-0.38	BPE/I/N-20 #3-0.52	BPE/I/N-20 #3-0.55	BPE/I/N-20 #3-0.76
Solid state polymerization time and temperature	No SSP	45 min @ 260°C	45 min @ 270°C	70 min @ 280°C
η_{inh}, dl/gm 0.5% in 60/40 wt% phenol/ 1,1,2,2-tetrachloroethane	0.38	0.52	0.55	0.76
DSC Properties				
Tg onset, °C	100,(and 195?)	110	110	110,(and 195?)
Tm and/or $T_{C\rightarrow N}$ peaks, °C	271, 281, 295	280, 288, 298	283, 290, 300	295, (302)
ΔH_m and/or $\Delta H_{C\rightarrow N}$, cal/gm polymer	5.0	6.2	6.1	5.6

*Monsanto identification: NBP 214671, D.H. Potthast, 3-17-82.

Melt Turbidity/Stir Opalescence

Melt turbidity and stir opalescence were examined for the BPE/I/N-20 #3 copolyesters, using the technique described in Chapter II. All four polymers displayed melt turbidity/stir opalescence immediately upon melting (onset ~266-300°C). In the three higher-molecular weight polymers, these characteristics persisted to temperatures greater than 400°C, the upper temperature limit of the apparatus. The BPE/I/N-20 #3-0.38 prepolymer, however, displayed an apparent "clearing temperature" at ~380°C, where the polymer became transparent. This probably indicates the nematic→isotropic transition.

The apparent clearing temperature of the prepolymer was difficult to observe, since it was coincident with the onset of degradation, accompanied by rapid bubble formation. The other three higher-molecular weight polymers also showed signs of degradation at the higher temperatures, but a clearing temperature was not observable.

Differential Scanning Calorimetry

DSC temperature scans for the four as-received BPE/I/N-20 #3 copolyesters were obtained at a heating rate of 10 °C/min, and are shown in Figure 63. Each curve is labelled with the inherent viscosity associated with the sample. The magnitudes of the curves may be visually compared, since they have been normalized on a per unit weight basis. The locations of the Tgs, Tms (and/or $T_{C \rightarrow N}$s), and

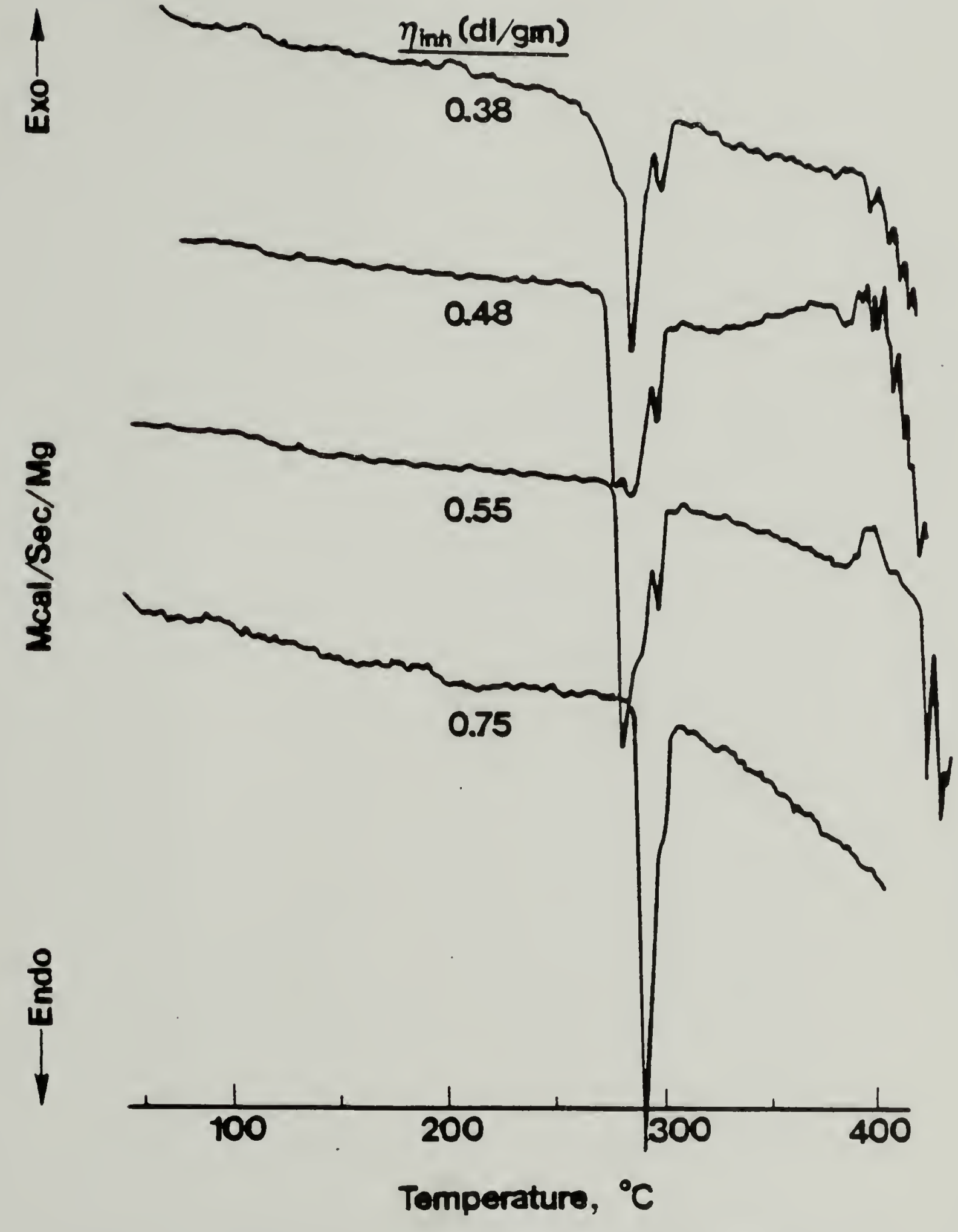

Fig. 63. DSC temperature scans of BPE/I/N-20 #3 polymers having four different molecular weights.

magnitudes of the $\Delta H_m S$ (and/or $\Delta H_{C \rightarrow N} S$) are given in Table 11.

An obvious feature of the thermograms is that the endotherms become more uniform (narrower, homogeneous) in samples polymerized to higher molecular weight. It is unclear, however, whether the homogeneity is a direct result of increased molecular weight, or a result of the increased solid-state polymerization temperature used to achieve higher molecular weight. The onset of melting for each polymer coincides with the temperature at which it was solid-state polymerized.

It was suggested earlier (Chapter VII) that the greater apparent heterogeneity at low molecular weight might arise from phase-separation of the isophthalate and naphthalate sequences, resulting in formation of crystals of different chemical compositions. There is other evidence that the comonomers may not be compatible, in that the copolyesters sometimes exhibit two Tgs. In Figure 63, the highest and lowest molecular weight polymers appear to have two Tgs (i.e., ~100°C and ~195°C), though the two intermediate molecular weight polymers do not. The reason for the inconsistency among the four polymers is unknown.

There are other factors which could account for multiple endotherms besides phase-separation of isophthalate and naphthalate groups. Crystals having differing degrees of perfection can result from different thermal environments during polymerization. Another source of heterogeneity is the distribution of molecular weights;

low molecular weight species tend to form less perfect crystals, which then have lower melting points.

Another feature of the DSC thermograms in Fig. 63 is a large, irregular endothermic response at ~400°C. This coincides with the onset of severe thermal degradation in the polyesters. Although a nematic→isotropic "clearing" temperature was found to occur at ~380°C in the lowest molecular weight polymer, it is not possible to assign such a transition in Fig. 63.

Melt Viscosities

Melt viscosities at 310°C were measured for the two higher-molecular weight BPE/I/N-20 #3 copolymers, using the same 20:1 L:D capillary and same techniques described in Chapter III. The melt viscosities of the two lower-molecular weight BPE/I/N-20 #3 copolymers are not reported, since they were too low to be measured with the 20:1 L:D capillary. The melt viscosities of BPE/I/N-20 #3 - 0.55 and BPE/I/N-20 #3 - 0.76 are shown in Figure 64, as compared to BPE/I/N-20 #1 and BPE/I/N-20 #2.

In order to visualize the dependence of melt viscosity upon molecular weight in the BPE/I/N-20 copolyesters, apparent viscosity (η_{app}) at $\dot{\gamma}$ = 10 s^{-1} has been plotted vs inherent viscosity (η_{inh}) in Figure 65. Melt viscosities of various BPE/I homopolyester samples (316°C) as a function of inherent viscosity have also been plotted, as taken from the study by Mendelson (37).

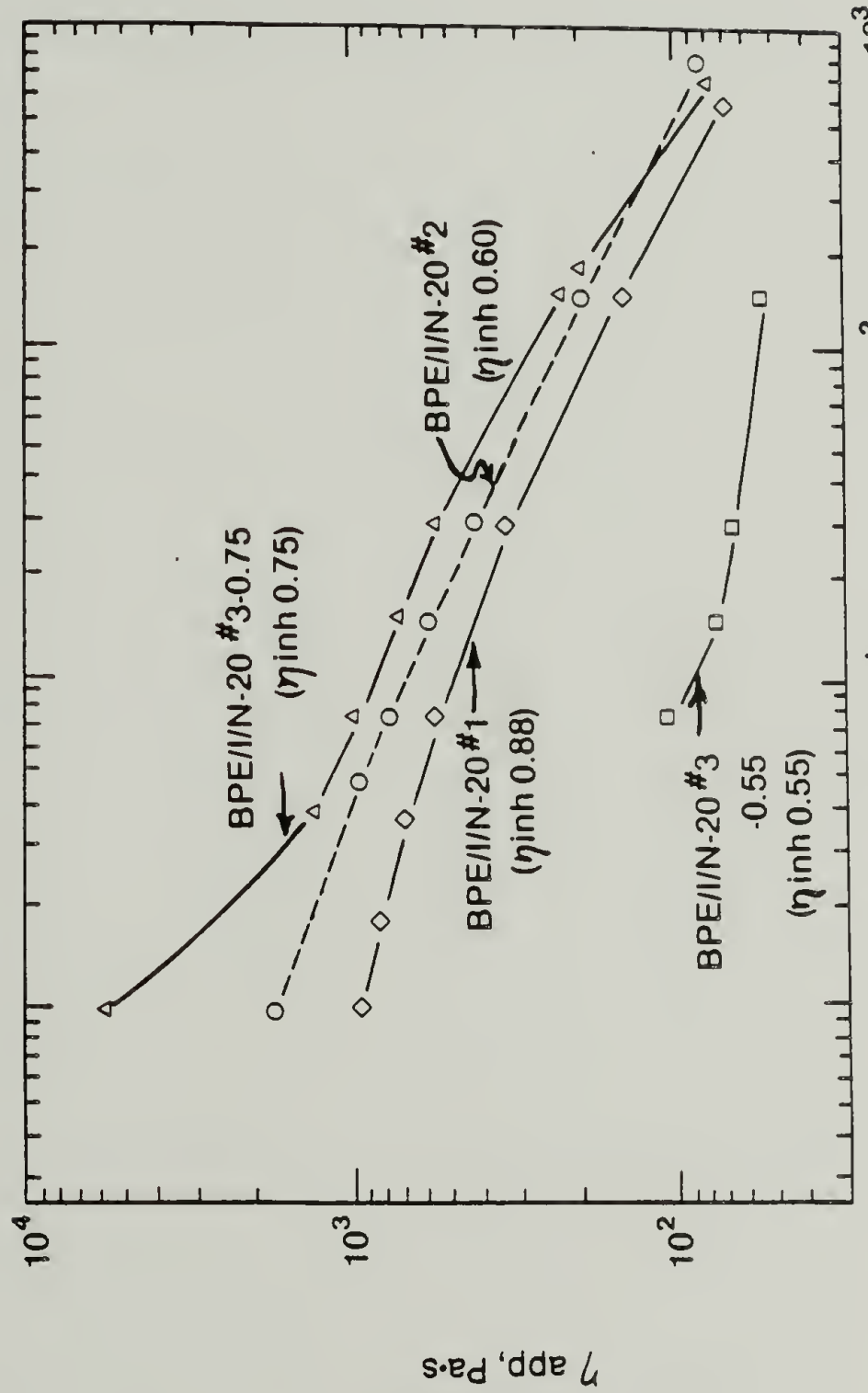

Fig. 64. Melt viscosity vs apparent shear rate for BPE/I/N-20 polymers having four different molecular weights. T = 310°C.

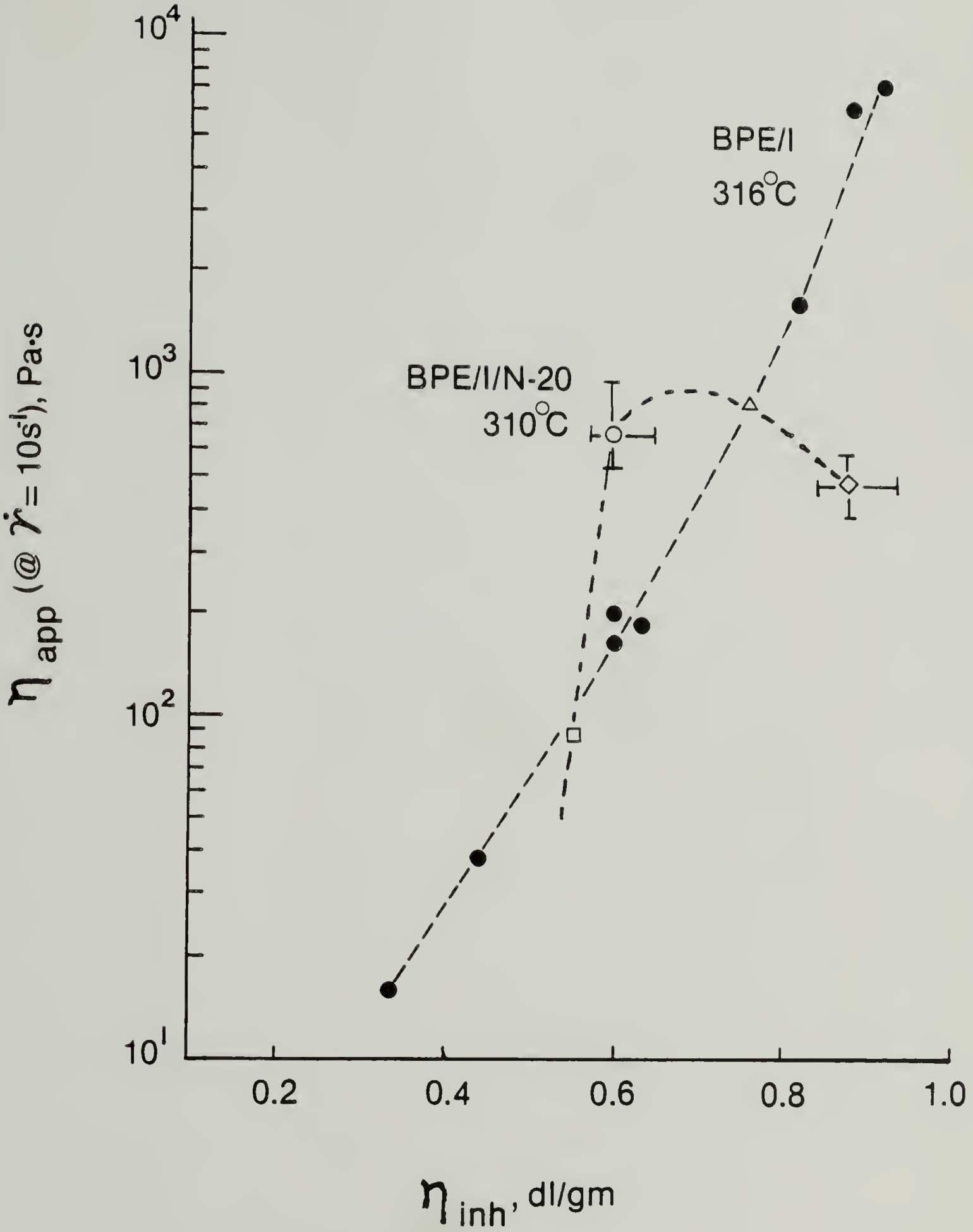

Fig. 65. Melt viscosity (η_{app}) vs apparent molecular weight (η_{inh}) for BPE/I and BPE/I/N-20 polyesters.

If a curve is placed through the BPE/I/N-20 data points, melt viscosity is observed to exhibit a maximum with molecular weight (η_{inh}). This phenomenon may be equivalent to the behavior observed for lyotropic PBA solutions, described in Chapter I (33). However, since all four of these copolymers were not prepared from the same prepolymer batch, there is still a concern that they could contain slightly different comonomer ratios which might have influenced the melt viscosities. Further work is necessary to establish whether the viscosity maximum results solely from differences in molecular weight.

C H A P T E R XI

SUMMARY

Thermotropic liquid crystalline polyesters having a novel Bisphenol E-isophthalate-co-naphthalate composition (designated BPE/I/N-20) have been obtained from Monsanto Co. For this thesis these polyesters have been characterized by a range of rheological and other properties. All BPE/I/N-20 polyesters contained the same nominal ratio of comonomers, but differed in apparent molecular weight (η_{inh}). Their properties have been compared and contrasted to those of a non-liquid crystalline Bisphenol E-isophthalate (BPE/I) reference polyester.

The properties that have been investigated include: viscosity-temperature-shear rate relationships and extrudate swell via capillary rheometry; thermal properties via differential scanning calorimetry; melt turbidity/stir opalescence; crystallinity and its orientation in extrudates by x-ray; extrudate morphology via scanning electron microscopy; composition by infrared spectroscopy, elemental analysis, and ^{1}H nuclear magnetic resonance; and tensile modulus.

Conclusions

Rheology. Several significant differences in rheology were observed between the BPE/I/N-20 liquid crystalline polyesters and the non-

liquid crystalline BPE/I reference polymer. One of the most unusual features exhibited by the BPE/I/N-20 polymers was a minimum in viscosity as a function of temperature. The BPE/I, in contrast, exhibited a conventional monotonic decrease in viscosity with temperature. The viscosity minimum (and subsequent increase) with temperature for the BPE/I/N-20 polymers may be equivalent to behavior observed for low-molecular weight nematic liquid crystals near their nematic→isotropic transitions.

The viscosity minima with temperature for the BPE/I/N-20 polyesters were unexpected, since - at the time the experiments were conducted - the most widely-studied rod-like thermotropic polymers had not exhibited any unusual temperature dependence of viscosity (4,7-11). Recently, however, several researchers have documented viscosity increases (or plateaus) with temperature for rod-like thermotropic polymers (12-18), indicating that this phenomenon may be a general characteristic of these systems.

Other differences observed in the rheology of the liquid crystalline BPE/I/N-20 copolyesters relative to the BPE/I include: 1.) more pronounced shear thinning, 2.) the absence of Newtonian viscosity plateaus at low shear 3.) an order-of-magnitude lower viscosity for one of the BPE/I/N-20 polymers (BPE/I/N-20 #1) as compared to BPE/I of similar apparent molecular weight (η_{inh}), and 4.) much lower (perhaps even negative) extrudate swell. The above features have also been observed in other rod-like thermotropic polymers, and seem to be attributable to the liquid crystalline nature of the

BPE/I/N-20 polymers.

An additional unusual finding in the rheology of the BPE/I/N-20 polymers was a maximum in viscosity (n_{app}) with apparent molecular weight (n_{inh}). In conventional polymers this would be anomalous, since viscosity normally increases markedly with molecular weight. However, such a maximum has been observed in at least one other liquid crystalline system (36): lyotropic solutions of poly(p-benzamide) (PBA). In the PBA system, the viscosity maximum with molecular weight seemed analogous to maxima which occur with concentration and temperature near the isotropic→nematic transition.

Since maxima in viscosity with molecular weight were observed for both the BPE/I/N-20 polymers and the lyotropic PBA solutions, this may represent a general characteristic of polymer liquid crystals. For the BPE/I/N-20 polymers, however, there is still some concern that undetected differences in comonomer ratios or comonomer sequence distribution may have influenced their viscosities. Further work is required to establish whether the viscosity maximum resulted solely from changes in molecular weight.

Orientation Studies. Generally, rod-like liquid crystals can be oriented more easily than isotropic fluids. Greater orientation was shown by BPE/I/N-20 #1 than by BPE/I in extrudates produced under similar conditions. The extrudates were examined via wide-angle x-ray scattering (WAXS), and scanning electron microscopy (SEM). Greater orientation in the BPE/I/N-20 #1 was manifested by a greater tendency

to form diffraction arcs (rather than rings) in WAXS, and by the exhibition of a unique fibrillar morphology via SEM.

Tensile modulus. The current high interest in rod-like liquid crystalline polymers is largely due to their potential for forming high-strength, high-modulus fibers. The moduli of BPE/I/N-20 #1 and BPE/I were compared in terms of rheometer extrudates produced under identical conditions. Neither polymer displayed a high modulus. The shear rate during extrusion was low ($30s^{-1}$) and little orientation was induced. However, the BPE/I/N-20 #1 did exhibit a modulus nearly twice that of the BPE/I, and may have the potential for achieving high modulus under optimized processing conditions.

Future Work

It would be highly desirable to complement the capillary rheometry in this study with rheological measurements in other geometries. In particular, the cone-and-plate rheometer offers a number of advantages. The cone-and-plate provides a homogeneous rate-of-shear throughout the sample, and also permits measurements at lower shear rates. These features would aid in establishing whether, and at what point, yield stresses occur in the liquid crystalline polymers. The cone-and-plate can also provide a measurement of normal stress differences, which are currently an area of uncertainty in polymer liquid crystal rheology. Do the BPE/I/N-20 polymers exhibit negative normal stresses, and under what conditions? Do the normal stresses

correlate with the very low, and perhaps negative, extrudate swell?

Another feature of the cone-and-plate geometry is that it can be adapted to study the response to start-up and cessation of steady shear. Anomalous behavior has been observed in these responses for other liquid crystalline polymers (10,17). For example, there have been reports of secondary maxima in shear stress during start-up of steady shear (10,17), and incomplete stress-relaxation after cessation of steady shear (17). It would be of interest to know whether such behavior patterns would be observed with the BPE/I/N-20 polymers, and whether they are general characteristics of rod-like liquid crystalline polymers.

A potential difficulty in using a cone-and-plate rheometer to study the BPE/I/N-20 liquid crystalline polymers is that > 300°C is required. At the time of this investigation, the only available cone-and-plate rheometers were unable to meet that requirement. Recently, however, a Rheometrics Mechanical Spectrometer has been purchased at the University of Massachusetts which is rated for use at temperatures to 400°C. Perhaps this instrument could be utilized for further work.

One of the more intriguing questions raised in this investigation is whether the BPE/I/N-20 polymers truly exhibit a maximum in viscosity as a function of molecular weight. With the limited number of copolymers studied, there is still some concern that the observed maximum was an artifact of undetected differences in comonomer ratios. A preliminary attempt was made to circumvent differences in comonomer ratio (Chapter X) by dividing a single batch of prepolymer into

portions, and polymerizing each to a different molecular weight. However, this first attempt failed to provide polymers in the necessary molecular weight range (ie, η_{inh} ~ 0.55-1.00 dl/gm) to confirm the maximum. This approach could be tried again. Any or all of the six BPE/I/N-20 polymers remaining from this study could be used as "prepolymers". Each could be divided into portions and subjected to continued solid-state polymerization to achieve the desired molecular weights.

If the maximum (and subsequent decrease) in viscosity with molecular weight is real, there are practical commercial benefits. Above a critical molecular weight, the molecular weights of rod-like polymer liquid crystals could be increased for improved mechanical properties (eg., strength), without there being a penalty in viscosity! Processing might actually be easier with higher molecular weight polymers.

A multitude of other ideas for future work suggest themselves, since the field of polymer liquid crystals is still in the frontier stage, and the BPE/I/N-20 polymers are themselves new to the literature. For example, the morphology and mechanical properties of the BPE/I/N-20 polyesters as a functon of processing conditions have not yet been explored.

The apparent incompatibility within the BPE/I/N-20 copolymers could also be investigated. There appeared to be a tendency for the naphthalate and isophthalate segments to phase-separate, based upon multiple endotherms and T_gs via differential scanning calorimetry. At

what temperatures, and on what time scale, does phase separation occur? Could the incompatibility in some way be responsible for the minima in viscosity and in extrudate swell with temperature?

Another extension of the studies of the BPE/I/N-20 polymers would be to investigate the effects of changing naphthalate and isophthalate proportions. Is there an optimum ratio of isophthalate-to-naphthalate to minimize viscosity and maximize mechanical properties? What is the minimum naphthalate content required to achieve liquid crystallinity?

Finally, all of the unusual phenomena observed for the BPE/I/N-20 polymers could be investigated in other thermotropic liquid crystalline polymers as well. The BPE/I/N-20 polymers were, in some ways, difficult to work with. Ie., their processing temperatures were rather high and their nematic→isotropic transitions were not accessible due to severe degradation. These problems might be avoided by choosing polymers which have lower transition temperatures and are not as susceptible to degradation.

REFERENCES

1. Preston, J., "Synthesis and Properties of Rod-like Condensation Polymers," in Liquid Crystalline Order in Polymers, A. Blumstein, ed., Academic Press, New York, (1978).
2. "Characteristics and Uses of Kevlar 49 Aramid High Modulus Organic Fiber," duPont Technical Information Bulletin K-5, September, 1981, Textile Fibers Department, Technical Service Station, E.I. du Pont de Nemours & Co.(Inc), Wilmington, DE 19898.
3. Jackson, W.J., Jr., and H.F. Kuhfuss, J. Polym. Sci., Chem. Ed., 14, 2043-2058 (1976).
4. Mc Farlane, F.E., V.A. Nicely, and T.G. Davis, "Liquid Crystal Polymers. II. Preparation and Properties of Polymers Exhibiting Liquid Crystalline Melts," in Contemporary Topics in Polymer Science, Vol. 2, E.M. Pearce and J.R. Schaefgen, ed., Plenum Press, New York, (1977).
5. Deex, O.D., and V.W. Weiss, U.S. Patent 4,102,864 (1978).
6. Baird, D.G., "Rheology of Polymers with Liquid Crystalline Order," in Liquid Crystalline Order in Polymers, A. Blumstein, ed., Academic Press, New York, (1978).
7. Wissbrun, K.F., J. Rheol., 25, No.6, 619-662 (1981).
8. Jackson, W.J., et al, Proc. Ann. Conf., Reinf. Plast./Compos., SPI, 1975, 30, 17D.

9. Jerman, R.E., and D.G. Baird, J. Rheol., 25, 275-292 (1981).

10. Wissbrun, K.F., "Observations on the Melt Rheology of Thermotropic Aromatic Polyesters," paper presented at Symposium on Liquid Crystal Polymers, Leeds, July 16-17, 1980; Br. Polym. J., 12, 163-169 (1980).

11. Baird, D.G., and G.L. Wilkes, ACS Polymer Preprints, Vol. 22, No. 2, p.357, August, 1981.

12. White, J.L., Bingham Award Address at Meeting of Soc. of Rheol., Louisville, Oct. 12-16, 1981.

13. Suto, S., J.L. White and J.F. Fellers, Univ. of Tennessee, Knoxville, PATRA Report No. 174, September, 1981. Also Rheol. Acta, 21, 62-71 (1982).

14. Prasadarao, M., E.M. Pearce, and C.D. Han, J. Appl. Polym. Sci., 27, 1343-1354 (1982).

15. Wissbrun, K.F., and A.C. Griffin, "Rheology of a Thermotropic Polyester in the Nematic and Isotropic States," in press.

16. Bickel, A., M.T. Shaw, and E.T. Samulski, "Rheological Properties of a Thermotropic Liquid Crystal Polyester," in press.

17. Baird, D.G., Paper presented at IUPAC 28th Macromolecular Symposium, Amherst, MA., July 12-16, 1982.

18. White, J.L., Paper presented at IUPAC 28th Macromolecular Symposium, Amherst, MA., July 12-16, 1982.

19. Porter, R.S., and J.F. Johnson, "The Rheology of Liquid Crystals," in Rheology, Vol. 4, F.R. Eirich, ed., Academic, New York (1967).

20. Landolt-Borstein, "Physikalisch - chemische Tabellen," Vol. I, p. 165, Springer, Berlin, 1923.

21. Berry, G.C., "Properties of Rigid Chain Polymers," in Contemporary Topics in Polymer Science, Vol. 2, E.M. Pearce and J.R. Schaefgen, ed., Plenum Press, New York (1977).

22. McFarlane, F.E., and T.G. Davis, U.S. Patent 4,011,199 (1977).

23. Barr, J.B., S. Chwastiak, R. Didchenko, I.C. Lewis, R.T. Lewis, and L.S. Singer, in New and Specialty Fibers, J. Economy, ed., Applied Polymer Symposia, No. 29, p. 161, Wiley, New York (1976).

24. Kiss, G., and R.S. Porter, J. Polym. Sci. Polym. Symp., 65, 193-211 (1978).

25. Kiss, G., Ph.D. Thesis, University of Massachusetts, Amherst, 1979.

26. Kiss, G., and R.S. Porter, J. Polym. Sci., Polym. Phys. Ed., 18, 361 (1980).

27. Hutton, J.F., Rheol. Acta, 14, 979-992 (1975).

28. Duke, R.W., and L.L. Chapoy, Rheol. Acta, 15, 548-557 (1976).

29. Huang, T.A., Ph.D. Thesis, University of Wisconsin, 1976; Dissert. Abs., 37, Ser. B, 5741 (1976).

30. Ghijsels, A. and J. Raadsen, Pure Appl. Chem., 52, 1359-1386 (1980).

31. Leslie, F.M., Advances in Liquid Crystals, Vol. 4, G.H. Brown, ed., Academic, New York (1979).

32. Bird, R.B., R.C. Armstrong, and O. Hassager, Dynamics of Polymeric Liquids, Vol. 1. Fluid Mechanics, John Wiley & Sons, New York (1977).

33. Papkov, S.P., V.G. Kulichikhin, V.D. Kalmykova, and A. Ya. Malkin, J. Polym. Sci., Polym. Phys. Ed., 12, 1753-1770 (1974).

34. Deex, O.D., private communication.

35. Ort, M., private communication.

36. Blumstein, A. Vilsagar, S., Ponrathnam, S., Clough, S.B., Blumstein, R.B., Maret, G., J. Polym. Sci., Polym. Phys. Ed., 20, 877 (1982).

37. Mendelson, R.A., Proceedings of IUPAC 28th Macromolecular Sym - posium, Amherst, MA July 12-16, 1982, p.791.

38. Graessley, W.W., J. Chem. Phys., 47, 1942 (1967).

39. Navard, P. and Haudin, J.-M., Br. Polym. J., 12 (1980).

40. NMR Spectrum 9199 M, Standard Spectra Collection, Sadtler Research Laboratories, 1970.

41. NMR Spectrum 20536M, Standard Spectra Collection, Sadtler Research Laboratories, 1975.

42. Ruland, W., Acta Cryst., 14, 1180 (1961).

43. Alexander, L.E., X-Ray Diffraction Methods in Polymer Science, Chapter 3, Wiley-Interscience, New York, 1969.

44. Capiati, N.J., and R.S. Porter, J. Polym. Sci., Polym. Phys. Ed., 13, 1177 (1975).

45. Modern Plastics Encyclopedia, Vol. 57, No. 10A, 1980-81.